The Dissertation Committee for Ellyn Cymbre Ranz Certifies that this is the approved version of the following dissertation:

Mobility in Individuals with Traumatic Lower-Limb Injuries: Implications for Device Design, Surgical Intervention and Rehabilitation Therapies

Committee:

Richard R. Neptune, Supervisor

Ronald E. Barr

Richard H. Crawford

James S. Sulzer

Jason M. Wilken

Mobility in Individuals with Traumatic Lower-Limb Injuries: Implications for Device Design, Surgical Intervention and Rehabilitation Therapies

by

Ellyn Cymbre Ranz, B.S.Bio.E.; M.S.M.E.

Dissertation

Presented to the Faculty of the Graduate School of

The University of Texas at Austin

in Partial Fulfillment

of the Requirements

for the Degree of

Doctor of Philosophy

The University of Texas at Austin

May 2016

Dedication

This dissertation is dedicated to Hans and the rest of my family, for their unconditional love and support.

Acknowledgements

I would like to thank my advisor, Dr. Richard Neptune, for his support and guidance throughout my graduate study, for motivating me to grow as a researcher, and for creating an exciting and collaborative research environment. I am incredibly grateful for everything he has done to help me pursue my graduate degree as well as my future career.

I am very appreciative of the past and present members of the Neuromuscular Biomechanics Laboratory for their unending encouragement, support, and inspiration. I have greatly enjoyed the collaborative work environment and I am privileged to complete my graduate study with a group of researchers who have also become close friends.

I would also like to thank our collaborators at the Center for the Intrepid in Fort Sam Houston, TX. Specifically, I wish to thank Dr. Jason Wilken, Dr. Elizabeth Russell Esposito, and Dr. Donald Gajewski for sharing their valuable expertise, their assistance with subject recruitment, data collection, and data analysis, and for their assistance in the development of my doctoral study.

I wish to thank Dr. Ronald Barr, Dr. Richard Crawford, Dr. James Sulzer, and Dr. Jason Wilken for serving on my dissertation committee. I am very appreciative of their feedback and guidance throughout the development and completion of my dissertation.

I am truly grateful for the support of my family and friends. Mom and Dad, thank you for always encouraging me to pursue my passions and for reminding me to focus on the important things in life. Austin and Holden, thank you for motivating and inspiring me. Hans, thank you for cheering me on and supporting me on this incredible journey. I cannot wait for the new adventure we are about to start.

Finally, I am very grateful to have received financial support from the Graduate School and the Cockrell School of Engineering through the Diversity Recruitment Fellowship, the Thrust 2000 – Flo Wells McGee Endowed Fellowship in Engineering, the Warren A. and Alice L. Meyer Endowed Scholarship in Engineering, the Graduate School Endowed Continuing Fellowship, and the Earnest E. and Elsie M. Clawson Endowed Scholarship in Engineering. I am also grateful to have received financial support from the Center for Rehabilitation Sciences Research (CRSR), Department of Physical Medicine and Rehabilitation, Uniformed Services University of Health Sciences, Bethesda, MD. The views expressed herein are those of the author and do not reflect the official policy or position of Brooke Army Medical Center, the U.S. Army Medical Department, the U.S. Army Office of the Surgeon General, the Department of the Army, Department of Defense or the U.S. Government.

Mobility in Individuals with Traumatic Lower-Limb Injuries: Implications for Device Design, Surgical Intervention and Rehabilitation Therapies

Ellyn Cymbre Ranz, Ph.D.

The University of Texas at Austin, 2016

Supervisor: Richard R. Neptune

Traumatic injuries to the extremities are commonly observed in emergency room patients and military personnel in combat. Restoring high mobility and functionality is a primary goal post-injury, which may require the use of rehabilitative devices, surgical interventions, and rehabilitation therapies. The research detailed in this dissertation investigates specific elements of these approaches through the use of experimental study and modeling and simulation.

In the first study, the influence of passive-dynamic ankle-foot orthosis bending axis on the gait performance of limb salvage subjects was investigated. Bending axis location was altered by fabricating customized orthosis components using additive manufacturing and was tested in a gait laboratory. Altering bending axis location did not result in large or consistent changes in gait measures, however subjects expressed strong preferences for bending axis condition and preference was strongly related to specific gait measures. This suggests that preference and comfort are important factors guiding the prescription of bending axis location. In the second study, musculoskeletal modeling was

used to examine the influence of transfemoral amputation surgical techniques on muscle capacity to generate forces and moments about the hip. Muscle reattachment tension and stabilization were shown to be critical parameters for post-amputation capacity, which supports the use of myodesis stabilization (muscle is reattached directly to bone) in amputation procedures. In the third study, a forward dynamics simulation of transfemoral amputee gait was developed and used to examine individual muscle and prosthesis contributions to walking subtasks. The residual hip muscles, and intact ankle, knee, and hip muscles worked synergistically to provide body support, anteroposterior propulsion, mediolateral control, and leg swing. Increased contributions of contralateral muscles to ipsilateral subtasks as well as increased duration of specific muscle contributions were observed in comparison to non-amputee and transtibial amputee walking. These findings can be used to help develop targeted rehabilitation therapies and improve transfemoral amputee locomotion.

Through elucidating the influence of PD-AFO bending axis on gait performance as well as the influence of transfemoral amputation surgical techniques on muscle capacity and function, this research provides a foundation for improved rehabilitation outcomes, and thus mobility for individuals who have experienced traumatic lower-limb injuries.

Table of Contents

List of Tables

List of Figures

Chapter 1: Introduction

Traumatic injuries to the extremities are commonly observed in emergency room patients, with over 587,000 recorded trauma admissions in the United States in 2014 related to these injuries (National Trauma Data Bank Annual Report, 2015). In addition to the general population, recent conflicts Operation Iraqi Freedom and Operation Enduring Freedom have resulted in a cohort of young, active individuals experiencing traumatic injuries (Owens et al., 2007). Over half of these injuries were to the extremities, with 26.5% occurring in the lower extremities (Owens et al., 2007). Many of these injuries are caused by high-energy impacts, which can lead to widespread damage that may require extensive surgery (Keeling et al., 2010; Tintle et al., 2010a; Tintle et al., 2010b) and rehabilitation (Granville et al., 2010; Owens, 2010). For these individuals, restoring high mobility and functionality post-injury is a primary goal, which can be accomplished through multiple approaches including the use of assistive devices, surgical techniques and rehabilitation therapies. The research detailed in this dissertation investigates specific elements of these approaches through the use of experimental and modeling and simulation studies.

Surgical advancements have enabled an increasing number of lower-limb salvage procedures, which can preserve an injured limb that may have previously required amputation (Shawen et al., 2010). However, extensive neurological and/or musculoskeletal injuries often exist post-surgery that require the use of an assistive

device, such as an orthosis, to restore function and mobility. Recent developments in ankle-foot orthosis (AFO) design include the development of passive-dynamic ankle-foot orthoses (PD-AFOs), which can help compensate for lost plantarflexor function by storing and releasing elastic energy during gait (Patzkowski et al., 2011). Previous studies have demonstrated the benefits (e.g., increased self-selected walking velocity and step length) of these devices (Desloovere et al., 2006; Patzkowski et al., 2012; Van Gestel et al., 2008) as well as investigated the influence of PD-AFO stiffness on specific biomechanical measures (Arch et al., 2015; Haight et al., 2015; Harper et al., 2014a; Russell Esposito et al., 2014) and energy cost (Bregman et al., 2011). However, there is still a limited understanding of the influence of other PD-AFO design characteristics on gait performance, and thus the prescription process remains largely qualitative.

Current PD-AFO designs include a molded footplate, cuff worn below the knee, and strut rigidly connecting them (e.g., Figure 2.1a) (Patzkowski et al., 2011). During walking, deflection occurs along the length of the strut, with the greatest deflection occurring at a central bending axis. Previous work has demonstrated that AFO bending axis location may vary with plantarflexion and dorsiflexion movements (Sumiya et al., 1997), and thus is a design characteristic that can potentially influence gait performance. However, this has largely been unexamined. The goal of the first study in Chapter 2 was to examine the influence of PD-AFO bending axis location on gait performance. A better understanding of the relationships between PD-AFO bending axis location and gait performance could allow for improved prescription guidelines and ultimately, better rehabilitation outcomes.

Although an increasing number of limb salvage procedures have been performed in recent years (Shawen et al., 2010), estimates indicate that in the United States over 769,000 individuals live with amputation resulting from trauma (Ziegler-Graham et al., 2008). Of these amputations, 29% are of the lower extremities, and the prevalence of traumatic amputation is continuing to rise (Ziegler-Graham et al., 2008). In addition to the general population, there has also been an increase in the rate of amputation per trauma admission resulting from combat injuries (Krueger et al., 2012). The vast majority of amputations resulting from recent combat injuries were of the lower extremities, 41.8% of which occurred at the transtibial level and 34.5% at the transfemoral level (Krueger et al., 2012). Advancements have been made in amputation technique and prosthetic technologies (for review, Fergason et al., 2010; Laferrier et al., 2010) and rehabilitation therapies (e.g., Granville and Menetrez, 2010; Owens, 2010), which have improved post-amputation mobility in recent years. While continued improvement of prosthesis designs and rehabilitation therapies is critical to improving patient outcomes, surgical technique directly influences residual limb function, and thus it is critical that optimal surgical techniques are used in amputation procedures. In a transfemoral amputation, significant musculature is removed and altered during surgery (Gottschalk, 2004). Important aspects of surgical technique include residual limb length, which muscles are reattached to the residual limb, the wrap or insertion position of the reattached muscles, and the tension and stabilization technique used in the reattachment. All of these factors may influence muscle balance and alignment of the residual limb during gait (Gottschalk, 2004). However, no study has investigated the influence of these

factors on the capacity of individual muscles to generate force and moments about the hip joint post-amputation.

While surgical advancements have been made, the highly invasive nature of such procedures makes systematic investigations of specific surgical techniques challenging. Musculoskeletal modeling and simulation is a powerful non-invasive framework through which to examine the influence of specific surgical techniques. Modeling and simulation has been used previously to investigate the influence of surgical interventions such as tendon transfer (Delp et al., 1994; Magermans et al., 2004), joint replacement (e.g., Marra et al., 2015; Piazza et al., 2001) and paraspinal muscle resection in posterior lumbar surgery (Bresnahan et al., 2010). Thus, musculoskeletal modeling provides an ideal framework through which to examine the influence of different amputation techniques. The goal of the second study in Chapter 3 was to examine the influence of different transfemoral amputation surgical techniques on muscle force- and moment-generating capacity using a musculoskeletal modeling approach. The insights gained from this study provide a foundation from which orthopedic surgeons may improve amputation procedures and thus rehabilitation outcomes.

In addition to investigating the influence of surgical technique, musculoskeletal modeling and simulation has also been used to provide insight into key clinical questions such as how specific patient populations compensate for impaired or lost muscles groups. Individual muscle contributions to the biomechanical subtasks of unimpaired walking (Anderson et al., 2003; Liu et al., 2006; McGowan et al., 2009; Neptune et al., 2004) as well as the individual muscle and prosthesis contributions, and corresponding

compensatory mechanisms, to unilateral transtibial amputee walking (Fey et al., 2013; Silverman et al., 2012; Zmitrewicz et al., 2007) have previously been examined. The insights gained through these studies provide a foundation from which targeted rehabilitation therapies and improved prostheses can be developed. However, the functional role of individual muscles in transfemoral amputee gait remains largely unexamined. Thus, the goal of the third study in Chapter 4 was to examine the individual muscle contributions to walking subtasks and identify compensatory mechanisms in transfemoral amputee gait.

The overall goal of this research was to improve mobility in individuals who have experienced traumatic lower-limb injuries using experimental and modeling and simulation techniques. Through elucidating the influence of PD-AFO bending axis on gait performance as well as the influence of transfemoral amputation surgical techniques on muscle capacity and function, this research investigates specific elements of device design, surgical techniques, and rehabilitations therapies, and provides a foundation for improved rehabilitation outcomes.

Chapter 2: The Influence of Passive-Dynamic Ankle-Foot Orthosis Bending Axis on Gait Performance in Individuals with Lower-Limb Impairments

INTRODUCTION

Recent military conflicts have resulted in a cohort of young, active individuals who have experienced traumatic injuries (Owens et al., 2007). Many injuries are the result of high energy blasts, frequently occurring at the foot or ankle (Tintle et al., 2010b). As a result of surgical advancements, these injuries can often be treated with limb salvage procedures as opposed to amputation (Shawen et al., 2010). However, due to extensive musculoskeletal or neuromuscular injury, deficits in ankle strength and mobility may persist post-surgery and often an assistive device, such as an orthosis, is needed to help restore function. Passive-dynamic ankle-foot orthoses (PD-AFOs) are commonly prescribed to augment impaired ankle muscle function and restore walking ability in individuals with various lower-limb mobility impairments by providing elastic energy storage and return. Previous studies have demonstrated the beneficial effects of PD-AFOs on individuals with gait limitations (Desloovere et al., 2006; Patzkowski et al., 2012; Van Gestel et al., 2008), and have specifically examined the influence of PD-AFO stiffness on gait performance (Arch et al., 2015; Haight et al., 2015; Harper et al., 2014a; Russell Esposito et al., 2014) and energy cost (Bregman et al., 2011). However, the design and prescription process remains largely qualitative and modifications to PD-AFO design characteristics other than stiffness may be advantageous.

One PD-AFO design includes a molded footplate, cuff below the knee, and strut directly connecting the two (e.g., Figure 2.1a) (Patzkowski et al., 2011). During walking, deflection occurs along the length of the strut, with the location of greatest deflection or bending axis occurring at the center. Sumiya et al. (1997) observed that the AFO instantaneous center of rotation (representing the axis of a hingeless AFO as determined by AFO deformation) was located at the level of the ankle joint during plantarflexion movements and was located even more distally for dorsiflexion movements. Thus, PD-AFO bending axis is a design characteristic that may potentially influence ankle mechanics, yet it has been largely uninvestigated.

The alignment of the PD-AFO bending axis with the natural ankle joint may be beneficial for improving gait mechanics. Previous studies have examined the influence of AFO and physiological joint alignment in articulated AFOs, suggesting that alignment of the AFO joint with the natural ankle joint minimizes spatiotemporal and foot kinematic deviations from barefoot walking (Leardini et al., 2014) and results in minimal resistance torque (Gao et al., 2011). This finding has also been observed in articulated external fixations of the ankle (Bottlang et al., 1999). In addition, research has shown that misalignment of articulated AFOs with the ankle joint can lead to increases in cuff movement (Fatone et al., 2007; Fatone et al., 2016), which may cause patient discomfort by generating skin and underlying tissue irritation on the shank.

To systematically study the effect of individual PD-AFO design characteristics, the ability to effectively replicate the features of clinical devices and manipulate design is required. To address this need, an additive manufacturing framework was previously

developed using selective laser sintering (SLS) (Harper et al., 2014b). SLS is an ideal additive manufacturing technique that can be used to efficiently fabricate customized, functional devices with precisely controlled design characteristics. SLS has previously been used to manufacture PD-AFOs (Faustini et al., 2008; Harper et al., 2014a; Schrank et al., 2011), as well as prosthetic sockets (Faustini et al., 2006; Rogers et al., 2007), feet (Fey et al., 2011; South et al., 2010) and ankles (Ventura et al., 2011a; Ventura et al., 2011b). In addition, PD-AFO components manufactured using SLS have been shown to influence gait performance in the same manner as clinically prescribed carbon fiber PD-AFOs (Harper et al., 2014b). Thus, SLS provides an ideal method to systematically alter PD-AFO bending axis.

Thus, the overall goal of this study was to use SLS to manufacture PD-AFOs with systematically varied bending axes and quantify the effect of the axis location on spatiotemporal, electromyographic, kinematic and kinetic measures. We hypothesize that subjects will prefer a more distal bending axis, which is located closer to the physiological ankle joint, and that this preference will correspond to improvements in biomechanical gait measures (closer to able-bodied). Insights gained by investigating the relationships between PD-AFO bending axis and gait performance will help identify the bending axis condition that results in the most normalized gait mechanics. This information can then be used to develop prescription guidelines for PD-AFOs to enhance locomotor function and rehabilitation outcomes.

METHODS

Subjects

A repeated-measures study design was used to compare across strut conditions. Thirteen participants who had experienced lower extremity trauma resulting in unilateral ankle muscle weakness and were undergoing rehabilitation at the Center for the Intrepid (Brooke Army Medical Center, JBSA Fort Sam Houston, TX) were enrolled in this study (Table 2.1). Each participant was clinically prescribed a PD-AFO (Intrepid Dynamic Exoskeletal Orthosis, Patzkowski et al., 2011). All participants provided institutionally-approved written informed consent prior to participation in this study and all data collection took place at the Military Performance Laboratory at the Center for the Intrepid.

Table 2.1: Participant demographics. R (L) indicates right (left) side impairment. Etiology as determined by medical assessment and record review.

Participant	Age (yr)	Height (m)	Body Mass (kg)	Leg Length (m)	Affected Side (R/L)	Etiology
1	30	1.75	79.1	0.95	L	Tibia/fibula fracture
2	30	1.76	78.2	0.98	L	Tibia/fibula fracture
3	36	1.78	75.5	0.99	L	Talar fracture, shrapnel
4	22	1.64	80.3	0.91	R	Shrapnel
5	27	1.82	92.9	0.98	R	Neuropathy
6	36	1.95	82.2	1.11	L	Multiple fractures, shrapnel
7	26	1.86	110.4	1.01	R	Soft tissue injury, neuropathy
8	33	1.77	90.7	0.98	L	Tibia fracture
9	36	1.76	83.6	0.93	R	Multiple fractures
10	21	1.75	88.3	0.94	L	Shrapnel, foot fracture
11	22	1.97	99.5	1.07	L	Tibia/fibula fracture
12	25	1.69	91.4	0.90	R	Soft tissue injury, neuropathy
13	40	1.77	90.8	0.98	R	Neuropathy
Average	29.54	1.79	87.92	0.98		
Std Dev	6.28	0.09	9.70	0.06		

SLS AFO Fabrication

The clinically prescribed carbon fiber PD-AFO consisted of three components: a footplate, cuff and a strut connecting the footplate and cuff (Figure 2.1a). In this study, a strut emulating the prescribed carbon fiber strut stiffness with a central bending axis was manufactured for each subject using Nylon 11 (PD D80-ST, Advanced Laser Materials, LLC, Temple, TX) with SLS (Vanguards HiQ/HS Sinterstation, 3D Systems, Inc., Rock Hill, SC). A previously described SLS framework for designing and manufacturing the strut was used and summarized here (Harper et al., 2014b). The stiffness of the prescribed carbon fiber strut was determined through mechanical testing in a three-point-bend configuration with a support span of 160 mm and a maximum load of 890 N (5000 N uniaxial load cell, Instron, Norwood, MA). Computer aided design (Solidworks, Dassault Systèmes Solidworks Corp., Waltham, MA) and a predictive stiffness model were used to design each SLS strut. Manufactured SLS struts were subsequently tested in the same three-point-bend configuration to verify the stiffness matched the prescribed carbon fiber strut within ± 5%.

The design and manufacture of an SLS strut possessing an off-center bending axis was performed using similar methods. The SLS strut design with a central bending axis was altered to offset the bending axis by decreasing the cross-sectional area of the strut, centered at 30% of the inner bolt hole-to-bolt hole distance from the center of the strut (Figure 2.1b). The cross-sectional area of the strut was decreased using a 2.54 cm (1 inch) radius circular extrusion in the posterior half of the strut thickness. The cross-sectional area alteration was selected in order to bias the bending axis of the strut while minimizing

stress concentrations. Finite element analyses were performed to adjust the altered SLS strut thickness to match the prescribed strut stiffness. Manufactured SLS struts were similarly tested in a three-point-bend configuration using a variable support span (the inner bolt hole-to-bolt hole distance) and a maximum load of 890 N (100 kN uniaxial load cell, MTS ReNew/Instron, Eden Prairie, MN) to verify the stiffness. Adequate part strength and ductility were verified through the testing of SLS tensile specimens (5000 N uniaxial load cell, Instron, Norwood, MA).

Experimental Data Collection

Participants performed overground walking trials while electromyographic (EMG), kinematic and kinetic data were collected. Participants were tested under three PD-AFO bending axis conditions: proximal bending axis (high), central bending axis (middle) and distal bending axis (low) (Figure 2.1b-d). The SLS strut manufactured with an off-center bending axis was used for both the high and low bending axis conditions, and strut orientation determined the bending axis location. The order of device testing was randomized, and participants were given a minimum of 30 minutes acclimation time to each PD-AFO bending axis condition prior to testing. Lead tape (Clubmaker^{TM}, Golf Smith, Austin, TX) was added along the length of each strut as needed to ensure equivalent PD-AFO masses across the bending axis conditions.

For each of the bending axis conditions, participants performed overground walking at both their self-selected and Froude (0.16) (Vaughan et al., 2005) speeds. Surface EMG data (Motion Laboratory Systems, Inc., Baton Rouge, LA) were collected

at 1200 Hz bilaterally from seven muscles: soleus (SOL), medial gastrocnemius (GAS), tibialis anterior (TA), rectus femoris (RF), biceps femoris long head (BF), vastus medialis (VAS) and gluteus medius (GMED). Three-dimensional (3D) kinematics were collected at 120 Hz using a 26 camera motion capture system (Motion Analysis Corp., Santa Rosa, CA) and a 6 degree-of-freedom body segment marker set with 57 markers (Wilken et al., 2012). Ground reaction forces (GRFs) were collected at 1200 Hz using force plates (AMTI, Inc., Watertown, MA) embedded along the walkway. After all sessions were completed, participants indicated their ranked-order preference of the PD-AFO bending axis conditions.

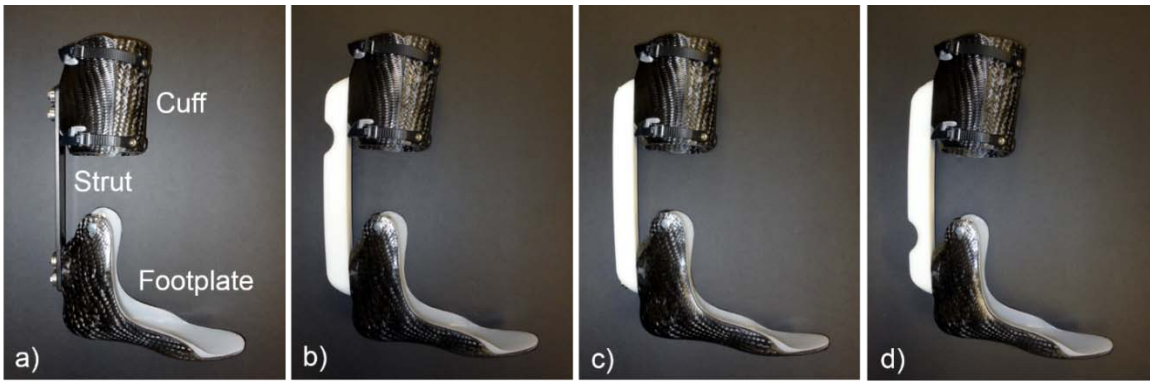

Figure 2.1: Passive-dynamic ankle-foot orthosis (PD-AFO). a) PD-AFO with the prescribed carbon fiber strut, b) with the proximal (high) bending axis SLS strut, c) with the central (middle) bending axis SLS strut, and d) with the distal (low) bending axis SLS strut.

Data Processing

Electromyography

Initial EMG processing was performed in Visual3D (C-Motion, Inc., Germantown, MD). EMG data were demeaned, filtered using a bandpass filter (cutoff frequencies of 20 Hz, 400 Hz), smoothed with a 50 ms sliding RMS window and time-normalized to a full gait cycle. Five full gait cycles for both the PD-AFO and non-PD-AFO limb were exported for additional processing and analysis. In Matlab (Mathworks, Inc., Natick, MA), EMG magnitudes were normalized by the peak value observed during the Froude speed condition for a given data collection session (Yang et al., 1984), and integrated EMG (iEMG) quantities were computed as the time integral of processed EMG data for each individual muscle. The iEMG quantities for each muscle were calculated within six regions of the gait cycle (Figure 2.2): 1) first double-leg support, 2) early single-leg support, 3) late single-leg support, 4) second double-leg support, 5) early swing, and 6) late swing. The iEMG quantities were averaged across gait cycles and normalized by the full gait cycle iEMG for the middle bending axis condition.

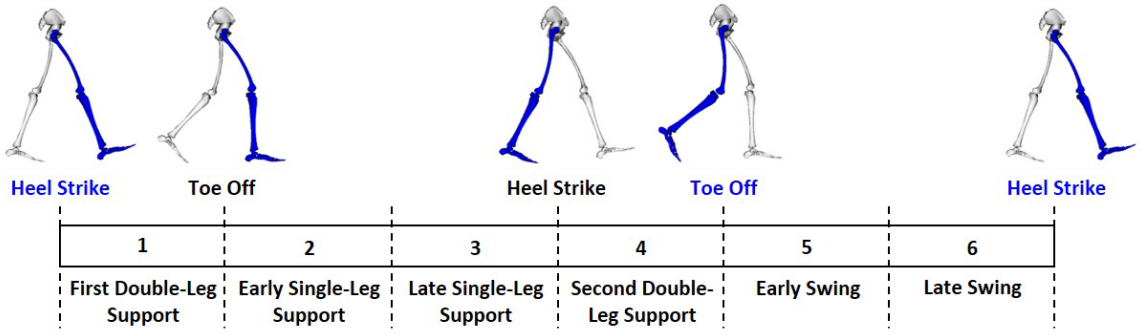

Figure 2.2: Six regions of the gait cycle: 1) first double-leg support, 2) early single-leg support, 3) late single-leg support, 4) second double-leg support, 5) early swing, and 6) late swing.

Kinematics and Kinetics

In Visual3D, a 13-segment model was created and scaled by both participant mass and height. Model joint centers and coordinate systems were defined via 20 bilateral anatomical landmarks, defined through a digitization process in accordance with the International Society of Biomechanics standards (Grood et al., 1983; Wu et al., 1995; Wu et al., 2002). 3D kinematic and analog data were interpolated using a cubic polynomial and filtered with a low-pass, 4^{th}-order Butterworth filter (cutoff frequencies of 6 and 50 Hz, respectively). Euler angles were used to determine the joint kinematics and pelvis, hip, knee, and ankle kinematics were defined using Cardan rotation sequences (Baker, 2001; Grood and Suntay, 1983; Wu et al., 2002). Inverse dynamics were used to compute intersegmental joint moments and powers, which were normalized by subject mass, and GRF data were normalized by subject weight. GRF data in addition to joint kinematics,

moments and powers were time normalized to a full gait cycle and five full gait cycles for each limb were exported for additional processing and analysis.

In subsequent processing and analysis in Matlab, changes in PD-AFO strut alignment between data collection sessions were normalized by subtracting the unloaded ankle angle during swing from the PD-AFO limb ankle angle across the full gait cycle. Peak joint kinematic and kinetic quantities were identified and GRF impulses and joint work were computed as the time integrals of GRFs and joint powers, respectively, during each of the six regions of the gait cycle (Figure 2.2) and averaged across all gait cycles.

Statistical Analyses

To determine the influence of PD-AFO bending axis, differences in biomechanical measures were analyzed using two-way (bending axis condition, limb) repeated-measures ANOVAs using SPSS (IBM Corp, Armonk, NY). Significant bending axis condition main effects and bending axis condition*limb interaction effects were adjusted using a Huynh-Feldt correction for sphericity violations and examined using post-hoc pairwise comparisons with a Bonferonni correction for multiple comparisons. The unadjusted criterion for statistical significance was set at $p < 0.05$. Significant pairwise comparisons between bending axis conditions for peak joint angles and moments were compared to previously-published minimal detectible change values calculated from data collected using identical methodology (Wilken et al., 2012).

In addition, a separate effect size analysis was conducted to assess the percent of variance in gait measures accounted for by participant PD-AFO bending axis preference

(Cohen, 2013). Eta-squared calculations were performed using a general linear model in SPSS with preference as the fixed factor, and gait measures as the dependent variables. The measure of association was considered to be large for $\eta^2 > 0.26$, and values of $\eta^2 > 0.50$ were additionally noted to highlight gait measures for which over half of the variance can be accounted for by preference.

RESULTS

Of the thirteen participants, four participants preferred the low bending axis, seven preferred the middle bending axis, and two preferred the high bending axis. The average walking speed was 1.32 (±0.07) m/s for their self-selected speed, and 1.25 (±0.05) m/s for their Froude speed. Similar trends across all variables were observed at their self-selected and Froude speeds, and thus the results for the Froude speed are included as supplemental material in Appendix A and the results for the self-selected walking speed are presented below. Further, there were no significant differences in walking speed, stride length and stride width across the bending axis conditions at either the self-selected or Froude speed.

iEMG

In Region 3, the bending axis location influenced GAS (bending axis main effect, $p = 0.040$; bending axis*limb interaction effect, $p = 0.043$) and TA (bending axis*limb interaction effect, $p = 0.047$) activity (Figure 2.3). For GAS, iEMG values were greater in the low compared to the middle condition (15.4%, $p = 0.030$), particularly in the PD-AFO limb (30.9%, $p = 0.009$).

Large participant bending axis preference effect sizes ($\eta^2 > 0.26$) were observed for iEMG values for all recorded muscles (Figure 2.3). During Region 1 in the PD-AFO limb, preference accounted for over half of the variance in the TA iEMG for the low condition ($\eta^2 = 0.62$), while in the non-PD-AFO limb, preference accounted for over half of the variance in the BF ($\eta^2 = 0.61$) and SOL ($\eta^2 = 0.58$) iEMG for the low condition and in the GAS iEMG for the high condition ($\eta^2 = 0.55$). In Region 4, preference accounted for over half of the variance in the PD-AFO limb TA iEMG for the low condition ($\eta^2 = 0.64$). In Region 5, preference accounted for over half of the variance in the PD-AFO limb SOL iEMG for the high condition ($\eta^2 = 0.64$) and in the non-PD-AFO limb VAS iEMG for the high condition ($\eta^2 = 0.52$). In Region 6, preference accounted for over half of the variance in the PD-AFO limb VAS ($\eta^2 = 0.59$) and SOL ($\eta^2 = 0.58$) iEMG for the high condition.

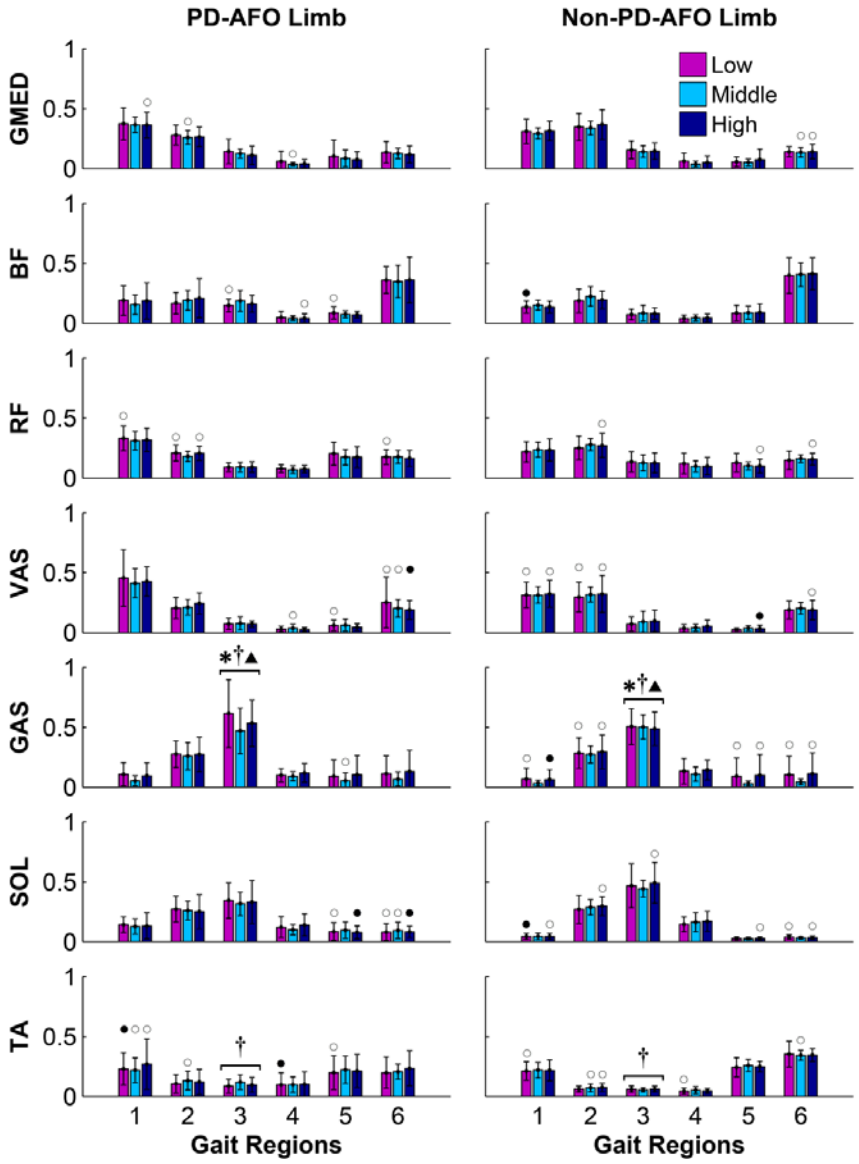

Figure 2.3: Average (± standard deviation) integrated electromyographic values at self-selected walking speed in the PD-AFO and non-PD-AFO limbs for the low, middle and high bending axis conditions during six regions of the gait cycle: 1) first double-leg support, 2) early single-leg support, 3) late single-leg support, 4) second double-leg support, 5) early swing, and 6) late swing. Data are presented for the gluteus medius (GMED), biceps femoris long head (BF), rectus femoris (RF), vastus medialis (VAS), medial gastrocnemius (GAS), soleus (SOL) and tibialis anterior (TA) muscles. Significant bending axis main effects (*), bending axis*limb interaction effects (†), low to middle bending axis comparisons (▲) and large effect sizes between preference and iEMG are indicated (○:$\eta^2 > 0.26$; ●:$\eta^2 > 0.50$).

Joint Kinematics and Kinetics

Peak plantarflexion angle (Region 1: bending axis main effect, $p = 0.002$), dorsiflexion moment (Region 1: bending axis main effect, $p = 0.006$) and knee extension moment (Region 2: bending axis main effect, $p = 0.010$) were influenced by PD-AFO bending axis condition (Table 2.2). In Region 1, the initial plantarflexion angle and dorsiflexion moment were greater in the low compared to the middle condition (angle: 24.3%, $p = 0.004$; moment: 12.9%, $p = 0.019$). In Region 2, the peak knee extension moment was lower in the middle compared to the high condition (11.9%, $p = 0.039$). However, each of these significant pairwise comparisons (i.e., Region 1 peak plantarflexion angle and dorsiflexion moment, and Region 2 peak knee extension moment) displayed differences that were less than previously-published minimal detectible change values for self-selected walking speeds (Wilken et al., 2012).

Large participant bending axis preference effect sizes ($\eta^2 > 0.26$) were observed for peak joint kinematics and kinetics at the ankle, knee and hip (Table 2.2). Preference accounted for over half of the variance in the Region 4 PD-AFO limb peak dorsiflexion angle with the low condition ($\eta^2 = 0.52$), and peak plantarflexion moment with the low ($\eta^2 = 0.86$), middle ($\eta^2 = 0.60$), and high ($\eta^2 = 0.67$) conditions. Preference accounted for over half of the variance in the Region 2 non-PD-AFO limb knee flexion angle with the middle condition ($\eta^2 = 0.55$) and Region 5 non-PD-AFO limb knee flexion angle with the high condition ($\eta^2 = 0.56$).

Table 2.2: Average (standard deviation) peak joint kinematics and kinetics at self-selected speed (positive values indicate dorsiflexion, knee flexion and hip flexion). The gait cycle regions during which the peaks occur are indicated as 1) first double-leg support, 2) early single-leg support, 3) late single-leg support, 4) second double-leg support, 5) early swing, and 6) late swing. Significant differences between the low and middle (▲) and high and middle (■) bending axis conditions are noted. Gait measures are shaded gray for preference effects sizes $\eta^2 > 0.26$ and dark gray for $\eta^2 > 0.50$.

			Peak Joint Kinematics (°)		
	Region	**Limb**	**Low**	**Middle**	**High**
Ankle Angle					
Plantarflexion ▲	1	PD-AFO	-7.40 (2.00)	-6.33 (1.89)	-6.77 (1.60)
		Non-PD-AFO	-2.03 (1.62)	-1.25 (1.98)	-1.87 (2.79)
Dorsiflexion	4	PD-AFO	5.83 (1.79)	5.19 (1.36)	4.87 (1.43)
		Non-PD-AFO	15.15 (2.38)	15.34 (2.39)	14.78 (2.61)
Plantarflexion	5	PD-AFO	-0.68 (0.54)	-0.61 (0.56)	-0.65 (0.51)
		Non-PD-AFO	-15.31 (3.83)	-15.40 (4.69)	-16.08 (5.17)
Knee Angle					
Flexion	2	PD-AFO	17.34 (7.45)	17.46 (4.19)	17.85 (5.97)
		Non-PD-AFO	16.19 (4.95)	16.41 (4.05)	16.80 (4.93)
Extension	3	PD-AFO	5.21 (6.82)	4.69 (5.05)	4.91 (4.19)
		Non-PD-AFO	1.84 (2.13)	3.24 (2.75)	2.73 (3.29)
Flexion	5	PD-AFO	63.45 (4.39)	63.34 (4.11)	63.34 (5.72)
		Non-PD-AFO	62.76 (4.01)	62.86 (4.10)	63.26 (4.78)
Hip Angle					
Extension	4	PD-AFO	-3.05 (4.71)	-3.07 (5.58)	-4.48 (5.13)
		Non-PD-AFO	-5.79 (4.18)	-5.38 (6.15)	-6.36 (5.97)
Flexion	6	PD-AFO	38.43 (4.52)	38.57 (5.11)	37.78 (5.60)
		Non-PD-AFO	34.97 (3.16)	35.09 (3.61)	34.72 (4.08)
			Peak Joint Kinetics (Nm/kg)		
Ankle Moment					
Dorsiflexion ▲	1	PD-AFO	0.45 (0.08)	0.40 (0.07)	0.43 (0.10)
		Non-PD-AFO	0.27 (0.07)	0.24 (0.08)	0.25 (0.07)
Plantarflexion	4	PD-AFO	-1.44 (0.23)	-1.50 (0.17)	-1.45 (0.19)
		Non-PD-AFO	-1.40 (0.21)	-1.43 (0.19)	-1.39 (0.22)
Knee Moment					
Flexion	1	PD-AFO	0.47 (0.11)	0.46 (0.06)	0.47 (0.11)
		Non-PD-AFO	0.62 (0.09)	0.60 (0.09)	0.61 (0.08)
Extension ■	2	PD-AFO	-0.64 (0.19)	-0.59 (0.19)	-0.68 (0.19)
		Non-PD-AFO	-0.52 (0.18)	-0.48 (0.12)	-0.53 (0.17)
Flexion	3	PD-AFO	0.38 (0.14)	0.43 (0.18)	0.35 (0.09)
		Non-PD-AFO	0.43 (0.12)	0.41 (0.12)	0.41 (0.16)
Hip Moment					
Extension	1	PD-AFO	-1.01 (0.22)	-1.00 (0.13)	-1.00 (0.23)
		Non-PD-AFO	-1.18 (0.15)	-1.17 (0.10)	-1.17 (0.15)
Flexion	4	PD-AFO	0.59 (0.11)	0.57 (0.16)	0.64 (0.16)
		Non-PD-AFO	0.57 (0.13)	0.54 (0.13)	0.58 (0.14)

Joint Work

PD-AFO bending axis influenced joint work at the ankle (Region 1 negative work: bending axis main effect, $p = 0.016$; Region 2 positive work: bending axis main effect, $p = 0.003$), knee (Region 2 positive work: bending axis main effect, $p = 0.011$) and hip (Region 1 positive work: bending axis main effect, $p = 0.008$; Region 3 negative work; bending axis main effect, $p = 0.046$) (Figure 2.4). In Region 1, positive hip work was 20.8% greater for the middle compared to the high condition ($p = 0.011$). During Region 2, positive ankle work was 34.1% lower for the middle compared to the low condition ($p = 0.002$) and positive knee work was 24.7% lower for the middle compared to the high condition ($p = 0.027$).

Large participant bending axis preference effect sizes ($\eta^2 > 0.26$) were observed in joint work at the ankle, knee and hip (Figure 2.4). In Region 2, preference accounted for over half of the variance in the non-PD-AFO limb positive hip work for the middle condition ($\eta^2 = 0.57$). In Region 3, preference accounted for over half of the variance in the PD-AFO limb negative knee work for the high condition ($\eta^2 = 0.58$). In Region 4, preference accounted for over half of the variance in the PD-AFO limb positive ankle work for the low condition ($\eta^2 = 0.59$) and positive hip work for the high condition ($\eta^2 = 0.51$). In Region 6, preference accounted for over half of the variance in the PD-AFO limb positive hip work for the high condition ($\eta^2 = 0.54$) and non-PD-AFO limb positive hip work for the low ($\eta^2 = 0.52$) and high ($\eta^2 = 0.60$) conditions.

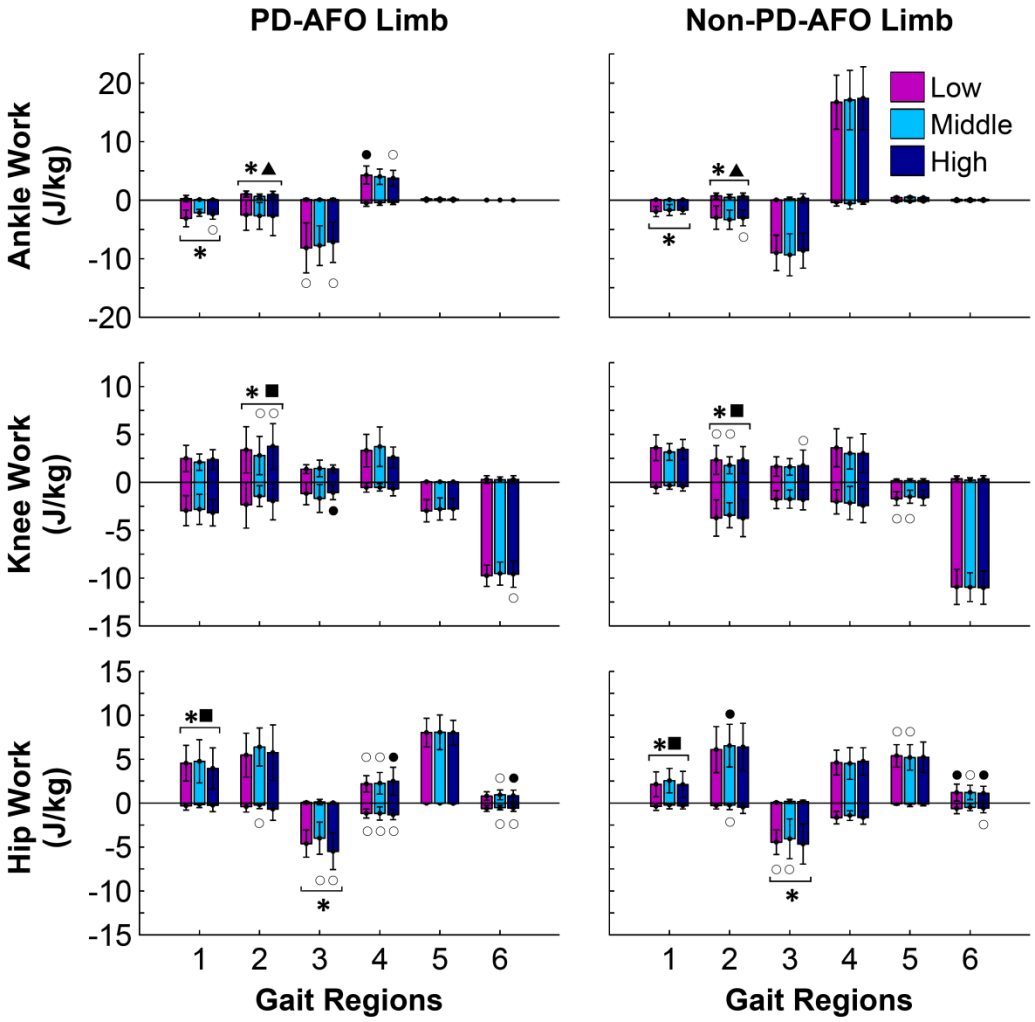

Figure 2.4: Average (± standard deviation) joint work at self-selected walking speed in the PD-AFO and non-PD-AFO limbs for the low, middle and high bending axis conditions during six regions of the gait cycle: 1) first double-leg support, 2) early single-leg support, 3) late single-leg support, 4) second double-leg support, 5) early swing, and 6) late swing. Average positive and negative joint work and respective standard deviations are presented separately. Significant bending axis main effects (*), low to middle bending axis comparisons (▲) and high to middle bending axis comparisons (■) are indicated. Large effect sizes between preference and joint work are also indicated (○: $\eta^2 > 0.26$; ●: $\eta^2 > 0.50$).

GRF Impulses

The only significant difference in GRF impulses across bending axis conditions occurred in the vertical GRF impulse (Region 3: bending axis main effect, $p = 0.011$) (Figure 2.5). In Region 3, the vertical GRF impulse with the middle condition was greater than both the low (3.2%, $p = 0.011$) and high (1.9%, $p = 0.003$) conditions.

Large participant bending axis preference effect sizes ($\eta^2 > 0.26$) were observed in the anteroposterior, vertical and mediolateral GRF impulses (Figure 2.5). Preference accounted for over half of the variance in the vertical GRF impulse during Region 1 for the non-PD-AFO limb with the high condition ($\eta^2 = 0.57$), as well as during Region 3 for the PD-AFO limb with the middle condition ($\eta^2 = 0.66$).

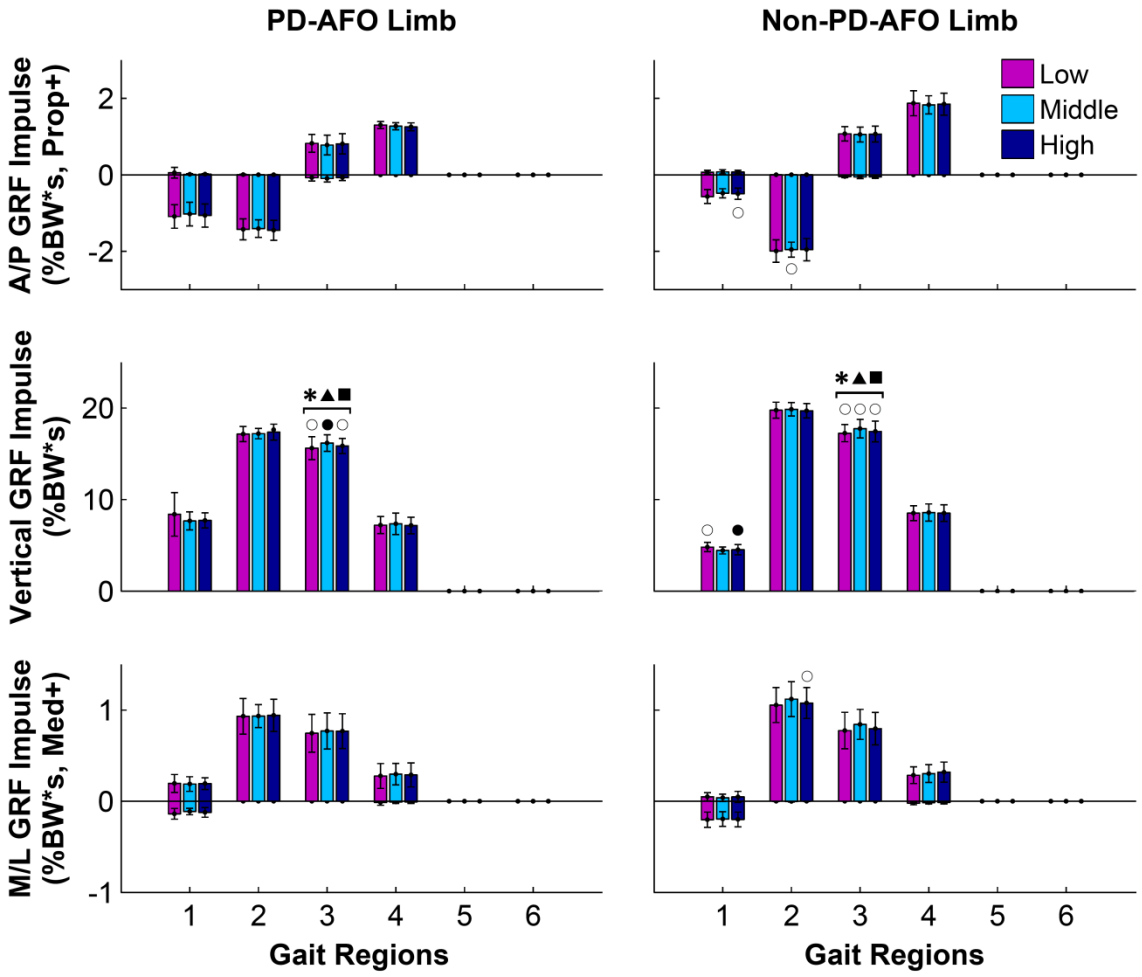

Figure 2.5: Average (± standard deviation) ground reaction force (GRF) impulses at self-selected walking speed in the PD-AFO and non-PD-AFO limbs for the low, middle and high bending axis conditions during six regions of the gait cycle: 1) first double-leg support, 2) early single-leg support, 3) late single-leg support, 4) second double-leg support, 5) early swing, and 6) late swing. Anteroposterior (A/P), vertical and mediolateral (M/L) positive and negative GRF impulses and respective standard deviations are presented separately. Significant bending axis main effects (*), low to middle bending axis comparisons (▲) and high to middle bending axis comparisons (■) are indicated. Large effect sizes between preference and GRF impulse are also indicated (○: $\eta^2 > 0.26$; ●: $\eta^2 > 0.50$).

DISCUSSION

The goal of this study was to investigate the influence of PD-AFO bending axis on gait performance. A better understanding of the relationship between bending axis and gait performance would help facilitate the development of evidence-based prescription guidelines for PD-AFOs and ultimately, improve rehabilitation outcomes for PD-AFO users.

PD-AFO bending axis altered GAS activity (iEMG) in late single-leg support. The low bending axis resulted in the greatest GAS activity, which has been previously shown to be an important contributor to both body support and forward propulsion in single-leg stance (Liu et al., 2006; Neptune et al., 2001). Harper et al. (2014a) similarly observed changes in GAS activity as a result of changes in PD-AFO stiffness in similar limb salvage subjects.

Altering PD-AFO bending axis had few effects on peak joint kinematics and kinetics. In first double-leg support, the peak plantarflexion angle and peak dorsiflexion moment were greater in the low condition, and in early single-leg support, the knee extension moment was greater in the high condition. Previous studies have observed a relationship between the instantaneous center of rotation of hingeless AFOs and ankle joint mechanics (Sumiya et al., 1997), as well as suggested that alignment of an articulated AFO joint with the physiological ankle joint minimizes foot kinematic deviations from barefoot walking (Leardini et al., 2014). This suggests that the use of the low bending axis, which lies closest to the physiological ankle joint, may allow for more normalized gait kinematics. However, the findings of the current study were not in

complete agreement, as the shift away from values previously observed in unimpaired subjects (Russell Esposito et al., 2014) was seen in both the high and low conditions (i.e., the increased knee extension moment observed in early single-leg support in the high condition as well as the increased peak dorsiflexion moment observed during first double-leg support in the low condition). It is important to note, however, that while significant peak joint kinematic and kinetic differences were observed in the current study, these values were lower than previously published minimal detectable change values for level walking at self-selected speeds (Wilken et al., 2012), and thus are likely not clinically relevant.

In the first half of stance, positive and negative ankle work, positive knee work and positive hip work were influenced by PD-AFO bending axis condition. In the second half of stance, negative hip work was influenced by PD-AFO bending axis condition. However, it should be noted that a consistent trend (e.g., increasing values as bending axis location moved from distal to proximal) was not observed.

Contrary to our hypothesis, the majority of participants preferred the middle bending axis, although at least two participants preferred each of the other bending axis locations. Inconsistent preferences in PD-AFO design between limb salvage subjects has also been observed when investigating PD-AFO stiffness in both level (Russell Esposito et al., 2014) and sloped walking (Haight et al., 2015). In addition, Raschke et al. (2015) suggested that there may be a link between prosthetic foot design preference and gait biomechanics, with individuals tending to prefer a prosthetic foot stiffness that minimized peak sagittal plane joint moments. The results of the current study also suggest a strong

relationship between bending axis preference and peak sagittal plane joint moments. A post-hoc analysis indicated that minimization of PD-AFO limb peak hip flexion moment and ankle plantarflexion moment during second double-leg support as well as the non-PD-AFO limb peak ankle dorsiflexion moment during first double-leg support and peak knee extension moment during early single-leg support each occurred in the preferred bending axis condition for over half of the participants. In addition to peak joint moments, peak joint kinematics, joint work, GRF impulses and muscle activity were also strongly related to bending axis preference. The differences in participant preference may have been influenced by diversity in etiology, and future work with larger preference subgroups may prove beneficial to addressing the relationship between etiology and preferred PD-AFO prescription.

In this study, there are a few limitations that warrant discussion. First, the participants enrolled in this study had a diverse range of injuries that led to the prescription of a PD-AFO. It is possible that etiology may be a confounding factor in the influence of PD-AFO bending axis on gait performance. The range of injuries and resulting functional limitations were diverse in this cohort and each participant's bending axis preference may have been directly related to their individual etiology. Although many of the participants had similar clinical presentations with respect to functional deficits, given the heterogeneity of injuries, very large cohorts of participants would likely be required to fully account for the role of etiology. By examining the relationships between preference and biomechanical measures through an effect size analysis, our goal was to indicate the presence of interactions between etiology and the influence of PD-

AFO bending axis on gait. Also, the participants enrolled in this study were young, highly active individuals and may not be representative of other populations of AFO and PD-AFO users. Therefore, future work examining the influence of PD-AFO bending axis in additional populations would be beneficial.

Finally, the contribution of the PD-AFO to ankle joint moments and work could not be distinguished from physiological contributions in this experimental setup. Previous studies have shown that alignment of an articulated AFO joint (Gao et al., 2011) and an articulated external ankle fixation joint (Bottlang et al., 1999) with the physiological ankle joint results in minimal resistance torque. Thus, it is likely that PD-AFO contributions to net ankle joint moments and work were influenced by bending axis location. Therefore, future work quantifying this contribution would improve the understanding of the influence of PD-AFO bending axis on compensatory mechanisms.

CONCLUSION

In conclusion, several significant differences were observed between the specified bending axis conditions, including the peak plantarflexion angle, peak dorsiflexion moment and positive hip work during first double-leg support, peak knee extension moment and positive ankle and knee work during early single-leg support, and GAS activity and vertical GRF impulse during late single-leg support. Although these differences were observed, peak joint kinematic and kinetic differences were less than previously published minimal detectable changes, and moving the bending axis proximally or distally did not produce large and consistent changes in other gait

measures. This suggests that choice of bending axis does not significantly change gait and other untested factors, such as etiology, may play a role in level ground walking mechanics. As very large cohorts of participants would be required to further evaluate the role of etiology, at present individual preference and comfort may be more important factors guiding the prescription of PD-AFO bending axis for level ground walking.

Chapter 3: The Influence of Limb Alignment and Transfemoral Amputation Technique on Muscle Capacity during Gait

INTRODUCTION

Recent estimates indicate there are over 1.7 million people living with amputation in the United States, with approximately 54% due to dysvascular disease, 45% due to trauma and less than 2% due to cancer (Ziegler-Graham et al., 2008). The prevalence of amputation is increasing and it is projected to reach 3.6 million people by 2050 (Ziegler-Graham et al., 2008). In addition to individuals in the general population, recent conflicts have resulted in a cohort of young active individuals with traumatic amputation (Krueger et al., 2012). For these individuals, restoring a high-level of mobility and functionality post-amputation is a primary goal when determining the optimal surgical technique and rehabilitation strategy. Previous work has examined the influence of residual limb length on gait performance in transfemoral amputees and found that amputees with longer residual limbs exhibit less excursion in their torso (Bell et al., 2013) and pelvis (Baum et al., 2008; Bell et al., 2013; Goujon-Pillet et al., 2008) and walk at faster self-selected speeds (Bell et al., 2013), but do not have lower energy expenditure (Bell et al., 2014). However, little research has been done to examine the influence of specific transfemoral amputation surgical techniques on the capacity of individual muscles to generate force and moments about the hip to maintain proper muscle balance and limb alignment during gait.

Important aspects of the surgical technique include the femur length, which muscles are reattached to the residual limb, the wrap position of the reattached muscles, and the tension and stabilization method used in the reattachment. These factors are critical in maintaining a muscle-balanced and aligned residual limb during gait (e.g., Gottschalk, 2004). In transfemoral amputations, essential muscles to reattach include the adductor magnus to maintain adductor-abductor balance, the rectus femoris to maintain hip flexor-extensor balance and the hamstrings to provide hip flexor-extensor and adductor-abductor balance (e.g., Gottschalk, 2004; Tintle et al., 2010a). Often smaller muscles (e.g., gracilis and sartorius) are left unattached to minimize suturing and surgery time.

Traditional muscle stabilization using myoplasty involves suturing agonist and antagonist muscles together over the residual end of the femur. However, this primarily provides distal end coverage and does not preserve muscle tension (Gottschalk, 2004). For this reason, some have recommended the use of myodesis stabilization for the adductor magnus (e.g., Gottschalk, 2004; Tintle et al., 2010a) and medial hamstrings (e.g., Tintle et al., 2010a), in which muscles are reattached directly to the femur under tension. Myodesis is a longer surgical procedure than the more traditional myoplasty, and thus evidence demonstrating that this technique improves the capacity of individual muscles to generate force and moments about the hip is needed to justify the increased cost and risk associated with the increased surgery time.

The influence of specific surgical techniques (e.g., reattachment tension) on muscle capacity has not been systematically examined in-vivo due to the highly invasive

nature of the procedure. However, musculoskeletal modeling is a powerful non-invasive framework through which to explore different surgical techniques, and it has been used previously to investigate the influence of surgical interventions such as tendon transfer (e.g., Delp et al., 1994; Magermans et al., 2004), joint replacement (Piazza and Delp, 2001) and paraspinal muscle resection in posterior lumbar surgery (Bresnahan et al., 2010). In addition, musculoskeletal modeling and simulation has been used to provide insight into key clinical questions such as the individual muscle contributions to walking mechanics (e.g., Anderson and Pandy, 2003; Liu et al., 2006; McGowan et al., 2009; Neptune et al., 2004), the influence of walking speed on muscle function (e.g., Arnold et al., 2007; Liu et al., 2008; Neptune et al., 2008), and the influence of assistive device design, such as prosthetic foot stiffness (Fey et al., 2012) and wheelchair seat position (Slowik et al., 2013), on metabolic cost. Thus, musculoskeletal modeling is an ideal framework to identify the optimal surgical techniques to maintain a muscle-balanced and aligned residual limb prior to clinical trials.

Therefore, the overall goal of this study was to systematically investigate the influence of residual limb alignment and transfemoral amputation technique (i.e., wrap position, femur length, muscle tension and stabilization) on the capacity of individual muscles to generate force and moments about the hip to maintain proper muscle balance during gait using advanced musculoskeletal modeling techniques. An improved understanding of how surgical technique effects muscle capacity can be used to guide the selection of specific techniques when considering factors such as surgical cost and risk. Further, those muscle groups found to be critical for maintaining muscle balance can be

identified and targeted in therapies to ensure optimal functionality and improve rehabilitation outcomes.

METHODS

To investigate the influence of limb alignment and surgical technique on muscle capacity, we systematically varied hip adduction angle, femur length, wrap position, muscle tension, and stabilization technique using a musculoskeletal modeling framework. Hip adduction angle was varied from -20 to 10 degrees relative to healthy gait kinematics, femur resection was varied from 10 to 14 cm, wrap position was varied from a medial insertion to an anterior insertion, muscle tension was varied relative to that of an intact muscle (80-100% of intact neutral tension) and stabilization techniques of myoplasty versus myodesis were compared.

Non-Amputee Model

A non-amputee subject was modeled using a well-established lower extremity musculoskeletal model in OpenSim 3.1 (Delp et al., 2007). The model had 23 degrees of freedom and 92 musculotendon actuators representing 76 major muscles in the lower extremities and torso. The muscle model used is based on the work of Thelen (2003). Musculotendon parameters were derived from Delp et al. (1990), and optimal fiber lengths and pennation angles were taken from Wickiewicz et al. (1983) and Friederich and Brand (1990). Twelve body segments were used to represent the torso, pelvis, and bilateral femur, tibia, calcaneus, talus and toes. The inertial properties of the body segments were derived from Anderson and Pandy (1999), and joint definitions were

derived from Delp et al. (1990). Experimentally-collected three-dimensional kinematics and kinetics of a healthy control subject performing overground walking at Froude 3 speed were used to perform inverse kinematics (Wilken et al., 2012). A residual reduction algorithm (RRA) was used to ensure dynamic consistency of the experimental kinematics and ground reaction forces, and computed muscle control (CMC) was performed to generate a set of muscle activations that, when the experimental ground reaction forces were applied, reproduced the experimental kinematics (Thelen et al., 2006).

Amputee Model

The musculoskeletal model was then modified to represent a transfemoral amputee. The lower-leg body segments (tibia, talus and foot) were removed from the residual limb, along with ankle and uniarticular knee muscles.

To investigate the influence of specific surgical techniques, muscles that are normally considered for reattachment during transfemoral amputation (i.e., adductor magnus, rectus femoris, biceps femoris long head, semimembranosus, semitendinosus, gracilis, sartorius and tensor fasciae latae) had their muscle geometry and properties systematically altered to represent the different surgical techniques. Muscle geometry was modified by adjusting the attachment points to the femur and adding cylindrical wrapping surfaces to emulate muscle wrapping over the residual end of the bone. Muscle parameters, specifically the tendon slack length (TSL), were modified to alter the muscle tension relative to that normally found in an intact muscle with the limb in a neutral position. This approach was used to replicate efforts to restore tension prior to

reattachment. The resting length of the musculotendon unit is the sum of the optimal fiber length and TSL. Decreasing TSL in the model is analogous to leaving a shorter muscle segment. Therefore, when the musculotendon unit is stretched to maintain its total length, muscle tension is increased. Conversely, increasing the TSL acts to lengthen the musculotendon unit, thus decreasing muscle tension. By altering TSL in the model, specific percentages of intact neutral tension can be preserved in a zero activation state (i.e., emulating the state of the relaxed muscle during surgery). In a myoplasty stabilization, muscle tension is not preserved, and thus stabilization by myoplasty was modeled by maintaining the intact TSL, and not the neutral muscle tension. In a myodesis stabilization, muscle tension is preserved as the muscle is anchored directly to bone, and thus stabilization by myodesis was modeled by preserving 100% of the intact neutral tension in a zero activation state.

A series of amputee models were generated to examine the influence of hip adduction, femur length, muscle wrap position, muscle tension and stabilization technique on the capacity of individual muscles to generate force and moments about the hip. Specifically, we quantified differences in hip adduction moment arm and contribution to the frontal plane hip moment. Analyses were performed using healthy gait kinematics and three different states of muscle activation for all muscles: zero activation, normal activation as determined by CMC, and full activation.

The influence of hip adduction position on muscle capacity was investigated by shifting the healthy gait kinematics by -20, -10, 0 and 10 degrees of hip adduction. The resulting muscle capacity was then assessed at mid-stance.

The influence of femur length was investigated by comparing the muscle capacity in amputee models with 10, 12 and 14 cm of femur resected at the points of initial contact, mid-stance and mid-swing. The resection lengths investigated represent the largest range in which myodesis stabilization could be performed. Muscle reattachments, relative reattachment locations and stabilization techniques were modeled consistently across femur lengths.

The influence of the adductor magnus wrap position on muscle capacity was examined by comparing four different amputee models (12 cm femur resection) with varying wrap positions. The muscle wrap positions modeled were a medial, non-wrapped insertion (Figure 3.1a), a lateral insertion (Figure 3.1b), an anterior-lateral insertion (Figure 3.1c) and an anterior insertion (Figure 3.1d). The resulting muscle capacity was assessed at initial contact, mid-stance and mid-swing.

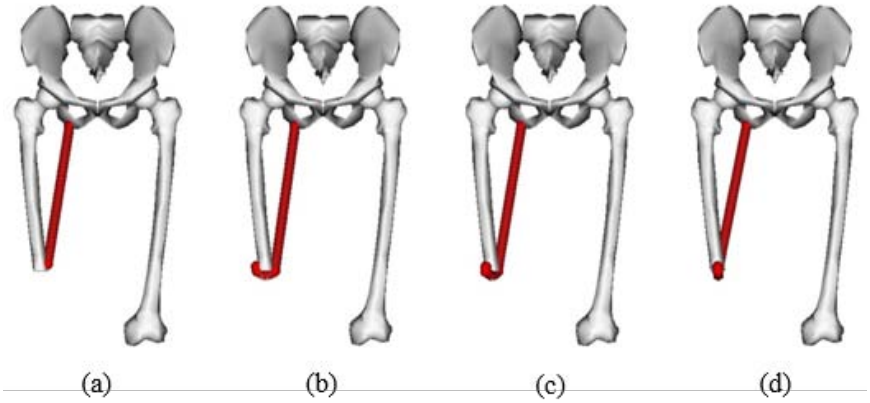

Figure 3.1: Adductor magnus wrap position. Wrap positions modeled in this study were: (a) medial insertion, (b) lateral insertion, (c) anterior-lateral insertion, and (d) anterior insertion.

To investigate the influence of muscle tension, a comparison of muscle capacity at initial contact, mid-stance and mid-swing was performed on amputee models (12 cm femur resection) with 80, 90 and 100% of the intact neutral tension preserved.

A comparison of muscle stabilization technique (i.e., myodesis versus myoplasty) was performed by computing the net hip joint frontal plane moment in the amputee models (12 cm femur resection) with either myodesis or myoplasty of the adductor magnus and semimembranosus. Joint moments of the non-amputee model, the myoplasty stabilization model, and the myodesis stabilization model were compared at initial contact, mid-stance and mid-swing.

RESULTS

The total frontal plane hip moment and gluteus medius contribution to the hip moment during mid-stance changed with variations in hip adduction angle (Figure 3.2). In all muscle activation states (zero, normal and full), the net frontal plane hip moment was least abducted when the femur was most abducted (i.e., -20 degree shift). Gluteus medius contribution to the hip abduction moment during mid-stance was affected by femur adduction angle. Under normal and full muscle activation, the gluteus medius contribution to the hip abduction moment was largest in the neutral position (i.e., 0 degree shift).

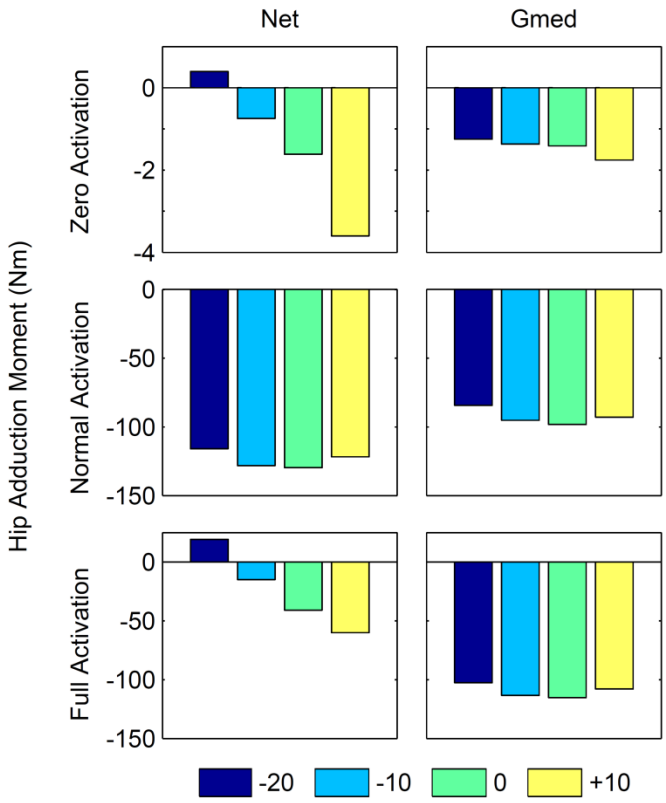

Figure 3.2: Net frontal plane hip moment (positive is adduction, negative is abduction) and gluteus medius (Gmed) contribution to the frontal plane hip moment (Nm) at mid-stance for zero, normal, and full activation. Results are shown for kinematics containing a -20 degree, -10 degree, 0 degree and +10 degree shift from normal hip adduction. Note that the scale is different for the zero activation state.

The frontal plane hip moment contributions from different muscles varied across femur lengths (Figure 3.3). Muscles that were candidates for reattachment and modeled with myodesis stabilization (adductor magnus and semimembranosus) remained similar across femur resections. At both 12 and 14 cm resections, biceps femoris long head no longer contributed to the frontal plane hip moment for all activation levels. At 10 and 12 cm resections, tensor fasciae latae contributed less than 10% of its intact moment for zero activation, and at a 14 cm resection it contributed less than 10% of its intact moment for all activation levels.

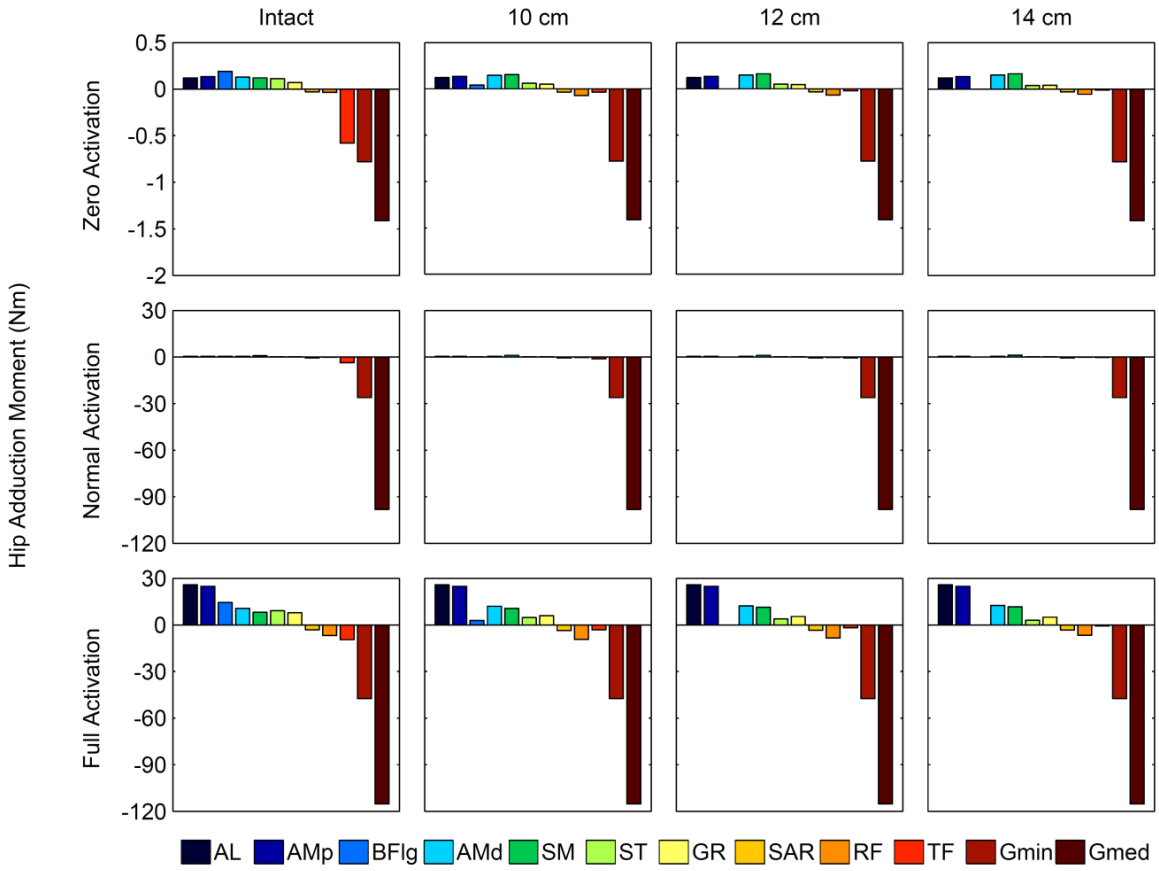

Figure 3.3: Frontal plane hip moment (Nm) contributions at mid-stance across activation level and length of femur resection. Positive frontal plane hip moment indicates adduction, negative indicates abduction. Hip moments are presented for large positive and negative contributors to the net hip moment, as well as for the reattachment candidates in the amputation procedure: adductor longus (AL), proximal adductor magnus (AMp), biceps femoris long head (BFlg), distal adductor magnus (AMd), semimembranosus (SM), semitendinosus (ST), gracilis (GR), sartorius (SAR), rectus femoris (RF), tensor fasciae latae (TF), gluteus minimus (Gmin), and gluteus medius (Gmed). Moments are presented for a non-amputee model (Intact) as well as 10 cm, 12 cm and 14 cm resections across three levels of muscle activation (zero, normal and full activation). Note that the scale differs for the zero activation state.

Adductor magnus wrap position did not meaningfully alter the hip adduction moment arm at any of the three points in the gait cycle examined (Figure 3.4). The largest difference in moment arm was observed during mid-stance where the anterior insertion produces a moment arm that is 3.3 mm greater than that of the lateral insertion (8.9 % difference).

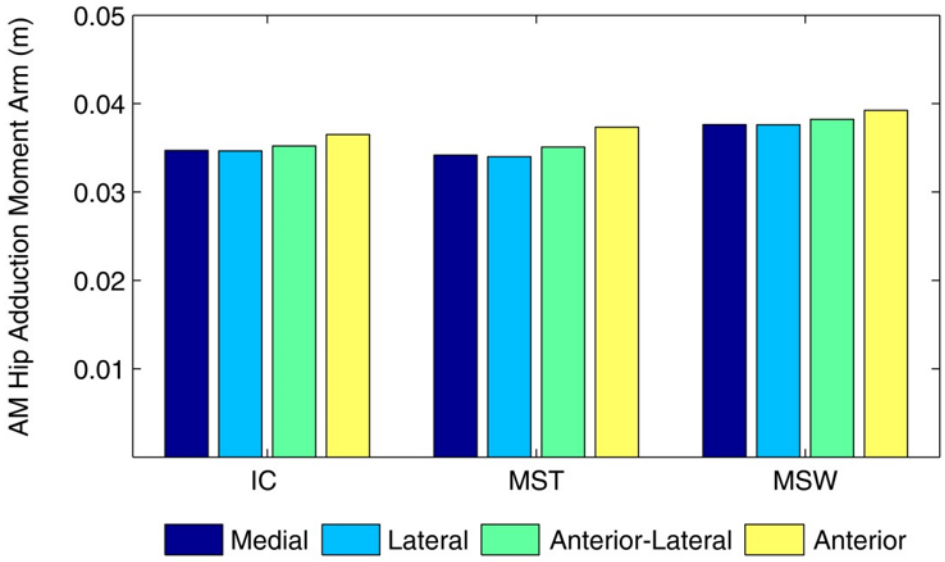

Figure 3.4: The influence of wrap position on adductor magnus (AM) hip adduction moment arm (m). Moment arms are shown at three different points in the gait cycle (initial contact (IC), mid-stance (MST), and mid-swing (MSW)), for four different wrap configurations: medial insertion, lateral insertion, anterior-lateral insertion and anterior insertion.

Muscle tension significantly influenced muscle capacity. Higher percentages of preserved tension resulted in larger fiber forces, thus resulting in a larger contribution (positive or negative) to the net frontal plane hip moment (Figure 3.5). For all activation

levels, the net hip adduction moment in the amputee model was larger with myodesis stabilization (Figure 3.6).

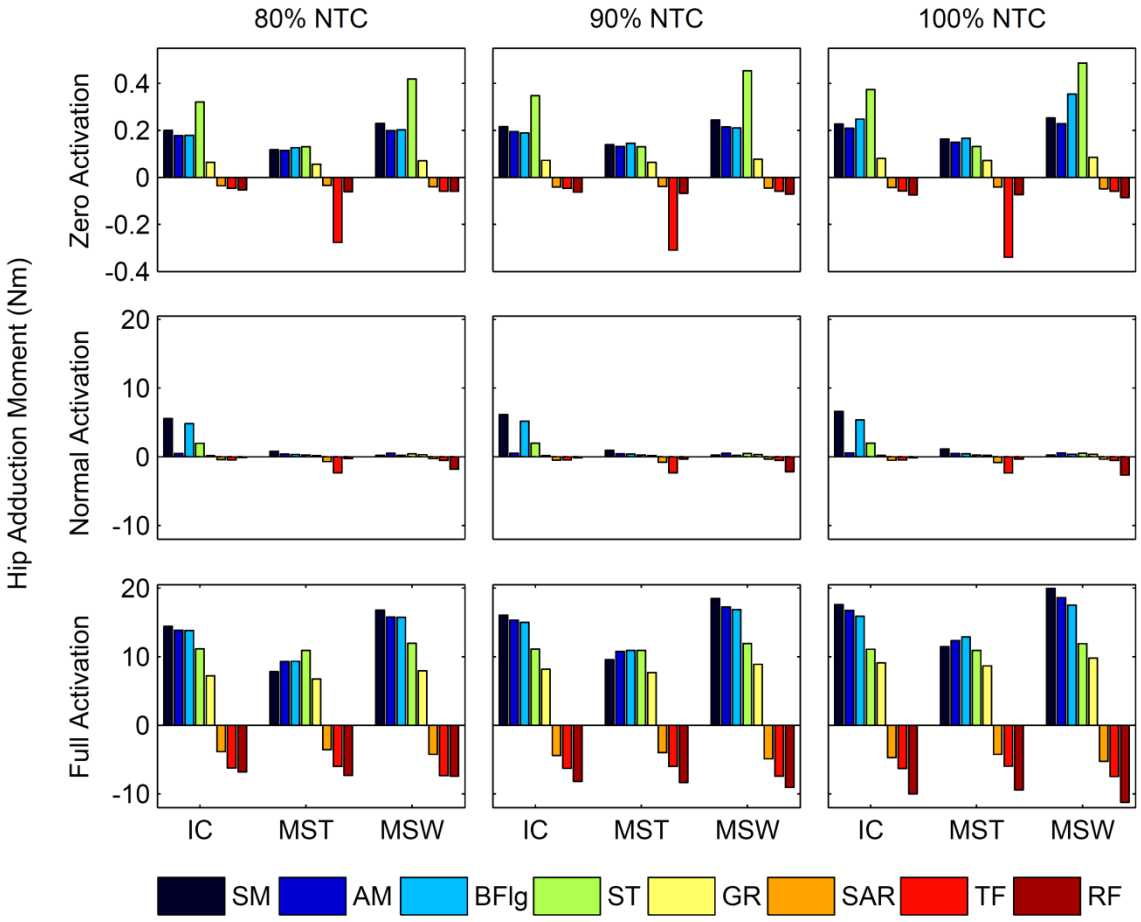

Figure 3.5: The influence of muscle reattachment tension on muscle contribution to the frontal plane hip moment. Hip moments (Nm) are shown at three different points in the gait cycle: initial contact (IC), mid-stance (MST), and mid-swing (MSW) for reattachment candidates at three different percentages of intact neutral tension preserved (80, 90, and 100%) and across three levels of muscle activation (zero, normal and full activation). Positive frontal plane hip moment indicates adduction, negative indicates abduction. Note that the scale differs for the zero activation state. Reattachment candidates are semimembranosus (SM), distal adductor magnus (AM), biceps femoris long head (BFlg), semitendinosus (ST), gracilis (GR), sartorius (SAR), tensor fasciae latae (TF), and rectus femoris (RF).

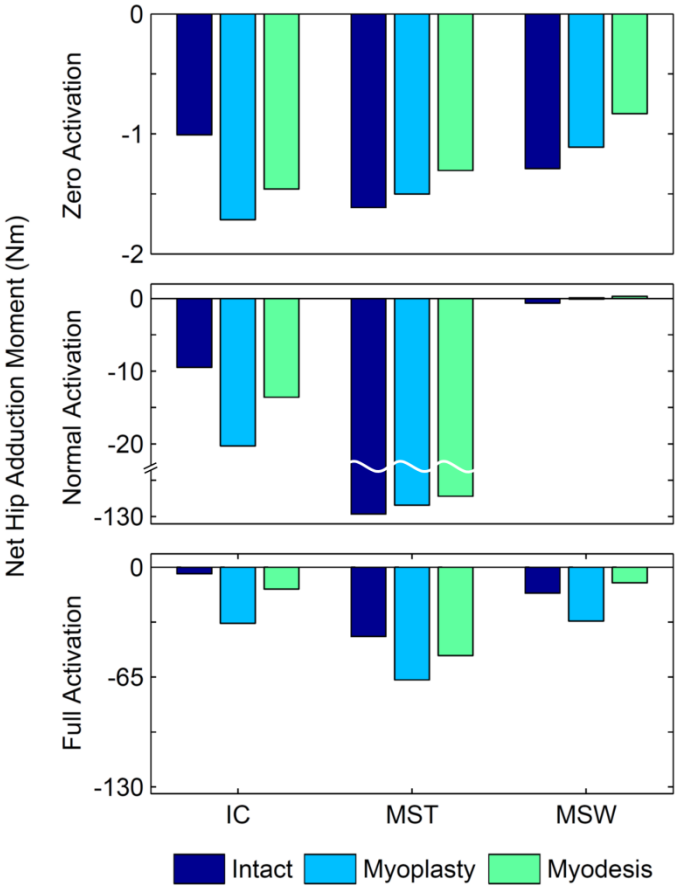

Figure 3.6: The net frontal plane hip moment (Nm) at initial contact (IC), mid-stance (MST) and mid-swing (MSW) of a non-amputee model (Intact), an amputee model with myoplasty stabilization, and an amputee model with myodesis stabilization of the adductor magnus and semimembranosus. Moments were compared across three levels of muscle activation (zero, normal and full activation). Positive frontal plane moment indicates hip adduction, negative indicates hip abduction. Note that the scales differ across the three rows of figures.

DISCUSSION

The goal of this study was to examine the influence of limb alignment and transfemoral amputation technique on the capacity of individual muscles to generate

force and moments about the hip to maintain proper muscle balance during gait. Through understanding which surgical techniques are critical to maintaining muscle capacity, and conversely those that have minimal effect, surgeons can streamline amputation procedures to maximize muscle capacity, minimize surgical cost and risk and improve rehabilitation outcomes.

The changes in muscle capacity associated with changes in hip alignment (Figure 3.2) highlight the importance of maintaining proper residual limb alignment during gait. If a limb is not well aligned and tends to abduct, there can be an increase in gait asymmetries resulting in inefficient gait patterns (e.g., Gottschalk, 1999). Thus, it is critical that surgical techniques (e.g., wrap position, tension preserved and femur length) maintain the dynamic balance of the residual limb to allow efficient and functional gait.

Residual limb length is often determined by the nature of the injury or condition requiring amputation. However, if there is flexibility in choosing limb length, the surgeon must decide the femur resection length. Previously, length preservation has been advocated (e.g., Gottschalk, 1999) as being important for positive functional outcomes, and studies have shown that residual femur length does influence self-selected walking speeds (Bell et al., 2013) and gait kinematics (Baum et al., 2008; Bell et al., 2013; Goujon-Pillet et al., 2008). The results of the present study indicate that a shorter residual limb may decrease frontal plane hip moment contribution of reattached muscles. However, this effect was not observed in muscles with myodesis stabilization, thus suggesting that muscle capacity can be preserved in shorter residual limbs by preserving neutral tension during reattachment. However, preserving tension in shorter residual

limbs can be challenging when the tendinous portion of the adductor magnus is missing, which makes it difficult to sufficiently stretch and attach the muscle. Thus, the present study only analyzed residual limb lengths that could utilize adductor tendon attachments and did not investigate shorter residual limbs which may have important implications for other factors such as socket fit.

Changes in adductor magnus wrap position resulted in only minor changes in hip adduction moment arm (Figure 3.3), indicating that this is not a critical surgical parameter. Some authors (e.g., Gottschalk, 2004; Tintle et al., 2010a) suggest a lateral attachment of the adductor myodesis, although this is likely due to the anatomical position of the adductor magnus with respect to the femur, which facilitates this particular wrap position. However, the present study suggests that wrap position should be selected that is most appropriate based on the available tissue (e.g., the wrap position that ensures preservation of muscle tension and a stable fixation). Thus, as muscle capacity in a medial attachment does not largely differ from a lateral attachment when tension is preserved, surgeons may have the option of leaving a longer residual limb, as a lateral attachment may require additional resection, which has important implications for socket fit and stabilization of the limb within the socket.

Although this study revealed that wrap position is not critical, the tension used in muscle reattachment was found to greatly influence the muscle's capacity to generate force. Increased initial tension results in greater muscle fiber forces and thus larger frontal plane hip moment generating capacity. Previous studies have recommended the use of myodesis stabilization for the adductor magnus and medial hamstrings (e.g., Tintle

et al., 2010a), which is consistent with the present study that highlights the importance of maintaining muscle tension. Reattaching muscles under tension allows for greater capacity to generate forces and moments, and thus could potentially provide greater limb functionality post-surgery.

Finally, we examined the difference in muscle balance between a non-amputee model, an amputee model in which the adductor magnus and semimembranosus were reattached using a myoplasty stabilization, and an amputee model in which they were reattached using a myodesis stabilization. The net hip adduction moments observed in these models indicate that myodesis stabilization may result in a larger hip adduction moment than myoplasty stabilization, and thus may produce a more favorable muscle balance. These findings, along with the reattachment tension sensitivity results support the use of myodesis stabilization on both the adductor magnus and medial hamstrings (e.g., Tintle et al., 2010a).

One potential limitation of this study is that kinematics of only one subject were represented. However, we performed similar analyses using additional kinematic data, including from younger and older subjects, which yielded similar findings. This highlights the robustness of these results to inter-subject differences in gait patterns. In addition, the subject kinematics were from a non-amputee subject, although differences between amputee and able-bodied gait have previously been shown (e.g., Jaegers et al., 1995), and more recently, the differences between transfemoral amputee and healthy muscle activity during walking have been observed (Wentink et al., 2013). However, while kinematic differences are often present in amputee gait, performing this study using

healthy kinematics allowed for a direct comparison between non-amputee and amputee models. Future analyses should include forward dynamic simulations of amputee models tracking transfemoral amputee data to further assess the efficacy of different surgical techniques on dynamic muscle capacity and function.

Another potential limitation of this study is that it does not account for changes that may occur in the residual limb post-surgery. However, reattached and functioning muscles may be less susceptible to atrophy and remodeling, and could potentially play a positive role in stabilizing the limb within the socket. In addition, this study did not consider other post-surgery factors such as muscle pull out strength or tissue healing. While changes may occur in the residual limb over time, the current findings highlight the surgical techniques critical to maintaining muscle capacity post-surgery, as well as potential targets for rehabilitation therapies.

CONCLUSION

In summary, muscle wrap orientation had little effect on muscle capacity. Similarly, if muscle tension is preserved, femur length had little effect. In contrast, limb alignment was found to influence the ability of muscles to generate forces and moments about the hip joint. Muscle reattachment tension had the greatest influence on muscle capacity, with increases in tension resulting in higher fiber forces and contributions to the hip adduction moment. Thus, myodesis stabilization, which allows for greater muscle tension, may provide superior hip muscle balance and function compared to myoplasty stabilization or when leaving muscles unattached.

Chapter 4: Muscle Function in Transfemoral Amputee Gait

INTRODUCTION

Unilateral, transfemoral amputee gait is characterized by several gait deviations compared to non-amputee gait, including slower self-selected walking speeds (Jaegers et al., 1995; Seroussi et al., 1996; Waters et al., 1976), increased energy cost (Schmalz et al., 2002; Waters et al., 1976), increased relative duration of residual limb swing and intact limb stance (Goujon-Pillet et al., 2008; Jaegers et al., 1995; Wentink et al., 2013), and increased range of motion of the trunk (Goujon-Pillet et al., 2008; Jaegers et al., 1995). These gait deviations are the result of the loss of musculature in the amputated limb and the resulting compensatory mechanisms that are used to restore mobility. Experimental studies have examined such compensations and identified increased residual limb hip flexor work during late stance (Seroussi et al., 1996), as well as increased intact limb hip extensor work during early stance and ankle plantarflexor work during push-off (Nolan et al., 2000; Seroussi et al., 1996) as the primary mechanisms by which transfemoral amputees restore mobility.

Differences in muscle coordination patterns have also been observed in transfemoral amputee gait compared to non-amputee gait, generally characterized by increases in muscle activation level and duration (Bae et al., 2009; Jaegers et al., 1996; Wentink et al., 2013). One study found that during late residual limb stance, tensor fasciae latae, vastus lateralis, biceps femoris, semitendinosus and adductor magnus each

had a second phase of activation, which was not observed in non-amputee walking (Wentink et al., 2013), and may correspond to increasing muscle volume to ensure a secure socket fit pre-swing (Hong et al., 2005). During the residual limb stance to swing transition, tensor fasciae latae and adductor magnus were active, contrary to non-amputee walking, and in the second half of swing gluteus medius and gluteus maximus were active, whereas in non-amputees they were active in late swing (Wentink et al., 2013). Additionally, during intact limb stance, soleus and tibialis anterior had longer activation durations (Wentink et al., 2013), which may correspond to increased ankle plantarflexor work during push-off (Nolan and Lees, 2000; Seroussi et al., 1996) and serve to facilitate foot clearance. While these previous studies have demonstrated various compensatory mechanisms that may be used by transfemoral amputees, it is still unclear how individual muscles contribute to specific walking subtasks such as body support, forward propulsion, mediolateral control and leg swing.

Musculoskeletal modeling and simulation provide a powerful, non-invasive framework through which quantities can be examined that may not be measured experimentally, and causal relationships between muscle activity and resulting motion can be identified (for review, Zajac et al., 2002). Previous studies investigating individual muscle contributions to walking subtasks have focused largely on non-amputee gait (Anderson and Pandy, 2003; Liu et al., 2006; McGowan et al., 2009; Neptune et al., 2001; Neptune et al., 2004). These studies have found that the vasti, gluteus maximus and gluteus medius are important contributors to body support in early stance and the ankle plantarflexors are important contributors in late stance (Liu et al., 2006; Neptune et al.,

2001). Gluteus maximus and vasti have been shown to be important contributors to forward propulsion in early stance (Neptune et al., 2004; Zajac et al., 2003), and the ankle plantarflexors are important contributors in late stance (Liu et al., 2006; Neptune et al., 2001). In addition, leg swing is primarily initiated by the gastrocnemius and iliacus, while rectus femoris opposes leg swing initiation (Neptune et al., 2004). The iliacus and biceps femoris short head accelerate the leg forward in early swing, while the biceps femoris short head and the hamstrings decelerate the leg in late swing (Neptune et al., 2004). The contributions of individual muscles to mediolateral control in non-amputee gait have also been examined. Lateral acceleration is provided by the hip adductors (Allen et al., 2012; Pandy et al., 2010; Silverman and Neptune, 2012) and hamstrings (Allen and Neptune, 2012; Silverman and Neptune, 2012) during early stance and the plantarflexors during late stance (Allen and Neptune, 2012; Pandy et al., 2010; Silverman and Neptune, 2012). Tensor fasciae latae acts to accelerate the body medially through mid-stance (Allen and Neptune, 2012; Silverman and Neptune, 2012), while the gluteus medius accelerates the body medially throughout stance (Allen and Neptune, 2012; Pandy et al., 2010; Silverman and Neptune, 2012). However, the specific role of the vasti is unclear, as previous studies have shown it provides both lateral (Pandy et al., 2010; Silverman and Neptune, 2012) and medial (Allen and Neptune, 2012) acceleration.

In amputees, the loss of lower-limb musculature and changes in muscle attachment points may influence contributions to the walking subtasks. The functional role of individual muscles and a prosthetic foot in transtibial amputee walking has previously been examined (Fey et al., 2013; Silverman and Neptune, 2012; Zmitrewicz et

al., 2007), demonstrating that the prosthesis can replace the function of the soleus, a uniarticular plantarflexor, by contributing to body support as well as forward (Fey et al., 2013; Silverman and Neptune, 2012; Zmitrewicz et al., 2007) and lateral (Silverman and Neptune, 2012) propulsion in late stance. However, the prosthesis does not fully replicate the function of the biarticular gastrocnemius (e.g., Silverman and Neptune, 2012; Zmitrewicz et al., 2007), which is important for body support and forward propulsion (Liu et al., 2006; Neptune et al., 2001) as well as leg swing initiation (Neptune et al., 2004). Compensatory mechanisms have also been observed in muscle contributions, including decreased braking contributions from the residual vasti and rectus femoris (Silverman and Neptune, 2012), increased propulsion contributions from both residual and intact rectus femoris and gluteus maximus (Zmitrewicz et al., 2007), increased medial propulsion by the residual sartorius, as well as medial propulsion (as opposed to lateral) from the vasti, soleus and gastrocnemius in the intact limb (Silverman and Neptune, 2012).

In transfemoral amputees, the additional losses in above-knee musculature and changes in prosthetic components (i.e., the addition of a prosthetic knee) will likely necessitate further changes in contributions to walking subtasks to restore mobility. Previous torque-driven simulations of transfemoral amputee gait have optimized knee joint position (Burkett et al., 2004) and knee motion controller (Pejhan et al., 2008; Shandiz et al., 2013; Tsai et al., 1986), and focused on spatiotemporal and joint kinetic and kinematic outcome measures. A previous muscle-driven simulation optimized knee joint friction (Suzuki, 2010) to minimize metabolic energy and additionally examined

changes in muscle forces when swing duration was minimized. However, to our knowledge no study has investigated the functional role and compensatory mechanisms of individual muscles in transfemoral amputee walking subtasks.

Therefore, the purpose of this study was to develop a three-dimensional forward dynamics simulation of transfemoral amputee walking and to use the simulation to determine how muscles and prostheses contribute to the walking subtasks of body support, forward propulsion, mediolateral control and leg swing. The results from this study will provide additional insights into individual muscle function and compensatory mechanisms used by transfemoral amputees, and may be used in the development of targeted rehabilitation therapies.

METHODS

Musculoskeletal Model

A three-dimensional musculoskeletal model of a non-amputee has previously been developed in SIMM/Dynamics Pipeline (MusculoGraphics, Inc., Santa Rosa, CA) (Peterson et al., 2010), and was altered to model a transfemoral amputee. The non-amputee model was comprised of rigid body segments including the trunk, pelvis, and bilateral thigh, patella, shank, talus, calcaneous, and toes. There were a total of 23 degrees-of freedom (DOF) in the model: a six DOF joint between the pelvis and ground, three rotational DOF between the trunk and pelvis, three rotational DOF between each thigh and the pelvis, and one rotational DOF at each knee, ankle, subtalar, and one metatarsolphalangeal joint per foot. Each leg in the model was driven by 38 Hill-type

musculotendon actuators (Table 4.1), with contraction dynamics governed by intrinsic muscle force-length-velocity relationships and a tendon force-strain relationship (Zajac, 1989).

Muscle excitations (u) were defined via bimodal patterns as:

$$u(t) = \begin{Bmatrix} \sum_{i=1}^{2} \frac{A_i}{2}\left[1 - \cos\left(2\pi \frac{t - onset_i}{offset_i - onset_i}\right)\right] & if\ onset_i \le t \le offset_i \\ 0 & else \end{Bmatrix} \quad (4.1)$$

For each muscle, the amplitude, *A*, as well as the onset and offset times for each mode *i* were optimized which results in six optimization parameters per muscle. The activation and deactivation dynamics of each muscle were modeled with a 1st order non-linear differential equation (Raasch et al., 1997) with previously defined activation and deactivation time constants (Winters et al., 1988). The contact between the foot and the ground was modeled using 31 visco-elastic elements with coulomb friction on the bottom of each foot, distributed between the calcaneous and toes segments (Neptune et al., 2000). To model the passive forces applied by tissues and structures at joints, passive torques were applied to each joint (Davy et al., 1987) .

The model was modified to represent a transfemoral amputee by removing and altering the lower-limb muscles (Table 4.1), and altering residual limb segments to model prosthetic components. All ankle muscles and uniarticular knee muscles were removed from the residual limb. Muscles that may be reattached to the residual limb during surgery (adductor magnus, rectus femoris, biceps femoris long head, semimembranosus,

semitendinosus, gracilis, sartorius and tensor fasciae latae) were reattached based on the results of Chapter 3. Adductor magnus and semimembranosus were reattached via myodesis stabilization, and the remaining muscles were reattached via myoplasty stabilization. Via points and wrapping surfaces (Delp et al., 2000) were used to wrap reattached muscles over the residual end of the femur, and muscles reattached using myodesis stabilization had musculotendon properties altered per Chapter 3 so that neutral tension was conserved in a passive state.

Table 4.1: Muscles included in the model. Asterisk (*) indicates muscles that are modeled with myodesis stabilization. Muscle group abbreviations are provided in parentheses.

Muscles Modeled		
In Both the Intact and Residual Limb	Modified Insertion in Residual Limb	Not Included in Residual Limb
Iliacus (IL)	Adductor magnus, inferior* (AM)	Vastus medialis (VAS)
Psoas (IL)	Sartorius (SAR)	Vastus intermedius (VAS)
Adductor longus (AL)	Rectus femoris (RF)	Vastus lateralis (VAS)
Adductor brevis (AL)	Tensor fascia lata (TFL)	Biceps femoris short head (BFSH)
Pectineus (AL)	Semimembranosus* (HAM)	Gastrocnemius, medial (GAS)
Quadratus femoris (AL)	Semitendinosus (HAM)	Gastrocnemius, lateral (GAS)
Gluteus medius, anterior (GMEDA)	Gracilis (HAM)	Soleus (SOL)
Gluteus medius, middle (GMEDA)	Biceps femoris long head (HAM)	Tibialis posterior (SOL)
Gluteus medius, posterior (GMEDP)		Flexor digitorum longus (SOL)
Gluteus minimus, anterior (GMEDA)		Tibialis anterior (TA)
Gluteus minimus, middle (GMEDA)		Extensor digitorum longus (TA)
Gluteus minimus, posterior (GMEDP)		
Gluteus maximus, superior (GMAX)		
Gluteus maximus, middle (GMAX)		
Gluteus maximus, inferior (GMAX)		
Gemellus (GMEDP)		
Piriformis (GMEDP)		
Adductor magnus, superior (AM)		
Adductor magnus, middle (AM)		

In addition, the mass and center of mass (COM) locations for the shank and thigh were altered for the residual limb to accurately reflect the prosthesis. The shank was separated into the lower portion of the prosthetic knee and pylon. The respective masses were calculated as half of the mass of the prosthetic knee, and the mass of an average prosthetic pylon for the specified length. The mass of the residual thigh was adjusted by subtracting the average percent of femur resected and adding half of the mass of the

prosthetic knee. The COM location was translated along the femur based on the altered composite mass distribution.

An energy storage and return (ESAR) prosthetic foot was modeled by applying a second-order torsional spring with damping at the ankle (Silverman and Neptune, 2012) as:

$$\tau_a = a_a + b_a\theta_a + c_a\dot{\theta}_a + d_a{\theta_a}^2 + e_a\theta_a\dot{\theta}_a \qquad (4.2)$$

where the torque (τ_a) applied is defined by the ankle joint angle (θ_a), the ankle joint angular velocity ($\dot{\theta}_a$), and constants a_a through e_a are determined by fitting the experimental ankle kinematic and kinetic data with Equation 4.2. The prosthetic foot torque was applied as a passive torque at the ankle.

A mechanical prosthetic knee was modeled after the Ossur Total Knee® 2100 (Ossur, Reykjavik, Iceland). The knee was modeled to lock during stance phase, and allow the shank and foot to swing forward during swing phase, while simultaneously shortening to assist with foot clearance. The knee was modeled with a hinge and slider joint, allowing for one rotation DOF at the knee, and longitudinal translation along the shank. The hinge joint had flexion and extension hydraulic resistance, modeled with a damper responding to speed, and directionally and position dependent as:

$$\tau_k = a_k + b_k\theta_k + c_k\dot{\theta}_k + d_k\dot{\theta}_k^2 \qquad (4.3)$$

where the torque (τ_k) applied is defined by the knee joint angle (θ_k), the knee joint angular velocity ($\dot{\theta}_k$), and constants a_k through d_k were determined by fitting the experimental knee kinematic and kinetic data with Equation 4.3. The prosthetic knee torque was applied as a passive torque at the knee. The knee extension stop and locking mechanism of the knee during stance was modeled by increasing knee joint stiffness during stance, and the swing phase segment shortening of the shank was modeled with the slider joint between the knee and pylon. This translation was a function of knee joint angle, in accordance with the experimental geometric translation of the Ossur Total Knee® with respect to knee angle.

Optimization Framework

A simulated annealing optimization algorithm (Goffe et al., 1994) was used to produce a forward dynamics simulation that emulated experimental tracking data (see below). The optimization algorithm iteratively modified the parameters for the muscle excitation timing and amplitude until the cost function was minimized. The cost function consisted of the difference between experimental and simulated kinematics and kinetics, as well as muscles stress to minimize co-contraction (Equation 4.4).

$$J = \sum_{i=1}^{n_{time}} \left[\sum_{j=1}^{n_{vars}} a_j \frac{\left(Y_{ij} - \hat{Y}_{ij}\right)^2}{SD_{ij}^2} + b \sum_{k=1}^{n_{musc}} \left(\frac{F_{ik}}{A_k}\right)^2 \right] \qquad (4.4)$$

where J is the value of the cost function, n_{time} is the number of time steps, n_{vars} is the number of variables that are being tracked, n_{musc} is the number of muscles, Y_{ij} is the experimental variable quantity for variable j at time step i, $\hat{Y}_{ij}$ is the corresponding simulation quantity, and SD_{ij} is the experimental standard deviation of variable j at time step i. F_{ik} is the force of muscle k at time step i, and A_k is the cross-sectional area of muscle k. The weightings for the error in variable j and the muscle stress are represented by constants a_j and b, respectively.

To help the optimization converge, a three-dimensional tracking force was applied to the pelvis COM and a tracking torque was applied to the prosthetic knee joint. The tracking force and torque were defined as a scaling factor (tracking force: 960, tracking torque: 5) multiplied by the difference between the simulated and experimental kinematics. The tracking force and torque were included in the objective function to be minimized (Equation 4.4).

Assessing Muscle and Prosthesis Function

The contribution of individual muscles to specific biomechanical functions was determined using a ground reaction force (GRF) decomposition and segment power analysis (Neptune et al., 2001; Neptune et al., 2004). At time step t, the total GRF and segment powers were calculated. At time step t-1, all muscle forces, except the muscle of interest, were applied to the model, and the equations of motion were integrated forward from time step t-1 to t. GRFs were recalculated, as were the segment powers, and the difference between the recalculated quantity and total quantity was determined. This

difference represented the muscle of interest's contribution to the GRF or segment power. This process was repeated for all muscles, gravity, and passive torques across all time steps. The contributions of the prosthetic knee and foot were assessed as their respective passive torque contributions to the GRFs or segment power. Contributions to the walking subtasks of forward propulsion, body support, and mediolateral control were investigated by examining each contribution to the anteroposterior, vertical and mediolateral GRF, respectively, as an impulse (time integral of GRF contribution) during the first and second halves of stance (Figure 2.2: Regions 1 and 2 (first half of stance), Regions 3 and 4 (second half of stance)). Contributions to leg swing were investigated by summing the mean power generated or absorbed for each segment of the leg, and examining component contributions during swing initiation, early swing and late swing (Figure 2.2: Regions 4, 5 and 6, respectively).

Experimental Data for Tracking Optimization

Previously collected experimental data from nine transfemoral amputees was used in this study to provide tracking data for the simulations. All subjects provided written, informed consent prior to data collection at the Military Performance Laboratory at the Center for the Intrepid (Brooke Army Medical Center, Fort Sam Houston, TX). Subjects performed overground walking at self-selected speeds. Three-dimensional kinematics were collected at 120 Hz using a 26 camera motion capture system (Motion Analysis Corp., Santa Rosa, CA) and a 6 DOF body segment marker set with 57 markers (Wilken et al., 2012), and GRFs were collected at 1200 Hz using five embedded force plates

(AMTI, Inc., Watertown, MA). In Visual3D, a 13-segment model was created, and scaled by subject height and mass. Twenty bilateral anatomical landmarks, defined using a digitization process, were used to define model joint centers and coordinate systems in accordance with the International Society of Biomechanics standards (Grood and Suntay, 1983; Wu and Cavanagh, 1995; Wu et al., 2002). Marker position and GRF data were interpolated and filtered using a low-pass 4th order Butterworth filter, with cutoff frequencies of 6 and 50 Hz, respectively. Joint kinematics were computed using Euler angles, and the pelvis, hip, knee, and ankle kinematics were defined using Cardan rotation sequences (Baker, 2001; Grood and Suntay, 1983; Wu et al., 2002). GRF data were normalized by subject weight, and GRF data and joint kinematics were time normalized to the full gait cycle, and exported. The group-averaged kinematics and kinetics were used for simulation tracking.

RESULTS

Simulation Quality

The optimization determined a set of muscle excitation parameters that produced a simulation representative of the experimental kinematics and kinetics (Figures B.1 – B.3). The average error between the simulated motion and experimental tracking data was 4.34 degrees for joint angles (2 SDs = 8.34), 0.10 for normalized GRFs (2 SDs = 0.11) and 0.07 meters for the pelvis translation (2 SDs = 0.09). Pelvis tracking forces were minimized, and both the vertical and anteroposterior forces were reduced to zero. The mediolateral pelvis force was reduced to peaks within 23% body weight, with an

average of less than 4.5% body weight. The prosthetic knee tracking torque was also minimized to an average 0.32 Nm (peaks < 7.04 Nm).

Body Support

During the first half of stance, the primary muscle contributors to body support for the intact limb were intact TA, GMEDA, GMAX, GMEDP and HAM (Figure 4.1). The primary muscle contributors to body support for the residual limb were residual HAM, GMAX, GMEDA, GMEDP and intact AL.

During the second half of stance, the primary muscle contributors to body support for the intact limb were the ankle plantarflexors (SOL and GAS) as well as intact IL, GMEDA and SAR. The primary muscle contributors to body support for the residual limb were residual GMED, GMEDP and HAM, and intact AL and HAM. The total (net) muscle contributions to body support during late stance were much less for the residual compared to the intact leg (Figure 4.1).

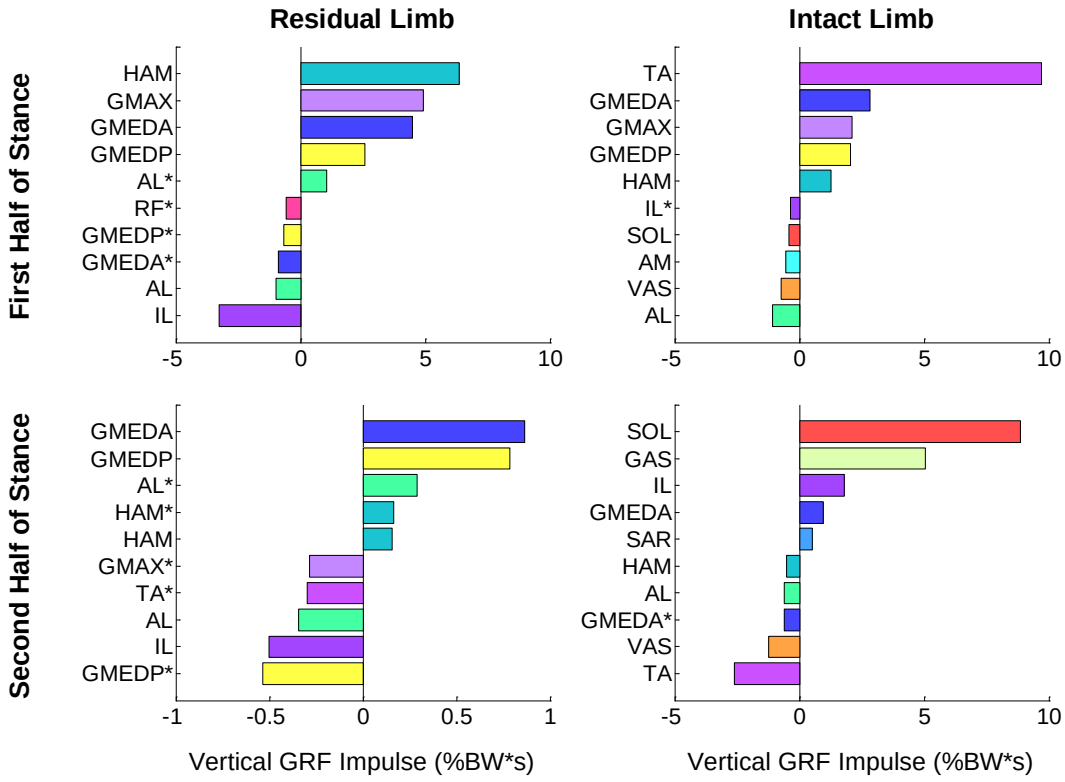

Figure 4.1: Primary positive and negative muscle group contributors to body support (vertical GRF impulse) during the first and second halves of residual and intact limb stance. Muscles listed are from the noted limb unless marked with an asterisk, which indicates the muscle is from the contralateral limb. Note that the axis range is different for the residual limb contributions during the second half of stance. Muscle group colors are consistent across figures in this chapter to allow for comparison. For muscle group abbreviations, refer to Table 4.1.

Anteroposterior Propulsion

During the first half of stance, the primary muscle contributors to forward propulsion for the intact limb were intact HAM, GMAX, GMEDP, GMEDA and AM (Figure 4.2). The primary muscle contributors to forward propulsion in the residual limb

were residual HAM, GMAX and AL and intact SOL and GMEDA. In opposition, the primary muscle contributors to braking for the intact limb were intact IL, TA, RF, VAS and TFL, and the primary muscle contributors to braking for the residual limb were residual IL, GMEDA and GMEDP in addition to intact HAM and AL.

During the second half of stance, the primary muscle contributors to forward propulsion for the intact limb were the ankle plantarflexors (SOL and GAS), and intact GMEDA, HAM and GMEDP. The primary muscle contributors to forward propulsion in the residual limb were residual HAM, GMEDA, GMEDP and GMAX in addition to intact AL. The total (net) muscle contributions to forward propulsion for the residual limb were notably less than the intact limb during late stance (Figure 4.2). In opposition, the primary muscle groups contributing to intact limb braking during the second half of stance were the intact IL, RF, AL, TA and VAS, which was similar to the first half of stance. The primary muscle contributor to residual limb braking was residual IL, with additional contributions from residual AL and AM as well as intact GMEDP and TA.

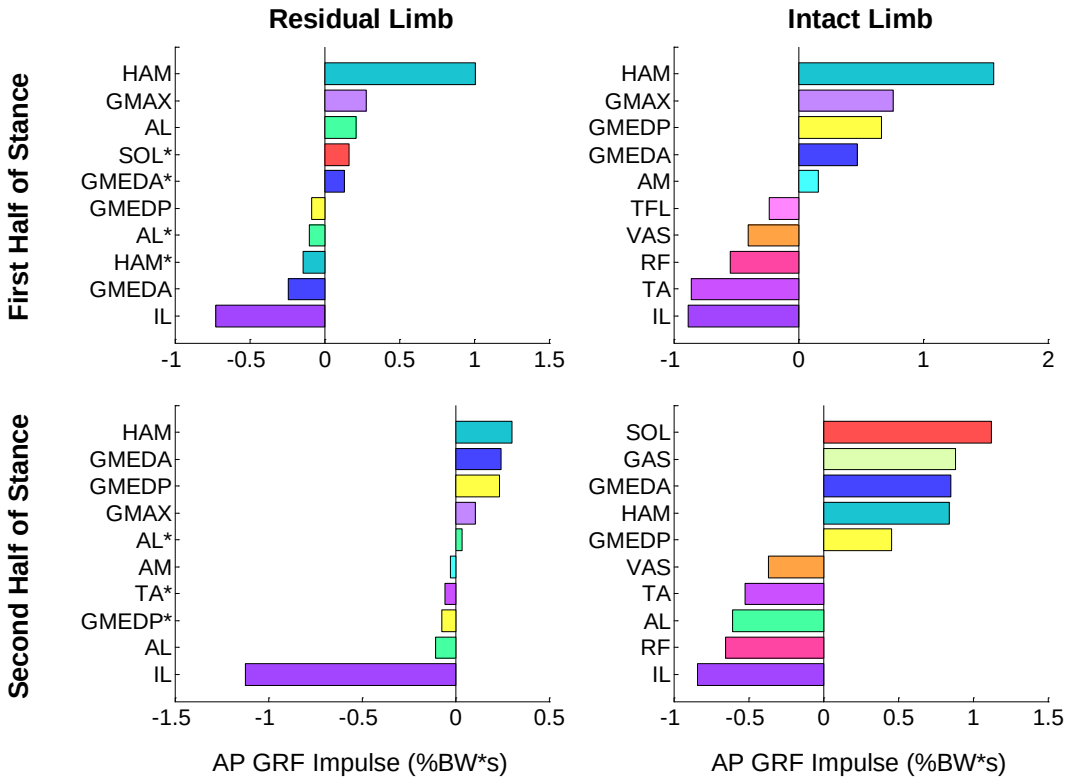

Figure 4.2: Primary positive and negative muscle group contributors to anteroposterior propulsion (AP GRF impulse) during the first and second halves of residual and intact limb stance. Positive (negative) GRF impulses indicate propulsion (braking). Note that axis ranges differ across plots. Muscles listed are from the noted limb unless marked with an asterisk, which indicates the muscle is from the contralateral limb. Muscle group colors are consistent across figures in this chapter to allow for comparison. For muscle group abbreviations, refer to Table 4.1.

Mediolateral Control

During the first half of stance, the primary muscle contributors to lateral propulsion for the intact limb were intact HAM, AL, AM and VAS in addition to residual AL (Figure 4.3). The primary muscle contributors to lateral propulsion in the residual

limb were similar, residual HAM, AL and GMAX, in addition to intact AL and HAM. The primary muscle contributors to medial propulsion for the intact limb were intact GMEDA, GMEDP, TFL, IL and SAR. The primary muscle contributors to medial propulsion for the residual limb were, similarly, residual GMEDA, GMEDP and IL in addition to intact GMEDA and GMEDP.

During the second half of stance, the primary muscle contributors to lateral propulsion in the intact limb were the ankle plantarflexors (SOL and GAS), and intact AL and HAM in addition to residual HAM. The primary muscle contributors to lateral propulsion in the residual limb were residual AL, AM and HAM in addition to intact AL and HAM. In opposition, the primary muscle contributors to medial propulsion for the intact limb were intact GMEDA, GMEDP, TA and IL in addition to residual GMEDA. The primary muscle contributors to medial propulsion for the residual limb were residual GMEDA and GMEDP in addition to intact GMEDA, GMEDP and SAR. The total residual limb muscle contributions to medial and lateral propulsion during the second half of stance were notably less than that of the intact limb (Figure 4.3).

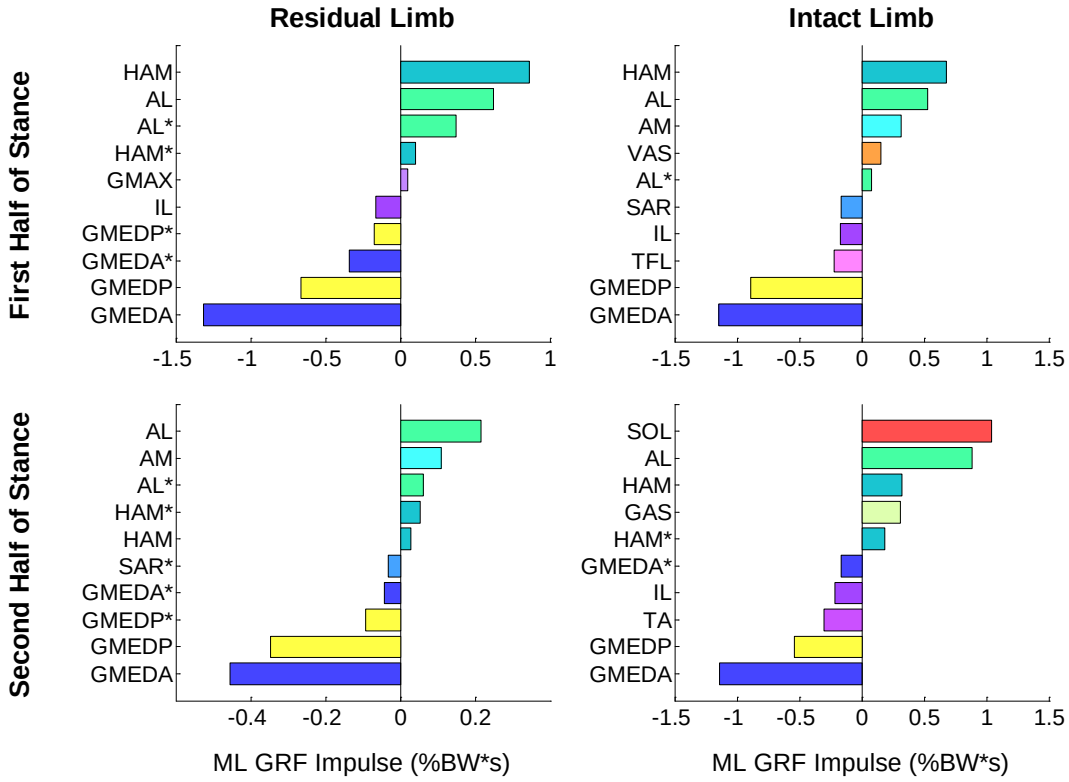

Figure 4.3: Primary positive and negative muscle group contributors to mediolateral control (ML GRF impulse) during the first and second halves of residual and intact limb stance. Positive (negative) GRF impulses indicate lateral (medial) propulsion. Note that axis ranges differ across plots. Muscles listed are from the noted limb unless marked with an asterisk, which indicates the muscle is from the contralateral limb. Muscle group colors are consistent across figures in this chapter to allow for comparison. For muscle group abbreviations, refer to Table 4.1.

Leg Swing

During leg swing initiation, the primary muscle contributors to power generation to the intact limb were intact AL and IL in addition to residual GMEDA (Figure 4.4). The primary muscle contributors to power generation to the residual limb were, similarly,

residual IL and AL in addition to intact GMEDA. In opposition to swing initiation, the primary muscle contributors to power absorption from the intact limb were intact GMEDA and VAS, and the primary muscle contributor to power absorption from the residual limb was residual GMEDA. The average muscle contributions to power generation and absorption during swing initiation were greater in the intact limb compared to the residual limb.

During early swing, the primary muscle contributors to power generation to the intact limb were residual HAM and GMEDA in addition to intact RF. The primary muscle contributors to power generation to the residual limb were intact HAM and residual IL. In opposition to early swing, the primary muscle contributor to power absorption from the intact limb was residual IL, and the primary muscle contributors to power absorption from the residual limb were intact IL and RF.

During late swing, the primary muscle contributors to power generation to the intact limb were intact GMEDP and TA. The primary muscle contributors to power generation to the residual limb were intact HAM and GMEDA. In opposition to late swing, the primary muscle contributor to power absorption from the intact limb remained the residual IL, and the primary muscle contributors to power absorption from the residual limb remained the intact IL and RF.

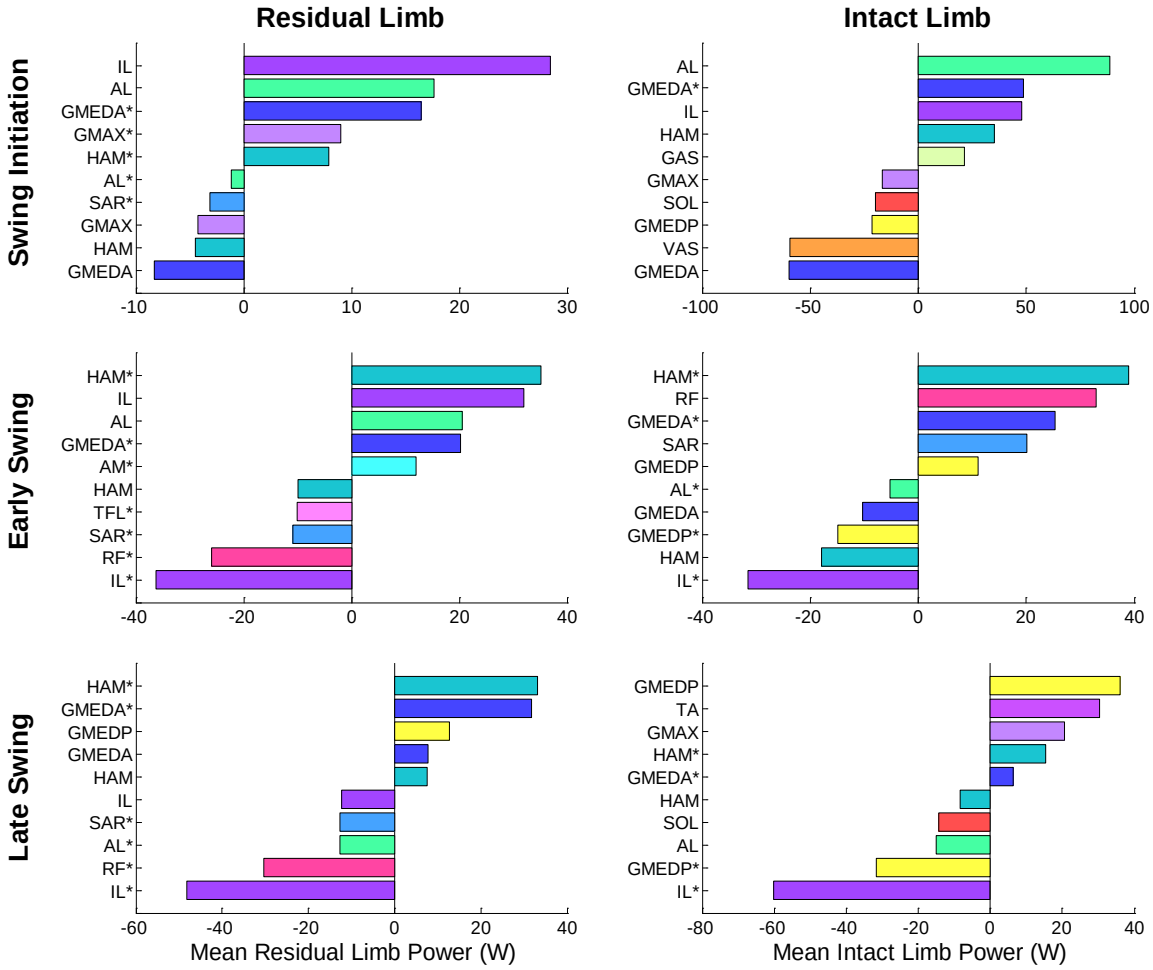

Figure 4.4: Primary muscle group contributors to the net mean mechanical power generation (positive) and absorption (negative) during swing initiation, early swing and late swing of the residual and intact limb. Note that axis ranges differ across plots. Muscles listed are from the noted limb unless marked with an asterisk, which indicates the muscle is from the contralateral limb. Muscle group colors are consistent across figures in this chapter to allow for comparison. For muscle group abbreviations, refer to Table 4.1.

Prosthesis Contributions

During the first half of stance, the prosthetic knee contributed to forward and medial propulsion, and during the second half of stance the prosthetic knee contributed to braking and medial propulsion (Figure 4.5). Throughout stance, the prosthetic foot contributed to body support as well as forward and lateral propulsion. The prosthetic foot opposed swing initiation by absorbing power, while the prosthetic knee opposed swing over its duration (Figure 4.6).

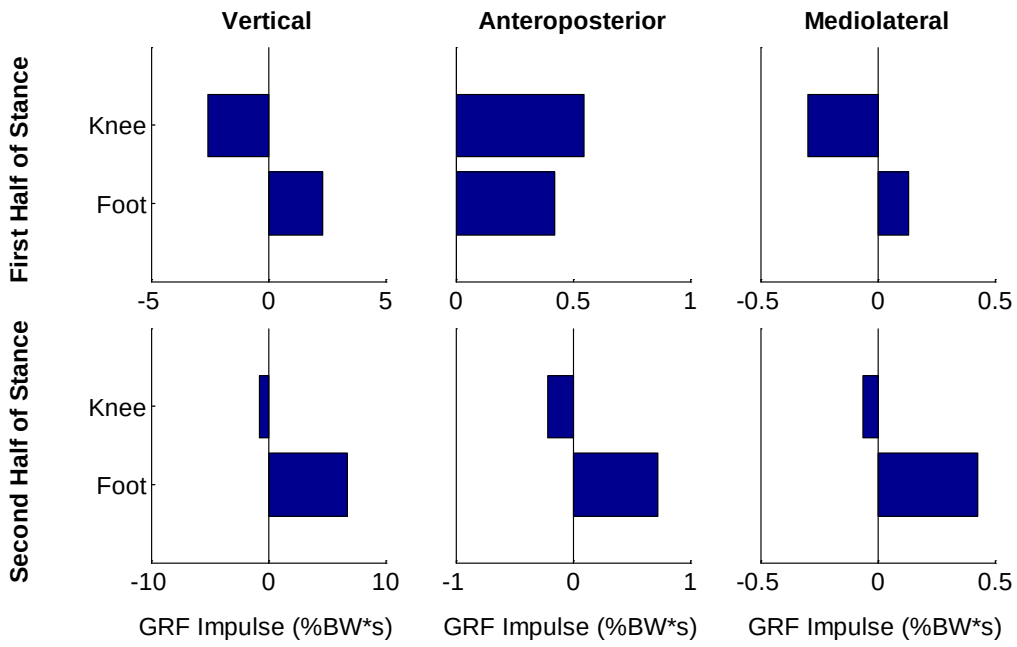

Figure 4.5: Prosthetic component contributions to body support (vertical GRF impulse), anteroposterior propulsion (anteroposterior GRF impulse), and mediolateral control (mediolateral GRF impulse) during the first and second halves of residual limb stance. Positive values indicate body support, anterior propulsion, and lateral propulsion. Contributions of the knee and foot prostheses are plotted separately.

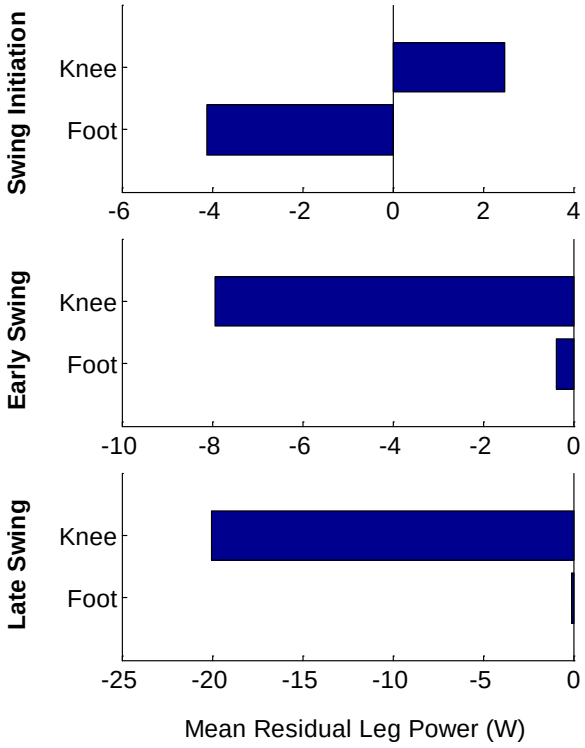

Figure 4.6: Prosthetic foot and knee contributions to the residual leg net mean mechanical power generation (positive) and absorption (negative) during swing initiation, early swing and late swing of the residual limb.

DISCUSSION

Body Support

Some of the identified muscle contributions to body support (GMAX, GMEDA and GMEDP during the first half of stance as well the ankle plantarflexors during the second half of stance) were consistent with muscle function previously examined in both non-amputee (Liu et al., 2006; Neptune et al., 2001; Silverman and Neptune, 2012) and

transtibial amputee (Silverman and Neptune, 2012) walking. However, the continued contributions of GMEDA (in addition to GMEDP in the residual limb) during the second half of stance differ from non-amputee and transtibial amputee walking, but do correspond with increased duration of gluteus medius activation during transfemoral amputee stance (Jaegers et al., 1996). VAS is also an important contributor to body support during early stance in non-amputee (Liu et al., 2006; Neptune et al., 2004; Silverman and Neptune, 2012) and transtibial amputee walking (Silverman and Neptune, 2012). However, VAS did not contribute to body support in transfemoral amputee walking. Although during a portion of the first half of stance intact VAS absorbed some power in the vertical direction from the residual and intact legs and provided power in the vertical direction to the trunk, at the very beginning of stance as well as 23% of the gait cycle after intact heel strike, VAS absorbed power in the vertical direction from the trunk (Figure B.8). VAS is also no longer functional in the residual limb after a transfemoral amputation, and thus compensations from additional muscle groups are necessary. The contributions of HAM to body support are minimal during non-amputee walking (Neptune et al., 2004), however in transfemoral amputee walking HAM transferred power in the vertical direction from both legs to the trunk (Figures B.4 and B.8), providing large contributions to body support. These contributions correspond with increased intact limb hip extensor work observed experimentally during early stance (Nolan and Lees, 2000; Seroussi et al., 1996).

Anteroposterior Propulsion

The propulsive role of GMAX during the first half of stance is consistent with findings for non-amputee walking (Neptune et al., 2004; Zajac et al., 2003). The propulsive role during the first half of stance of HAM for both limbs as well as GMEDA and GMEDP for the intact limb are also consistent with non-amputee and transtibial amputee walking (Silverman and Neptune, 2012). In addition, experimental studies have observed increased intact ankle plantarflexor work during push-off for transfemoral amputees compared to non-amputees (Nolan and Lees, 2000; Seroussi et al., 1996), which corresponds to the contralateral contributions of intact SOL to residual limb propulsion during early stance observed in this study. During the first half of both residual and intact limb stance, IL was a major contributor to braking, primarily by absorbing power in the anterior direction from the contralateral leg (Figure B.5 and B.9). The braking contributions of VAS (Neptune et al., 2004; Silverman and Neptune, 2012) and RF (Silverman and Neptune, 2012) in the intact limb are consistent with some previous investigation of non-amputee and transtibial amputee walking. As VAS is no longer functional in the residual limb, and RF, while reattached, has diminished capacity (via myoplasty stabilization, see Chapter 3), additional compensations were needed for residual limb braking. This included contributions from residual GMEDA, which absorbed power in the anterior direction from the residual leg and trunk, as well as intact HAM, which absorbed power in the anterior direction from the intact leg and trunk (Figures B.5 and B.9).

During the second half of stance, the propulsive role of the intact ankle plantarflexors is consistent with findings of studies examining non-amputee and transtibial amputee walking (Liu et al., 2006; Neptune et al., 2001; Silverman and Neptune, 2012), and the continued contributions of GMEDA and GMEDP correspond with increased duration of gluteus medius activation observed during transfemoral amputee stance (Jaegers et al., 1996). During the second half of stance, IL remained a primary contributor to braking for both the residual and intact limbs. For the intact limb, late stance braking contributions from RF are consistent with non-amputee walking (Neptune et al., 2004). Similar to the first half of stance, the changes in residual limb musculature required braking contribution compensations, including from residual AL and intact GMEDP, which absorbed power in the anterior direction from the trunk and contralateral leg, and transferred power to the ipsilateral leg (Figures B.5 and B.9).

Mediolateral Control

The role of the hip adductors to provide lateral propulsion during the first half of stance is consistent with both non-amputee (Allen and Neptune, 2012; Pandy et al., 2010; Silverman and Neptune, 2012) and transtibial amputee (Silverman and Neptune, 2012) walking, as is the laterally propulsive role of HAM (Allen and Neptune, 2012; Silverman and Neptune, 2012). The role of VAS in mediolateral control for non-amputees is unclear, with previous studies indicating they provide both lateral (Pandy et al., 2010; Silverman and Neptune, 2012) and medial (Allen and Neptune, 2012) acceleration. In the present study, VAS contributed to lateral propulsion during the first half of intact limb

stance primarily by transferring power in the lateral direction from the intact limb to the trunk and residual limb (Figure B.10). The roles of GMEDA and GMEDP to provide medial propulsion during the first half of stance in both limbs are consistent with non-amputee (Allen and Neptune, 2012; Pandy et al., 2010; Silverman and Neptune, 2012) and transtibial amputee walking (Silverman and Neptune, 2012). GMEDA provided medial propulsion by absorbing more power in the lateral direction from both legs than it provided to the trunk, and GMEDP provided medial propulsion by absorbing more power in the lateral direction from the trunk and contralateral leg than it provided to the ipsilateral leg (Figures B.6 and B.10). The medial contributions of TFL (Allen and Neptune, 2012; Silverman and Neptune, 2012) and SAR (Silverman and Neptune, 2012) in the intact limb are also consistent with non-amputee and transtibial amputee walking. The residual limb TFL and SAR while reattached, have diminished capacity (via myoplasty stabilization, see Chapter 3), necessitating compensatory medial propulsion contributions for the residual limb, including from the intact GMEDA and GMEDP.

During the second half of stance, the intact plantarflexors provided lateral propulsion for the intact limb, which is consistent with both non-amputee (Allen and Neptune, 2012; Silverman and Neptune, 2012) and transtibial amputee (Silverman and Neptune, 2012) walking. The continued lateral contribution of the hip adductors throughout stance is also consistent with a previous investigation of non-amputee and transtibial amputee walking (Silverman and Neptune, 2012). However, the continued lateral contribution of HAM is not. During the second half of stance, HAM absorbed power in the lateral direction from the legs and delivered power in the lateral direction to

the trunk (Figures B.6 and B.10). The primary contributors to medial propulsion during the second half of stance were similar to the first half, and the continued contributions of GMEDA and GMEDP throughout stance are consistent with both non-amputee (Allen and Neptune, 2012; Pandy et al., 2010; Silverman and Neptune, 2012) and transtibial amputee (Silverman and Neptune, 2012) walking.

Leg Swing

The contributions of IL and AL to swing initiation for both legs, as well GAS for the intact leg, are consistent with their function observed in both non-amputee (Neptune et al., 2001; Neptune et al., 2004; Silverman and Neptune, 2012) and transtibial amputee walking (Silverman and Neptune, 2012). While HAM does not contribute to swing initiation in non-amputees and transtibial amputees, its contributions in transfemoral amputee walking may correspond to additional muscle activity observed experimentally (Jaegers et al., 1996; Wentink et al., 2013).

Throughout swing for both legs, contralateral HAM and GMEDA acted to accelerate the leg forward by transferring power from the trunk and/or contralateral leg to the ipsilateral leg (Figures B.7 and B.11). In addition, residual IL accelerated the residual leg during early swing and residual GMEDA accelerated the residual leg during late swing by transferring power from the intact leg and/or trunk to the residual leg (Figure B.7). The contribution of residual IL to early residual leg swing is consistent with non-amputee walking (Neptune et al., 2004), however IL begins to decelerate the leg during late swing when it absorbs power from the residual leg (Figure B.7). Intact RF

accelerated the intact leg during early swing and intact GMEDP and TA accelerated the intact leg during late swing by transferring power from the trunk or residual leg to the intact leg and/or by directly generating power to the intact leg (Figure B.11). Contralateral IL acted to decelerate the legs throughout swing by absorbing significant power from the contralateral leg (Figures B.7 and B.11). Intact HAM acted to decelerate the intact leg during late swing by absorbing power from the leg, which is consistent with non-amputee walking (Neptune et al., 2004). However residual HAM acts to accelerate the residual leg, as during late swing HAM stops absorbing power from the residual leg and starts generating power to the residual leg (Figure B.7).

Prosthesis Contributions

The prosthetic foot contributed to body support throughout stance, with increased contributions in the second half, which is consistent with previous studies that have examined the functional role of a prosthetic foot in transtibial amputee walking (Fey et al., 2013; Silverman and Neptune, 2012; Zmitrewicz et al., 2007). The prosthetic foot also provided forward and lateral propulsion throughout stance, more so during the second half of stance. The lateral propulsion throughout stance (Silverman and Neptune, 2012), as well as the forward propulsion during the second half of stance is also consistent with previous investigations of a prosthetic foot in transtibial amputee walking (Fey et al., 2013; Silverman and Neptune, 2012; Zmitrewicz et al., 2007). The prosthetic foot absorbed power from the leg and transferred it to the trunk, behaving similar to the uniarticular SOL (Figures B.11 and B.12). The prosthetic knee provided forward

propulsion (braking) during the first (second) half of stance and medial propulsion throughout stance. The knee also acted to decelerate the leg throughout swing, in accordance with its damping mechanism.

Limitations

Some assumptions are required for the musculoskeletal parameters used in the model, such as the musculoskeletal geometry, musculotendon properties, and body segment mass and inertia properties. However, the optimization algorithm is capable of compensating for small deviations in model parameters from physiologic quantities by adjusting muscle excitation magnitudes. Thus, the simulation generates muscle forces that produce a motion that emulates the experimental motion, and variations in the model parameters and corresponding adjustments to the muscle excitations should have a minimal influence on the study results and conclusions.

Due to the nature of experimental data collection, it would not be possible to collect in vivo data on quantities such as muscle forces. Thus, the results of this study cannot be directly validated with experimental results. However, indirect forms of validation were used in this study. First, the simulated joint kinematics and ground reaction forces were compared to the experimental data. The average errors between simulated and experimental motion were less than two standard deviations, which indicates that the simulation quantities are statistically indistinguishable from the experimental quantities. In addition, the muscle excitation timings were compared to experimentally collected EMG of unilateral transfemoral amputee gait (Jaegers et al.,

1996; Wentink et al., 2013) to ensure that muscles are generating force at times in the gait cycle that correspond to what has been observed experimentally (Figures B.13 and B.14).

CONCLUSION

The residual limb hip muscles and the intact limb hip, knee, and ankle muscles in addition to the prosthetic foot and knee acted synergistically to complete the subtasks of transfemoral amputee walking. In comparison to non-amputee and transtibial amputee walking, increased contralateral muscle contributions were observed to compensate for the lost residual limb muscles. In addition, some muscle groups contributed to walking subtasks for longer durations than observed in non-amputee or transtibial amputee walking, which corresponds to the increased muscle activity durations observed experimentally. The results from this study provide further understanding of the functional role of individual muscles and prosthetic components in transfemoral amputee gait, which can be used in the future to design targeted rehabilitation therapies to improve locomotion.

Chapter 5: Conclusions

The overall goal of this research was to provide a foundation for improving mobility in individuals who have experienced traumatic lower-limb injuries through better understanding the influence of passive-dynamic ankle-foot orthosis (PD-AFO) design characteristics on gait performance, the influence of transfemoral amputation techniques on muscle capacity, and the functional role of muscles in transfemoral amputee walking.

In Chapter 2, the influence of PD-AFO bending axis location on gait performance in individuals with unilateral ankle muscle weakness was examined in an experimental framework. Some differences were observed in gait measures between bending axis conditions, including the peak plantarflexion angle, peak dorsiflexion moment and positive hip work during first double-leg support, peak knee extension moment and positive ankle and knee work during early single-leg support, and GAS activity and vertical GRF impulse during late single-leg support. However, differences in peak joint kinematics and kinetics were less than previously published minimal detectible changes, and no large or consistent changes in gait biomechanics were observed as a result of changes in bending axis location. However, subject bending axis location preference was strongly related to specific biomechanical quantities. This indicates that preference and comfort may be more important factors guiding the prescription of PD-AFO bending axes.

In Chapter 3, the influence of different transfemoral amputation surgical techniques on muscle capacity to generate forces and moments about the hip joint was examined using a musculoskeletal modeling framework. Residual femur alignment greatly influenced the net frontal plane hip moment and gluteus medius contribution to the frontal plane hip moment, which demonstrates the critical nature of maintaining an aligned residual limb during gait. Reattached muscle tension and stabilization method had a drastic influence on muscle capacity, and when tension was preserved in a myodesis stabilization, muscle wrap position and residual limb length had negligible influence on muscle capacity. This study supports the use of myodesis in transfemoral amputation procedures, and provides a foundation for more efficient and effective amputations.

In Chapter 4, the functional roles and compensatory mechanisms of individual muscles in the biomechanical subtasks of transfemoral amputee walking were examined using a modeling and simulation approach. The residual hip and intact hip, knee and ankle muscles worked synergistically to complete the walking subtasks of body support, anteroposterior propulsion, mediolateral control and leg swing. As result of the losses in below- and above-knee musculature in the residual limb, a number of contralateral muscle contributions to ipsilateral limb tasks were observed. In addition, some muscle groups contributed to walking subtasks for a longer duration of the gait cycle compared to non-amputee and transtibial amputee walking, which may correspond to the increased durations of muscle activity observed experimentally in transfemoral amputee walking.

These investigations explored specific elements of mobility restoration approaches, and provide a foundation for improved PD-AFO prescription guidelines,

transfemoral amputation surgical approaches and targeted rehabilitation therapies for transfemoral amputees. This research has the potential to improve mobility, and thus quality of life, for individuals who have experience traumatic lower-limb injuries.

Chapter 6: Future Work

The goal of this research was to help improve mobility in individuals who have experienced traumatic lower-limb injuries by providing foundations from which to improve orthosis design, amputation techniques, and targeted rehabilitation therapies. While this work has the potential to improve rehabilitation outcomes it also may be further explored in several areas.

In Chapter 2, the relationship between passive-dynamic ankle-foot (PD-AFO) bending axis location and gait performance was examined. While altering bending axis location did not produce large or consistent changes in gait performance, a strong qualitative preference was expressed by participants, and bending axis condition had a strong statistical measure of association with gait measures. Future work should further examine the relationship between etiology and functional deficits and bending axis preference. In order to do this, a much larger sample size would be required, particularly given the diverse range of injuries of the subjects included in this study. In addition, the individuals tested in this study were young and highly active. Populations of less-active PD-AFO users (e.g., post stroke) may not be able to compensate for changes in orthosis design as easily, and the influence of orthosis design on gait performance may be more significant. The influence of PD-AFO bending axis on gait performance should be examined in such populations so that prescription guidelines may be improved for all PD-AFO users.

In Chapter 3, the influence of transfemoral amputation surgical techniques on the capacity of individual muscles to generate forces and moments about the hip joint was examined. In this study, a generic model was scaled by the height and weight of a non-amputee. This did not account for subject-specific changes in bone or muscle morphology, which have been shown to influence muscle force predictions during gait (Bosmans et al., 2015). In order to use this framework to investigate the influence of surgical techniques on a given individual, a detailed subject-specific model should be developed and corresponding experimental data used. Current medical imaging (e.g., MRI) offers the ability to customize a musculoskeletal model based on physiologic musculoskeletal geometry, including not only personalized bone morphology and muscle attachment sites, but also potentially the tracking of muscle atrophy and remodeling to allow for the model to be revised with the subject's ongoing rehabilitation and healing. The use of such subject-specific models would allow for a tailored understanding of different surgical interventions. In addition, this study demonstrated the benefits of myodesis stabilization in transfemoral amputation through a modeling framework, thus providing a first step towards clinical trials. Future work should also investigate the influence of muscle stabilization technique in a clinical setting, in order to create universally improved and accepted surgical procedures.

In Chapter 4, the functional roles of individual muscles in transfemoral amputee walking were examined. By understanding individual muscle contributions and corresponding compensations, targeted rehabilitation therapies may be developed to ensure that primary contributors to walking subtasks are strengthened as needed. Future

work should focus on developing these therapies and assessing their efficacy in an experimental setting. The model and tracking data used in Chapter 4 were group-averaged. However, variable gait strategies exist in transfemoral amputees, and variability in muscle activity has been observed (Jaegers et al., 1996; Wentink et al., 2013). Future work should use subject-specific musculoskeletal models to generate subject-specific forward dynamics simulations. Such a framework would allow clinicians to provide customized, targeted rehabilitation recommendations. Lastly, the model used in this study assumed a rigid fixation at the interface between the residual limb and prosthesis; however, pistoning is known to occur during walking. Creating a model of the socket interface would not only further improve model accuracy, but also allow the examination of muscle contributions to the interface. For example, it has been postulated that a secondary activation of residual hip muscles prior to swing may be a socket-fitting compensation (Wentink et al., 2013). The increased muscle activation would increase muscle volume and thus socket interface pressure (Hong and Mun, 2005), providing a more secure fit. By including this interface in the model, simulations of transfemoral amputee gait may be able to capture and analyze such additional muscle compensations.

The studies investigated in this dissertation provide an important step towards improving mobility in individuals who have experienced traumatic lower-limb injuries. These studies may be expanded upon in several exciting avenues for future work, which have the potential to further customize rehabilitation approaches and thus improve rehabilitation outcomes and quality of life for these individuals.

Appendix A: Supplemental Material for Chapter 2

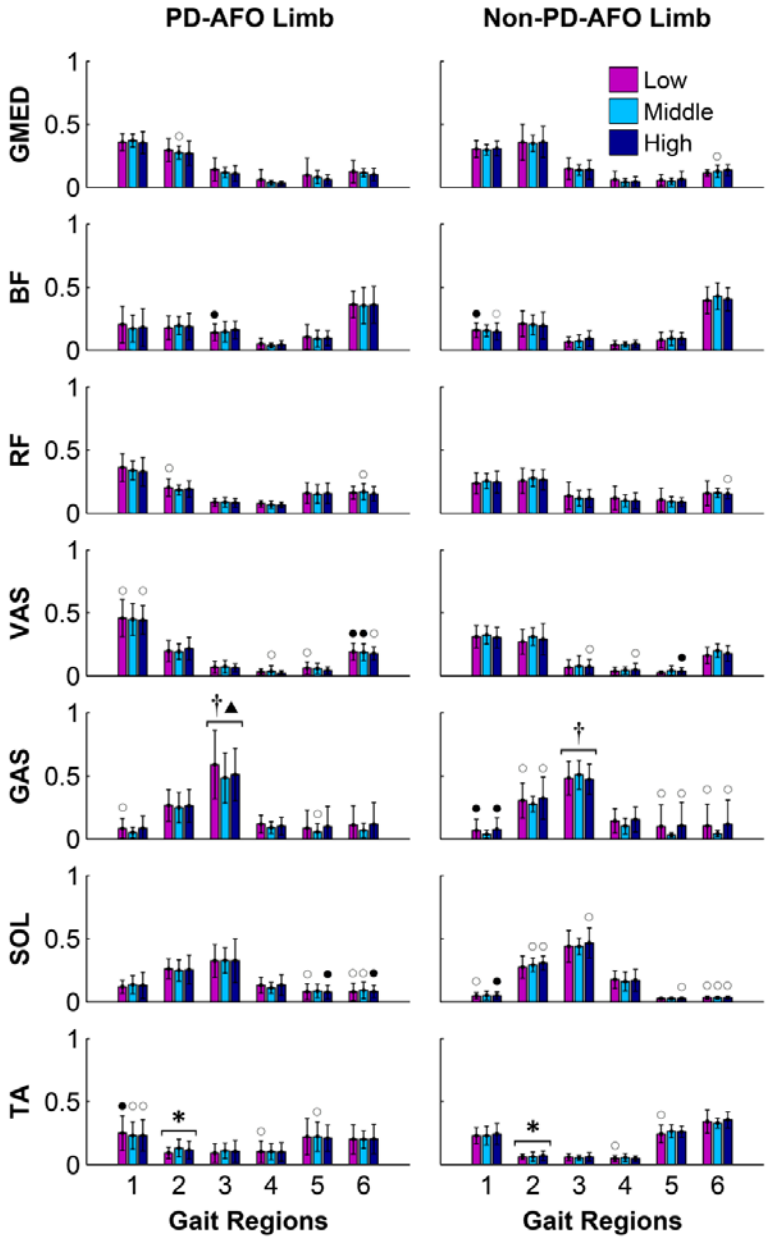

Figure A.1: Average (±standard deviation) integrated electromyographic values at Froude speed for the low, middle and high bending axes during six regions of the gait cycle: 1) first double-leg support, 2) early single-leg support, 3) late single-leg support, 4) second double-leg support, 5) early swing, and 6) late swing. Data are presented for the gluteus medius (GMED), biceps femoris long head (BF), rectus femoris (RF), vastus medialis (VAS), medial gastrocnemius (GAS), soleus (SOL) and tibialis anterior (TA). Significant bending axis main effects (*), bending axis*limb interaction effects (†), low to middle bending axis comparisons (▲) and large effect sizes between preference and iEMG are indicated (○: $\eta^2 > 0.26$; ●: $\eta^2 > 0.50$).

Table A.1: Average (standard deviation) peak joint kinematics and kinetics at Froude speed (positive values indicate dorsiflexion, knee flexion and hip flexion). The gait cycle regions during which the peaks occur are indicated as 1) first double-leg support, 2) early single-leg support, 3) late single-leg support, 4) second double-leg support, 5) early swing, and 6) late swing. Significant differences between the low and middle (▲) bending axis conditions are noted. Gait measures are shaded gray for preference effects sizes $\eta^2 > 0.26$ and dark gray for $\eta^2 > 0.50$.

			Peak Joint Kinematics (°)		
	Region	**Limb**	**Low**	**Middle**	**High**
Ankle Angle					
Plantarflexion ▲	1	PD-AFO	-7.30 (2.01)	-6.16 (1.94)	-6.75 (1.62)
		Non-PD-AFO	-2.45 (1.67)	-1.85 (1.92)	-1.97 (2.81)
Dorsiflexion	4	PD-AFO	5.98 (1.58)	5.23 (1.38)	4.92 (1.24)
		Non-PD-AFO	15.27 (2.50)	15.22 (2.40)	14.97 (2.49)
Plantarflexion	5	PD-AFO	-0.66 (0.63)	-0.51 (0.51)	-0.56 (0.52)
		Non-PD-AFO	-15.53 (3.78)	-14.86 (4.15)	-15.67 (5.01)
Knee Angle					
Flexion	2	PD-AFO	16.36 (6.82)	17.20 (5.02)	17.41 (6.10)
		Non-PD-AFO	14.98 (5.67)	16.25 (4.45)	15.86 (5.94)
Extension	3	PD-AFO	4.79 (5.84)	4.71 (4.98)	5.31 (4.64)
		Non-PD-AFO	2.10 (2.37)	3.10 (2.97)	2.76 (3.36)
Flexion	5	PD-AFO	62.82 (5.29)	62.60 (4.17)	62.78 (5.10)
		Non-PD-AFO	62.32 (4.37)	62.67 (4.08)	62.35 (4.21)
Hip Angle					
Extension	4	PD-AFO	-3.39 (4.07)	-3.07 (5.49)	-4.30 (5.41)
		Non-PD-AFO	-5.54 (3.91)	5.41 (6.25)	-6.00 (5.96)
Flexion	6	PD-AFO	38.10 (4.58)	38.31 (5.65)	37.16 (5.53)
		Non-PD-AFO	34.31 (3.81)	34.76 (4.06)	33.80 (4.33)
			Peak Joint Kinetics (Nm/kg)		
Ankle Moment					
Dorsiflexion ▲	1	PD-AFO	0.43 (0.06)	0.38 (0.06)	0.40 (0.10)
		Non-PD-AFO	0.23 (0.07)	0.22 (0.07)	0.24 (0.08)
Plantarflexion	4	PD-AFO	-1.43 (0.23)	-1.46 (0.19)	-1.43 (0.18)
		Non-PD-AFO	-1.36 (0.18)	-1.38 (0.19)	-1.34 (0.18)
Knee Moment					
Flexion	1	PD-AFO	0.44 (0.09)	0.43 (0.07)	0.42 (0.08)
		Non-PD-AFO	0.57 (0.11)	0.59 (0.09)	0.56 (0.11)
Extension	2	PD-AFO	-0.64 (0.18)	-0.59 (0.17)	-0.65 (0.19)
		Non-PD-AFO	-0.46 (0.17)	-0.47 (0.13)	-0.50 (0.20)
Flexion	3	PD-AFO	0.36 (0.16)	0.41 (0.16)	0.35 (0.10)
		Non-PD-AFO	0.40 (0.13)	0.40 (0.13)	0.39 (0.15)
Hip Moment					
Extension	1	PD-AFO	-0.93 (0.18)	-0.96 (0.20)	-0.93 (0.21)
		Non-PD-AFO	-1.08 (0.20)	-1.12 (0.17)	-1.08 (0.20)
Flexion	4	PD-AFO	0.57 (0.12)	0.57 (0.16)	0.59 (0.17)
		Non-PD-AFO	0.55 (0.15)	0.54 (0.15)	0.55 (0.13)

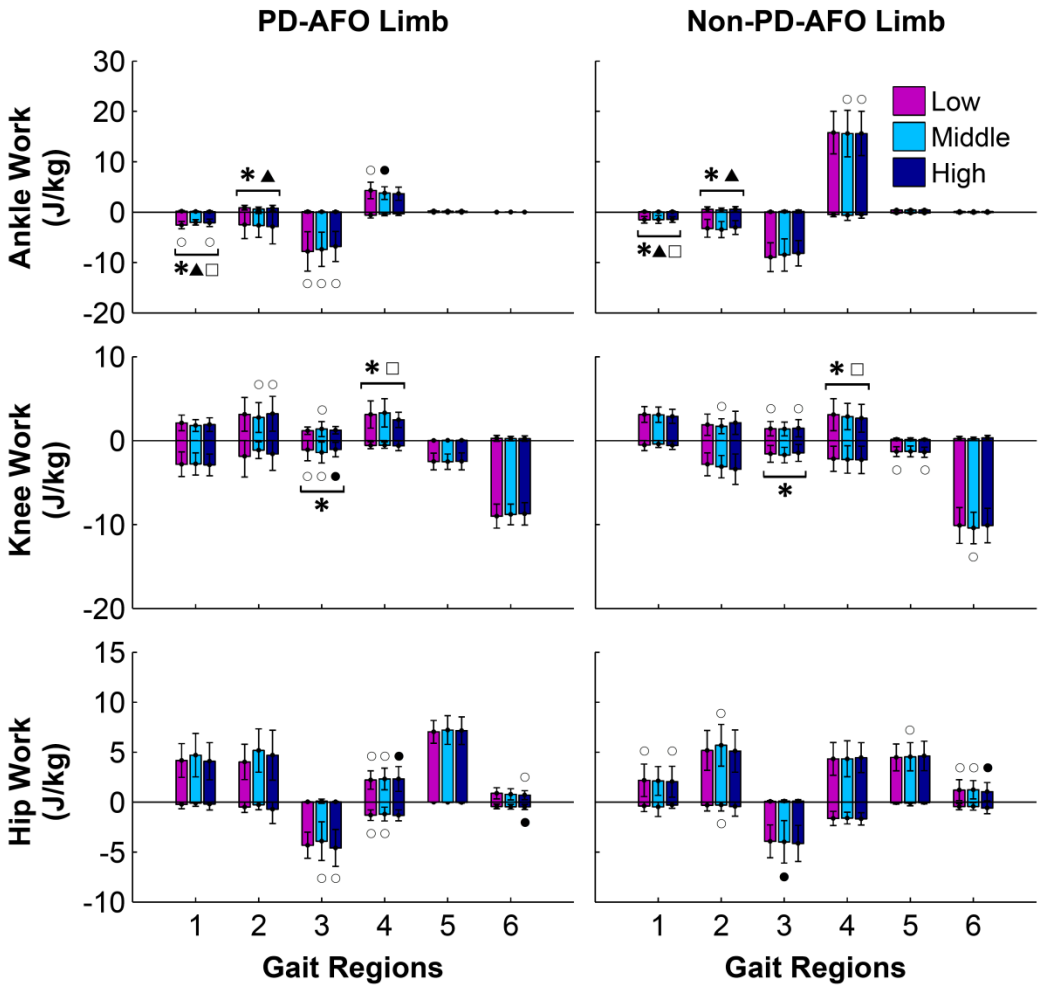

Figure A.2: Average (± standard deviation) joint work at Froude walking speed in the PD-AFO and non-PD-AFO limbs for the low, middle and high bending axis conditions during six regions of the gait cycle: 1) first double-leg support, 2) early single-leg support, 3) late single-leg support, 4) second double-leg support, 5) early swing, and 6) late swing. Average positive and negative joint work and respective standard deviations are presented separately. Significant bending axis main effects (*), low to middle bending axis comparisons (▲) and low to high bending axis comparisons (□) are indicated. Large effect sizes between preference and joint work are also indicated (○: $\eta^2 > 0.26$; ●: $\eta^2 > 0.50$).

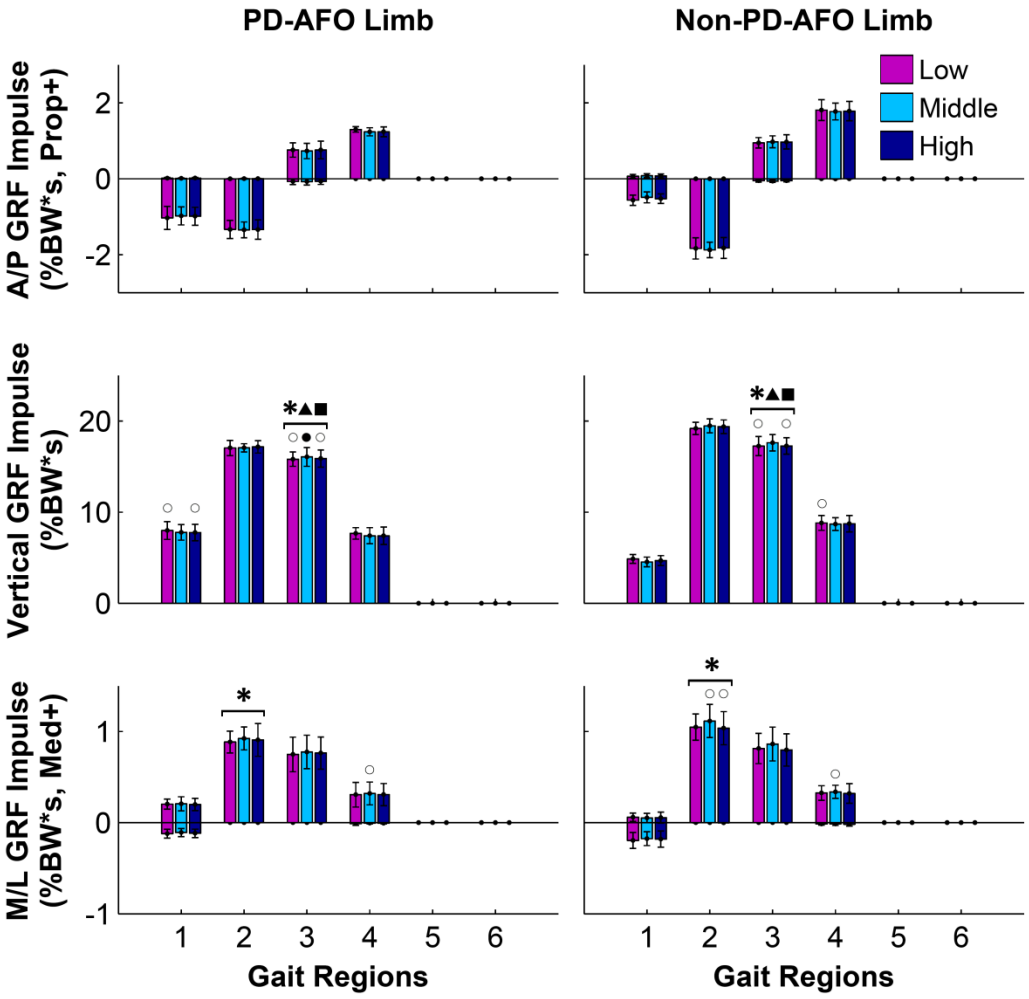

Figure A.3: Average (± standard deviation) ground reaction force (GRF) impulses at Froude walking speed in the PD-AFO and non-PD-AFO limbs for the low, middle and high bending axis conditions during six regions of the gait cycle: 1) first double-leg support, 2) early single-leg support, 3) late single-leg support, 4) second double-leg support, 5) early swing, and 6) late swing. Anteroposterior (A/P), vertical and mediolateral (M/L) positive and negative GRF impulses and respective standard deviations are presented separately. Significant bending axis main effects (*), low to middle bending axis comparisons (▲), and high to middle bending axis comparisons (■) are indicated. Large effect sizes between preference and GRF impulse are also indicated (○: $\eta^2 > 0.26$; ●: $\eta^2 > 0.50$).

Appendix B: Supplemental Material for Chapter 4

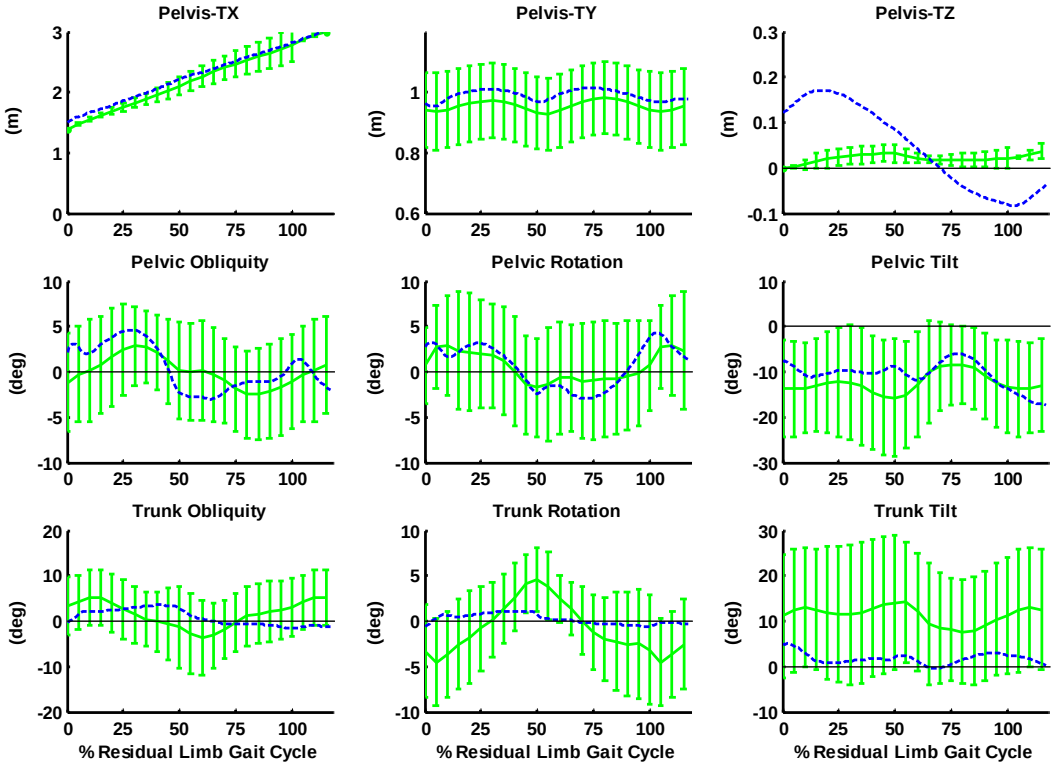

Figure B.1: Trunk and pelvis kinematics of average experimental motion (standard deviation bars, green solid line) and simulated motion (dashed blue line).

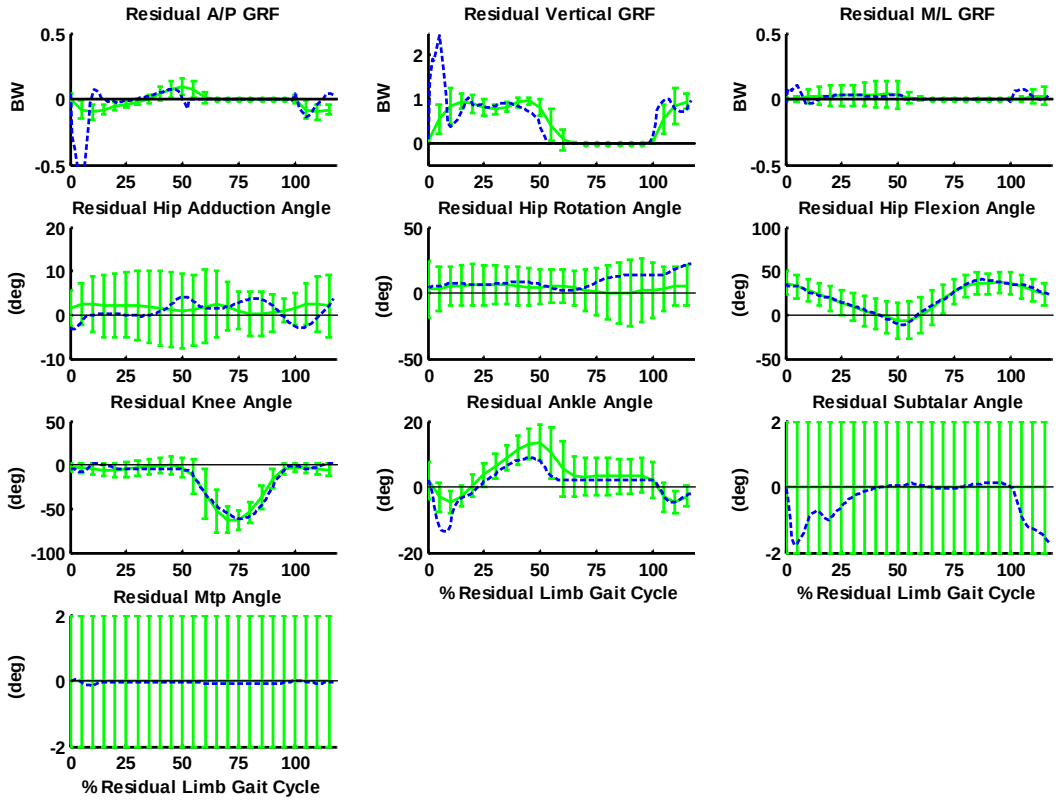

Figure B.2: Residual limb kinematics and ground reaction forces (GRFs) of average experimental motion (standard deviation bars, green solid line) and simulated motion (dashed blue line). The residual knee, ankle, subtalar and mtp angles represent prosthetic components.

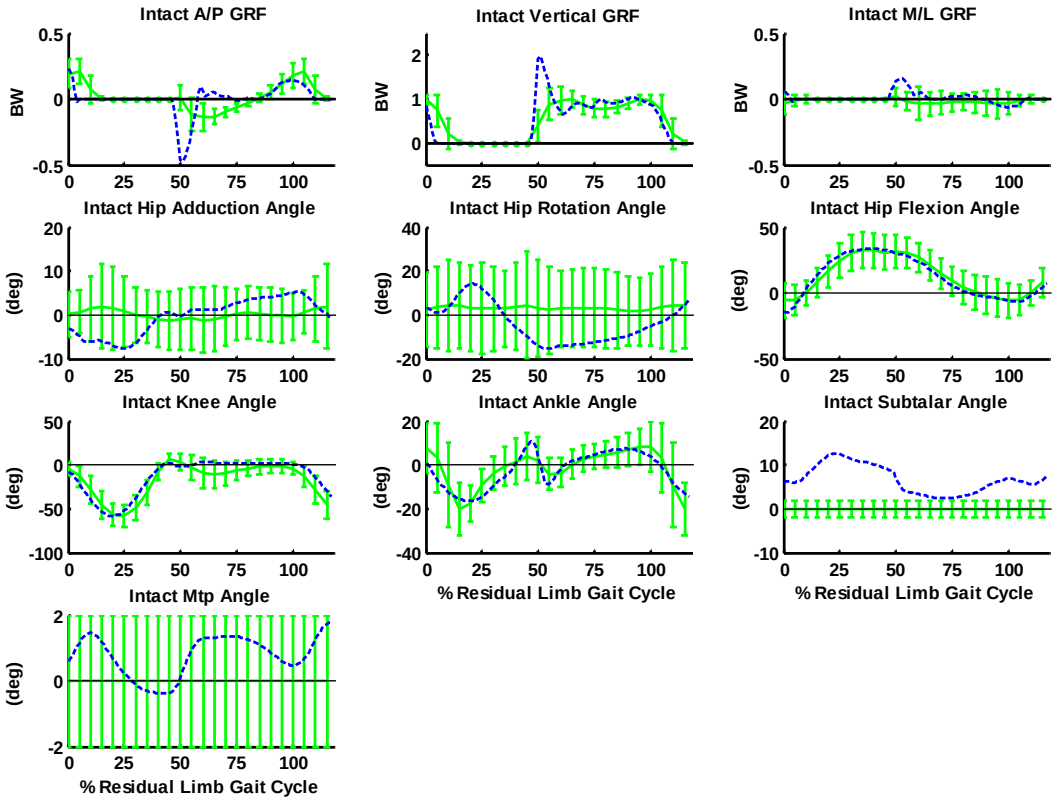

Figure B.3: Intact limb kinematics and ground reaction forces (GRFs) of average experimental motion (standard deviation bars, green solid line) and simulated motion (dashed blue line).

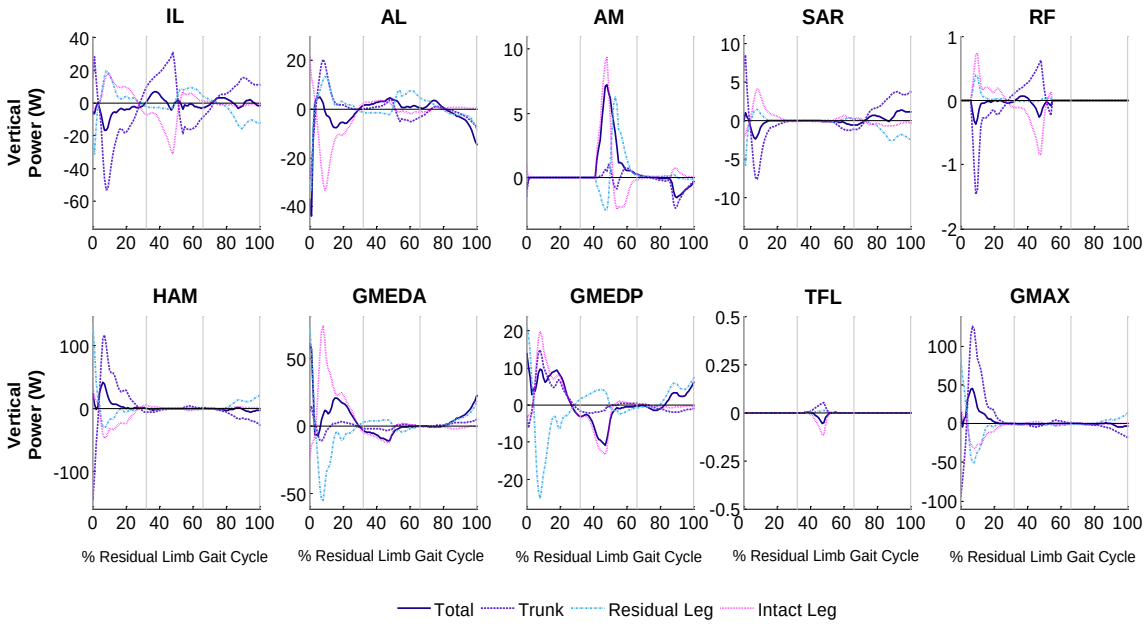

Figure B.4: Musculotendon mechanical power output for the residual limb muscle groups over the residual limb gait cycle and power generated to (positive) and absorbed from (negative) the trunk, residual leg, and intact leg in the vertical direction. The gray lines on the plots divide the gait cycle into the first and second halves of stance, and swing. For muscle group abbreviations, refer to Table 4.1.

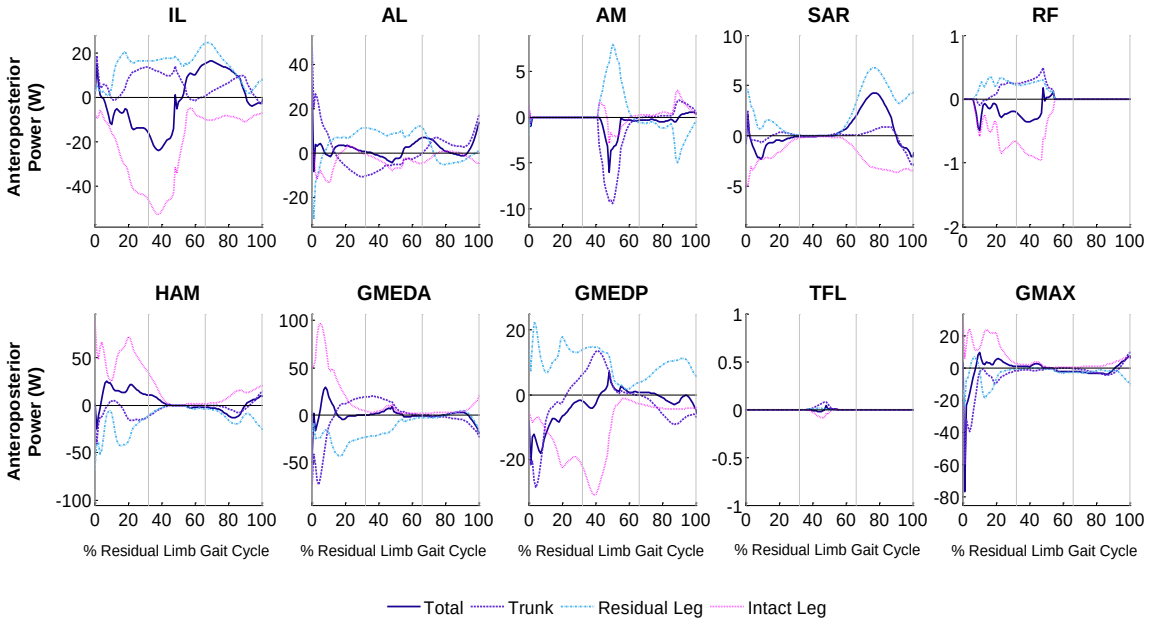

Figure B.5: Musculotendon mechanical power output for the residual limb muscle groups over the residual limb gait cycle and power generated to (positive) and absorbed from (negative) the trunk, residual leg, and intact leg in the anteroposterior direction. The gray lines on the plots divide the gait cycle into the first and second halves of stance, and swing. For muscle group abbreviations, refer to Table 4.1.

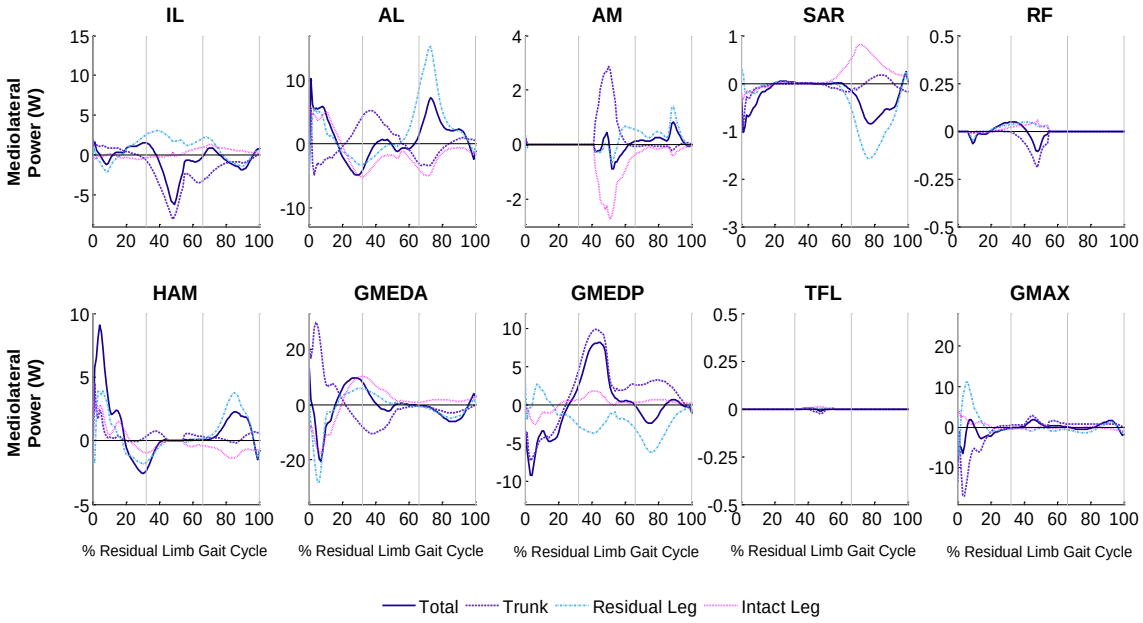

Figure B.6: Musculotendon mechanical power output for the residual limb muscle groups over the residual limb gait cycle and power generated to (positive) and absorbed from (negative) the trunk, residual leg, and intact leg in the mediolateral direction. The gray lines on the plots divide the gait cycle into the first and second halves of stance, and swing. For muscle group abbreviations, refer to Table 4.1.

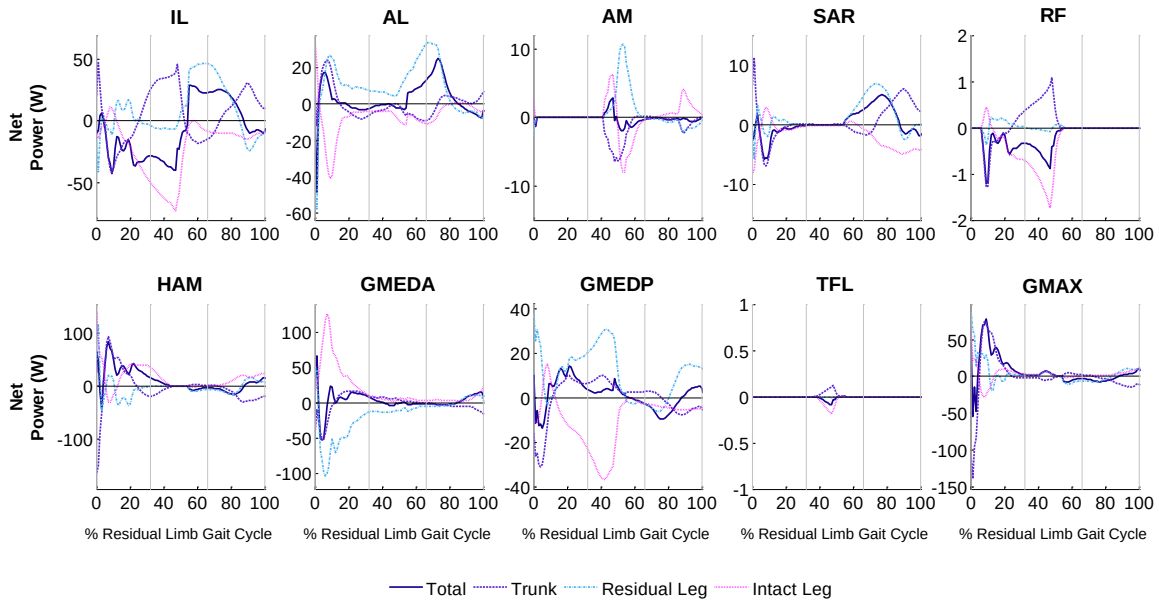

Figure B.7: Musculotendon mechanical power output for the residual limb muscle groups over the residual limb gait cycle and power generated to (positive) and absorbed from (negative) the trunk, residual leg, and intact leg. The gray lines on the plots divide the gait cycle into the first and second halves of stance, and swing. For muscle group abbreviations, refer to Table 4.1.

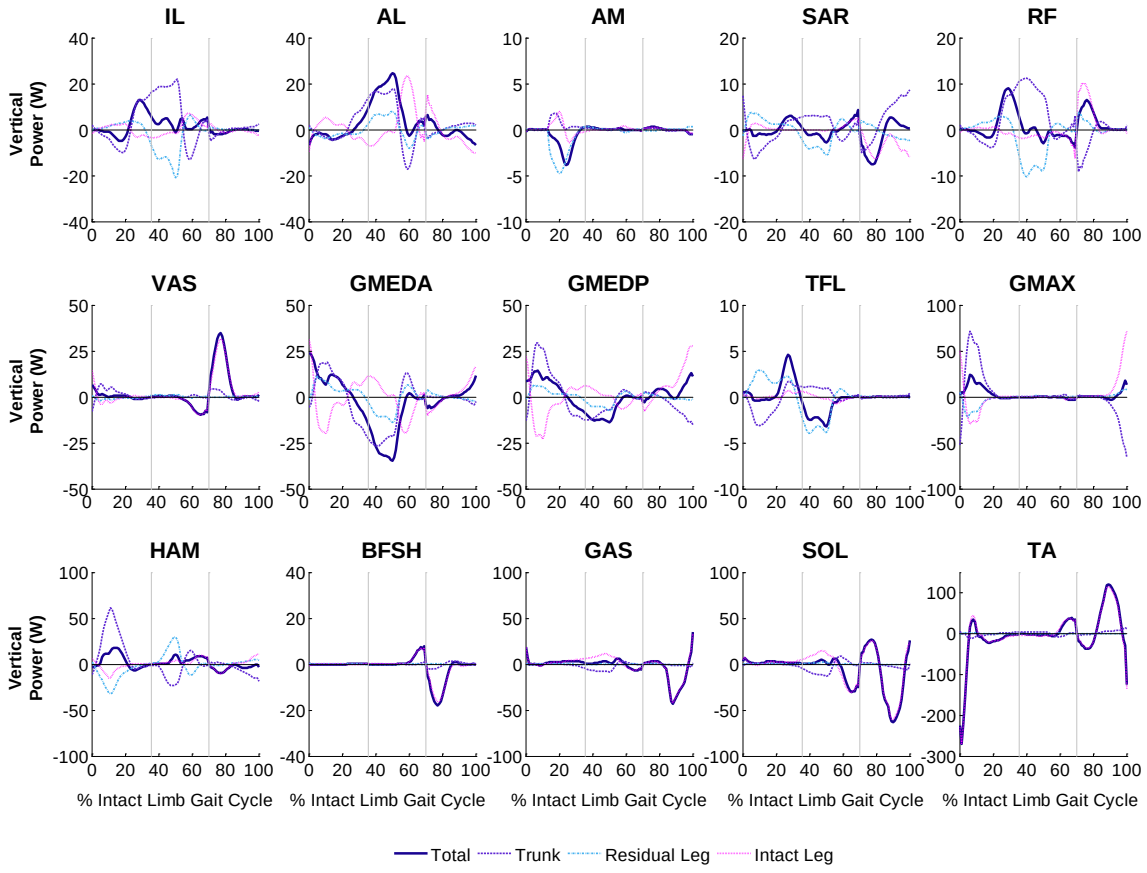

Figure B.8: Musculotendon mechanical power output for the intact limb muscle groups over the intact limb gait cycle and power generated to (positive) and absorbed from (negative) the trunk, residual leg, and intact leg in the vertical direction. The gray lines on the plots divide the gait cycle into the first and second halves of stance, and swing. For muscle group abbreviations, refer to Table 4.1.

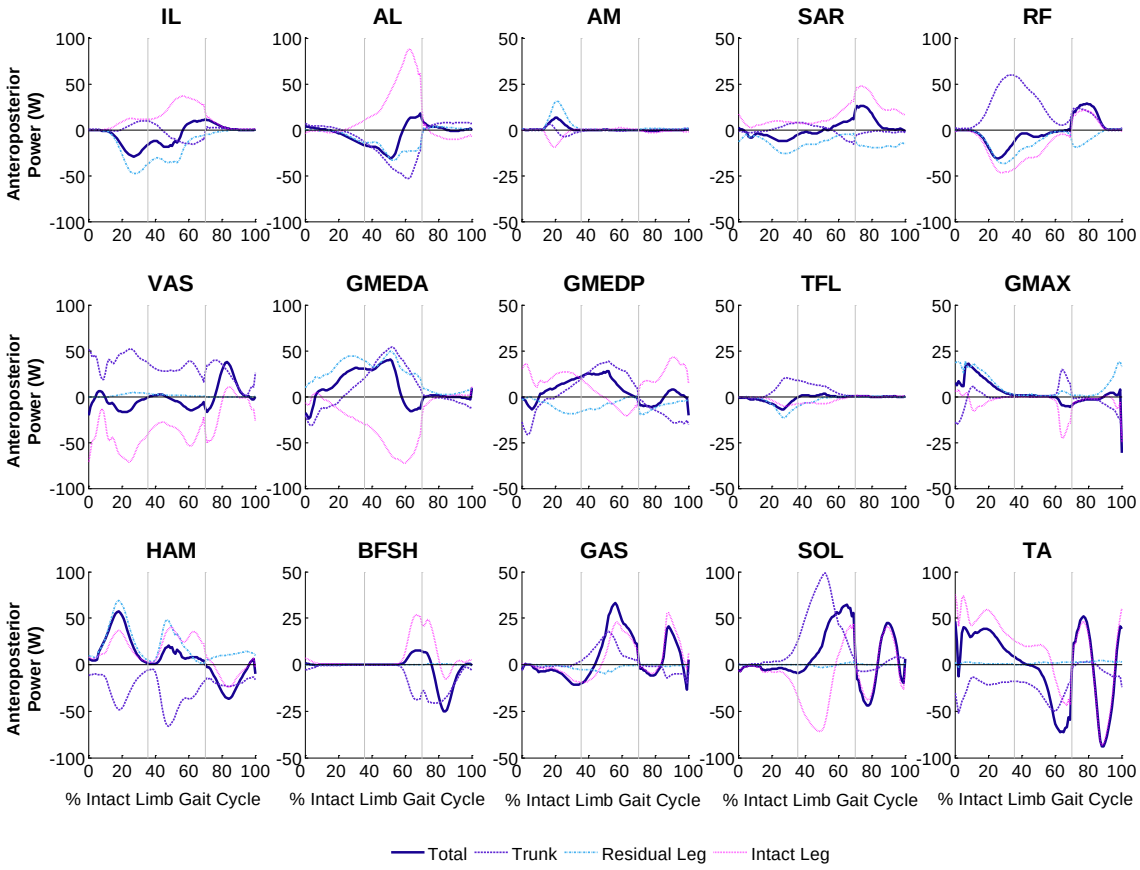

Figure B.9: Musculotendon mechanical power output for the intact limb muscle groups over the intact limb gait cycle and power generated to (positive) and absorbed from (negative) the trunk, residual leg, and intact leg in the anteroposterior direction. The gray lines on the plots divide the gait cycle into the first and second halves of stance, and swing. For muscle group abbreviations, refer to Table 4.1.

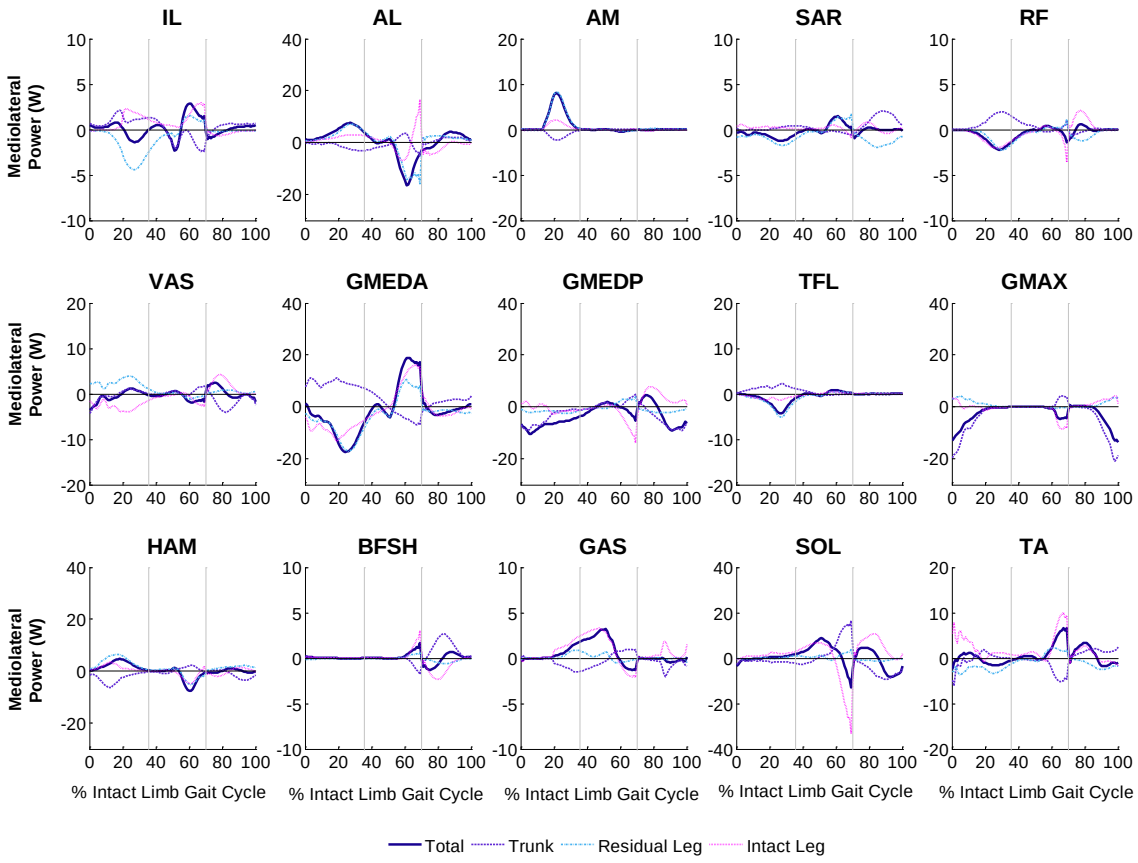

Figure B.10: Musculotendon mechanical power output for the intact limb muscle groups over the intact limb gait cycle and power generated to (positive) and absorbed from (negative) the trunk, residual leg, and intact leg in the mediolateral direction. The gray lines on the plots divide the gait cycle into the first and second halves of stance, and swing. For muscle group abbreviations, refer to Table 4.1.

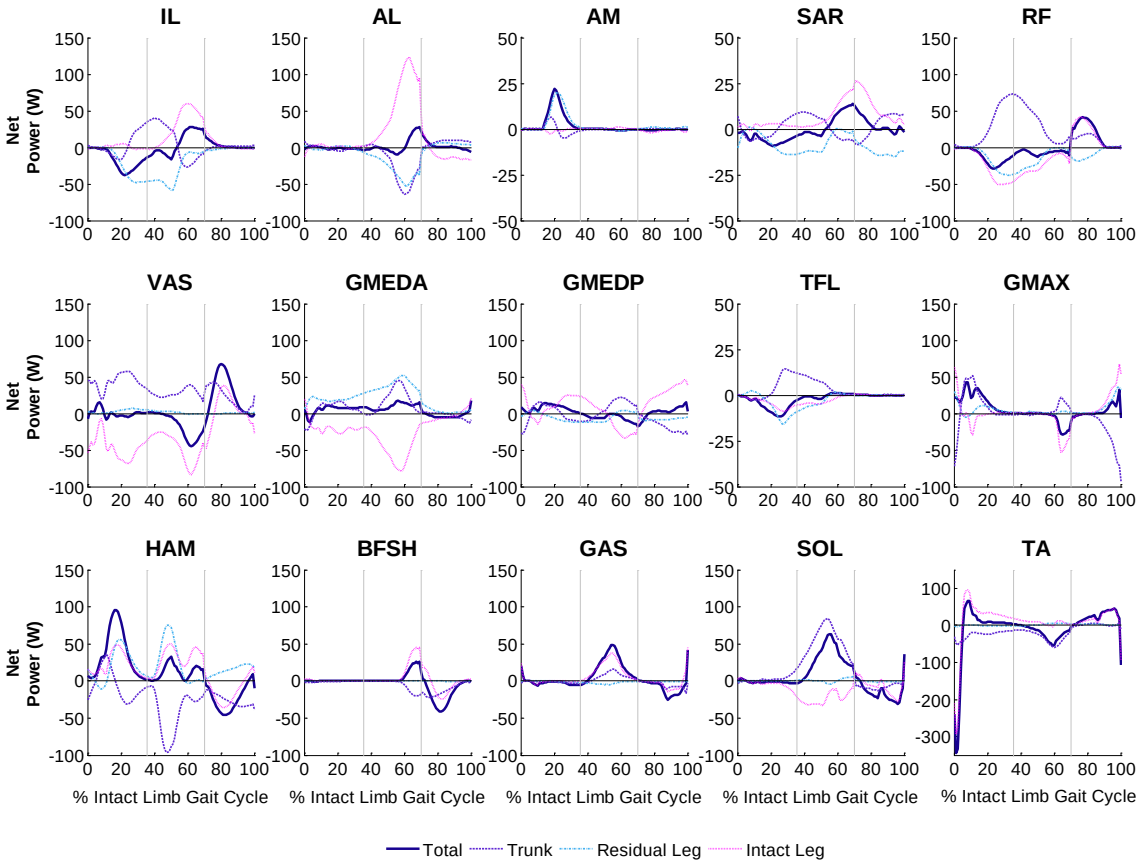

Figure B.11: Musculotendon mechanical power output for the intact limb muscle groups over the intact limb gait cycle and power generated to (positive) and absorbed from (negative) the trunk, residual leg, and intact leg. The gray lines on the plots divide the gait cycle into the first and second halves of stance, and swing. For muscle group abbreviations, refer to Table 4.1.

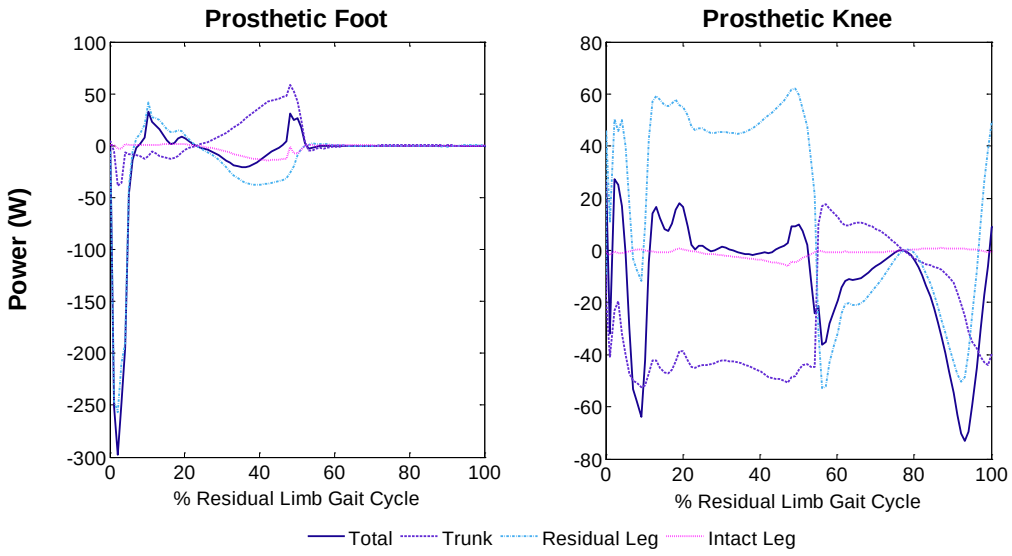

Figure B.12: Mechanical power output for the prosthetic foot and knee over the residual limb gait cycle and power generated to (positive) and absorbed from (negative) the trunk, residual leg, and intact leg.

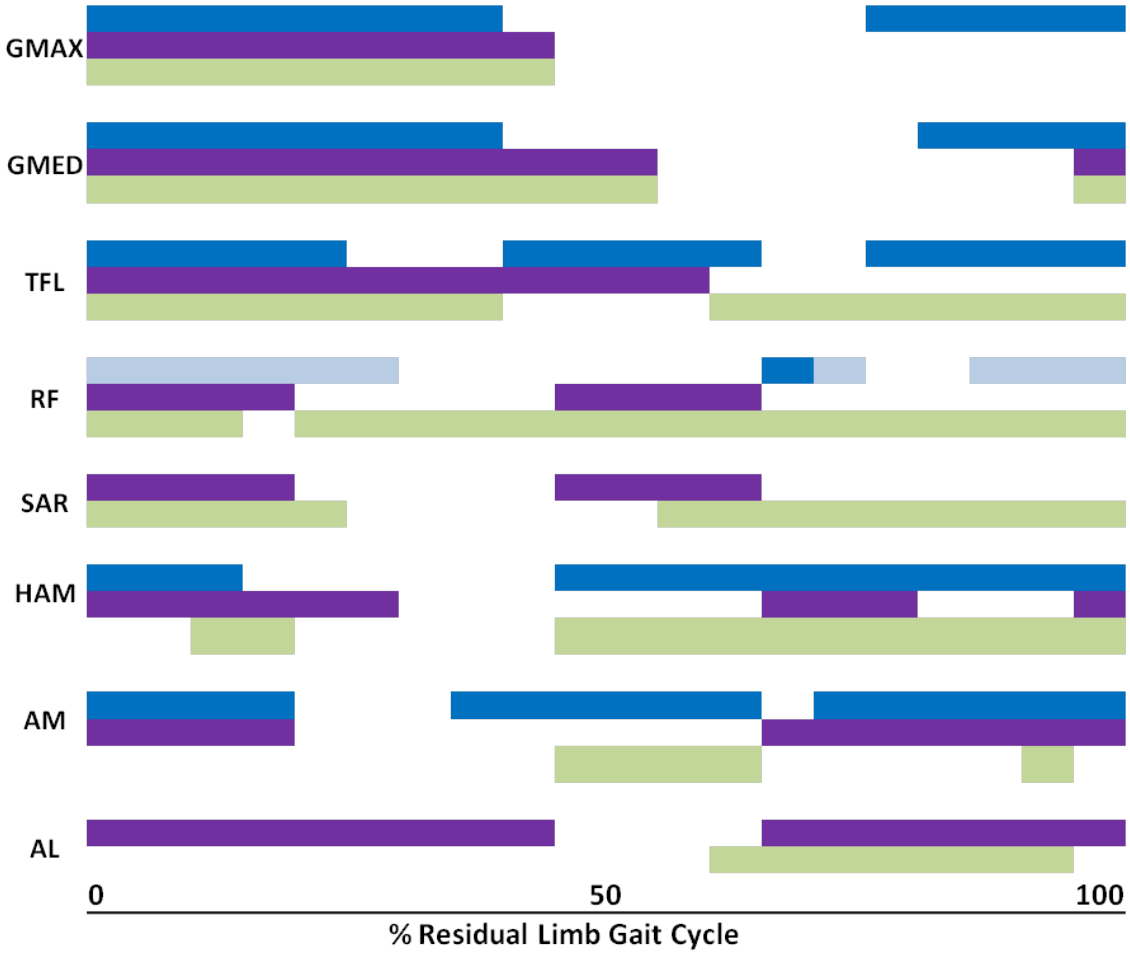

Figure B.13: Residual limb muscle activity timings for the simulated (green) and experimental data (blue and purple). The blue data represents the group average muscle activity timings observed by Wentink et al. (2013) (light blue indicates data that may be due to cross-talk) and the purple data represents timings observed by Jaegers et al. (1996).

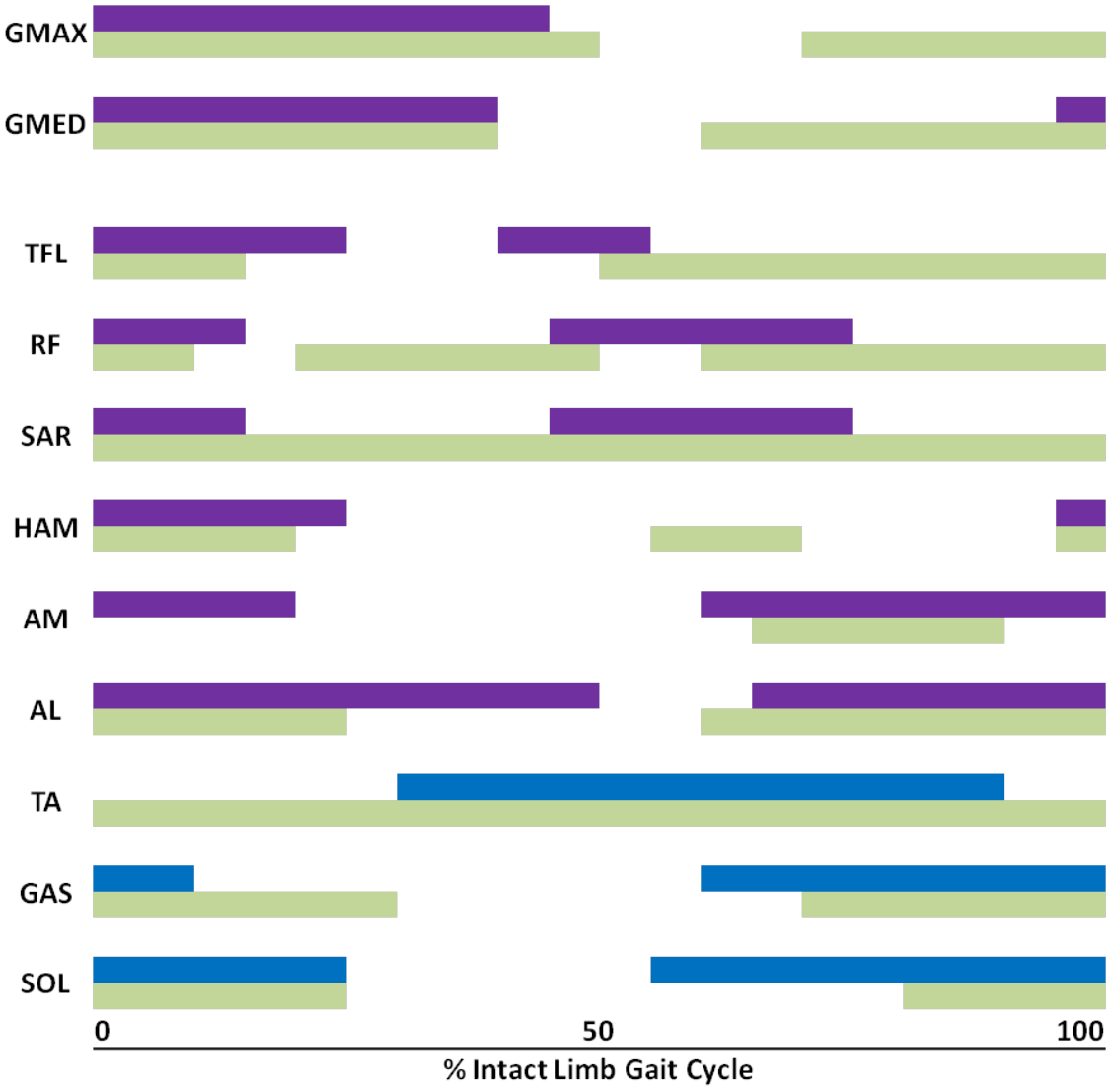

Figure B.14: Intact limb muscle activity timings for the simulated (green) and experimental data (blue and purple). The blue data represents the group average muscle activity timings observed by Wentink et al. (2013) (light blue indicates data that may be due to cross-talk) and the purple data represents timings observed by Jaegers et al. (1996).

References

(2015). *Incidents by ais body region*. National Trauma Data Bank Annual Report 2015. Nance, M. L. Chicago, IL, Committee on Trauma, American College of Surgeons.

Allen, J. L. and Neptune, R. R. (2012). *Three-dimensional modular control of human walking.* J Biomech **45**(12): 2157-63.

Anderson, F. C. and Pandy, M. G. (1999). *A dynamic optimization solution for vertical jumping in three dimensions.* Comput Methods Biomech Biomed Engin **2**(3): 201-31.

Anderson, F. C. and Pandy, M. G. (2003). *Individual muscle contributions to support in normal walking.* Gait Posture **17**(2): 159-69.

Arch, E. and Stanhope, S. (2015). *Passive-dynamic ankle–foot orthoses substitute for ankle strength while causing adaptive gait strategies: A feasibility study.* Ann Biomed Eng. **43**(2): 442-50.

Arnold, A. S., Schwartz, M. H., Thelen, D. G. and Delp, S. L. (2007). *Contributions of muscles to terminal-swing knee motions vary with walking speed.* J Biomech **40**(16): 3660-71.

Bae, T. S., Choi, K. and Mun, M. (2009). *Level walking and stair climbing gait in above-knee amputees.* J Med Eng Technol **33**(2): 130-5.

Baker, R. (2001). *Pelvic angles: A mathematically rigorous definition which is consistent with a conventional clinical understanding of the terms.* Gait Posture **13**(1): 1-6.

Baum, B. S., Schnall, B. L., Tis, J. E. and Lipton, J. S. (2008). *Correlation of residual limb length and gait parameters in amputees.* Injury **39**(7): 728-33.

Bell, J. C., Wolf, E. J., Schnall, B. L., Tis, J. E. and Potter, B. K. (2014). *Transfemoral amputations: Is there an effect of residual limb length and orientation on energy expenditure?* Clin Orthop Relat Res **472**(10): 3055-61.

Bell, J. C., Wolf, E. J., Schnall, B. L., Tis, J. E., Tis, L. L. and Potter, B. K. (2013). *Transfemoral amputations: The effect of residual limb length and orientation on gait analysis outcome measures.* J Bone Joint Surg Am **95**(5): 408-14.

Bosmans, L., Valente, G., Wesseling, M., Van Campen, A., De Groote, F., De Schutter, J. and Jonkers, I. (2015). *Sensitivity of predicted muscle forces during gait to anatomical variability in musculotendon geometry.* J Biomech **48**(10): 2116-23.

Bottlang, M., Marsh, J. L. and Brown, T. D. (1999). *Articulated external fixation of the ankle: Minimizing motion resistance by accurate axis alignment.* J Biomech **32**(1): 63-70.

Bregman, D. J., van der Krogt, M. M., de Groot, V., Harlaar, J., Wisse, M. and Collins, S. H. (2011). *The effect of ankle foot orthosis stiffness on the energy cost of walking: A simulation study.* Clin Biomech **26**(9): 955-61.

Bresnahan, L., Fessler, R. G. and Natarajan, R. N. (2010). *Evaluation of change in muscle activity as a result of posterior lumbar spine surgery using a dynamic modeling system.* Spine (Phila Pa 1976) **35**(16): E761-7.

Burkett, B., Smeathers, J. and Barker, T. (2004). *A computer model to simulate the swing phase of a transfemoral prosthesis.* J Appl Biomech **20**: 25-37.

Cohen, J. (2013). *The analysis of variance*. Statistical power analysis for the behavioral sciences, Taylor and Francis**:** 274-88.

Davy, D. T. and Audu, M. L. (1987). *A dynamic optimization technique for predicting muscle forces in the swing phase of gait.* J Biomech **20**(2): 187-201.

Delp, S. L., Anderson, F. C., Arnold, A. S., Loan, P., Habib, A., John, C. T., Guendelman, E. and Thelen, D. G. (2007). *Opensim: Open-source software to create and analyze dynamic simulations of movement.* IEEE Trans Biomed Eng **54**(11): 1940-50.

Delp, S. L. and Loan, J. P. (2000). *A computational framework for simulating and analyzing human and animal movement.* Comput Sci Eng. **2**(5): 46-55.

Delp, S. L., Loan, J. P., Hoy, M. G., Zajac, F. E., Topp, E. L. and Rosen, J. M. (1990). *An interactive graphics-based model of the lower extremity to study orthopaedic surgical procedures.* IEEE Trans Biomed Eng **37**(8): 757-67.

Delp, S. L., Ringwelski, D. A. and Carroll, N. C. (1994). *Transfer of the rectus femoris: Effects of transfer site on moment arms about the knee and hip.* J Biomech **27**(10): 1201-11.

Desloovere, K., Molenaers, G., Van Gestel, L., Huenaerts, C., Van Campenhout, A., Callewaert, B., Van de Walle, P. and Seyler, J. (2006). *How can push-off be preserved during use of an ankle foot orthosis in children with hemiplegia? A prospective controlled study.* Gait Posture **24**(2): 142-51.

Fatone, S. and Hansen, A. H. (2007). *A model to predict the effect of ankle joint misalignment on calf band movement in ankle-foot orthoses.* Prosthet Orthot Int **31**(1): 76-87.

Fatone, S., Johnson, W. B. and Kwak, S. (2016). *Using a three-dimensional model of the ankle-foot orthosis/leg to explore the effects of combinations of axis misalignments.* Prosthet Orthot Int. **40**(2): 247-52.

Faustini, M. C., Neptune, R. R., Crawford, R. H., Rogers, W. E. and Bosker, G. (2006). *An experimental and theoretical framework for manufacturing prosthetic sockets for transtibial amputees.* IEEE Trans Neural Syst Rehabil Eng **14**(3): 304-10.

Faustini, M. C., Neptune, R. R., Crawford, R. H. and Stanhope, S. J. (2008). *Manufacture of passive dynamic ankle-foot orthoses using selective laser sintering.* IEEE Trans Biomed Eng **55**(2 Pt 1): 784-90.

Fergason, J., Keeling, J. J. and Bluman, E. M. (2010). *Recent advances in lower extremity amputations and prosthetics for the combat injured patient.* Foot Ankle Clin **15**(1): 151-74.

Fey, N. P., Klute, G. K. and Neptune, R. R. (2011). *The influence of energy storage and return foot stiffness on walking mechanics and muscle activity in below-knee amputees.* Clin Biomech **26**(10): 1025-32.

Fey, N. P., Klute, G. K. and Neptune, R. R. (2012). *Optimization of prosthetic foot stiffness to reduce metabolic cost and intact knee loading during below-knee amputee walking: A theoretical study.* J Biomech Eng **134**(11): 111005.

Fey, N. P., Klute, G. K. and Neptune, R. R. (2013). *Altering prosthetic foot stiffness influences foot and muscle function during below-knee amputee walking: A modeling and simulation analysis.* J Biomech **46**(4): 637-44.

Friederich, J. A. and Brand, R. A. (1990). *Muscle fiber architecture in the human lower limb.* J Biomech **23**(1): 91-5.

Gao, F., Carlton, W. and Kapp, S. (2011). *Effects of joint alignment and type on mechanical properties of thermoplastic articulated ankle-foot orthosis.* Prosthet Orthot Int **35**(2): 181-9.

Goffe, W. L., Ferrier, G. D. and Rogers, J. (1994). *Global optimization of stastitical functions with simulated annealing.* Journal of Econometrics **60**: 65-99.

Gottschalk, F. (1999). *Transfemoral amputation. Biomechanics and surgery.* Clin Orthop Relat Res(361): 15-22.

Gottschalk, F. (2004). *Transfemoral amputation: Surgical management*. Atlas of amputation and limb deficiencies: Surgical, prosthetic and rehabilitation principles. DG Smith, J. M., JH Bowker, American Academy of Orthopedic Surgeons**:** 533-40.

Goujon-Pillet, H., Sapin, E., Fode, P. and Lavaste, F. (2008). *Three-dimensional motions of trunk and pelvis during transfemoral amputee gait.* Arch Phys Med Rehabil **89**(1): 87-94.

Granville, R. and Menetrez, J. (2010). *Rehabilitation of the lower-extremity war-injured at the center for the intrepid.* Foot Ankle Clin **15**(1): 187-99.

Grood, E. S. and Suntay, W. J. (1983). *A joint coordinate system for the clinical description of three-dimensional motions: Application to the knee.* J Biomech Eng **105**(2): 136-44.

Haight, D. J., Russell Esposito, E. and Wilken, J. M. (2015). *Biomechanics of uphill walking using custom ankle-foot orthoses of three different stiffnesses.* Gait Posture **41**(3): 750-6.

Harper, N. G., Esposito, E. R., Wilken, J. M. and Neptune, R. R. (2014a). *The influence of ankle-foot orthosis stiffness on walking performance in individuals with lower-limb impairments.* Clin Biomech **29**(8): 877-84.

Harper, N. G., Russell, E. M., Wilken, J. M. and Neptune, R. R. (2014b). *Selective laser sintered versus carbon fiber passive-dynamic ankle-foot orthoses: A comparison of patient walking performance.* J Biomech Eng **136**(9): 091001.

Hong, J. H. and Mun, M. S. (2005). *Relationship between socket pressure and emg of two muscles in trans-femoral stumps during gait.* Prosthet Orthot Int **29**(1): 59-72.

Jaegers, S. M., Arendzen, J. H. and de Jongh, H. J. (1996). *An electromyographic study of the hip muscles of transfemoral amputees in walking.* Clin Orthop Relat Res(328): 119-28.

Jaegers, S. M. H. J., Arendzen, J. H. and Dejongh, H. J. (1995). *Prosthetic gait of unilateral transfemoral amputees - a kinematic study.* Arch Phys Med Rehab **76**(8): 736-43.

Keeling, J. J., Hsu, J. R., Shawen, S. B. and Andersen, R. C. (2010). *Strategies for managing massive defects of the foot in high-energy combat injuries of the lower extremity.* Foot Ankle Clin **15**(1): 139-49.

Krueger, C. A., Wenke, J. C. and Ficke, J. R. (2012). *Ten years at war: Comprehensive analysis of amputation trends.* J Trauma Acute Care Surg **73**(6 Suppl 5): S438-44.

Laferrier, J. Z. and Gailey, R. (2010). *Advances in lower-limb prosthetic technology.* Phys Med Rehabil Clin N Am **21**(1): 87-110.

Leardini, A., Aquila, A., Caravaggi, P., Ferraresi, C. and Giannini, S. (2014). *Multi-segment foot mobility in a hinged ankle-foot orthosis: The effect of rotation axis position.* Gait Posture **40**(1): 274-7.

Liu, M. Q., Anderson, F. C., Pandy, M. G. and Delp, S. L. (2006). *Muscles that support the body also modulate forward progression during walking.* J Biomech **39**(14): 2623-30.

Liu, M. Q., Anderson, F. C., Schwartz, M. H. and Delp, S. L. (2008). *Muscle contributions to support and progression over a range of walking speeds.* J Biomech **41**(15): 3243-52.

Magermans, D. J., Chadwick, E. K., Veeger, H. E., Rozing, P. M. and van der Helm, F. C. (2004). *Effectiveness of tendon transfers for massive rotator cuff tears: A simulation study.* Clin Biomech **19**(2): 116-22.

Marra, M. A., Vanheule, V., Fluit, R., Koopman, B. H. F. J. M., Rasmussen, J., Verdonschot, N. and Andersen, M. S. (2015). *A subject-specific musculoskeletal modeling framework to predict in vivo mechanics of total knee arthroplasty.* J Biomech Eng. **137**(2): 020904.

McGowan, C. P., Kram, R. and Neptune, R. R. (2009). *Modulation of leg muscle function in response to altered demand for body support and forward propulsion during walking.* J Biomech **42**(7): 850-6.

Neptune, R. R., Kautz, S. A. and Zajac, F. E. (2001). *Contributions of the individual ankle plantar flexors to support, forward progression and swing initiation during walking.* J Biomech **34**(11): 1387-98.

Neptune, R. R., Sasaki, K. and Kautz, S. A. (2008). *The effect of walking speed on muscle function and mechanical energetics.* Gait Posture **28**(1): 135-43.

Neptune, R. R., Zajac, F. E. and Kautz, S. A. (2004). *Muscle force redistributes segmental power for body progression during walking.* Gait Posture **19**(2): 194-205.

Nolan, L. and Lees, A. (2000). *The functional demands on the intact limb during walking for active trans-femoral and trans-tibial amputees.* Prosthet Orthot Int **24**(2): 117-25.

Owens, B. D., Kragh, J. F., Jr., Macaitis, J., Svoboda, S. J. and Wenke, J. C. (2007). *Characterization of extremity wounds in operation iraqi freedom and operation enduring freedom.* J Orthop Trauma **21**(4): 254-7.

Owens, J. G. (2010). *Physical therapy of the patient with foot and ankle injuries sustained in combat.* Foot Ankle Clin **15**(1): 175-86.

Pandy, M. G., Lin, Y.-C. and Kim, H. J. (2010). *Muscle coordination of mediolateral balance in normal walking.* J Biomech **43**(11): 2055-64.

Patzkowski, J. C., Blanck, R. V., Owens, J. G., Wilken, J. M., Blair, J. A. and Hsu, J. R. (2011). *Can an ankle-foot orthosis change hearts and minds?* J Surg Orthop Adv **20**(1): 8-18.

Patzkowski, J. C., Blanck, R. V., Owens, J. G., Wilken, J. M., Kirk, K. L., Wenke, J. C. and Hsu, J. R. (2012). *Comparative effect of orthosis design on functional performance.* J Bone Joint Surg Am **94**(6): 507-15.

Pejhan, S., Farahmand, F. and Parnianpour, M. (2008). *Design optimization of an above-knee prosthesis based on the kinematics of gait.* Conf Proc IEEE Eng Med Biol Soc **2008**: 4274-7.

Peterson, C. L., Hall, A. L., Kautz, S. A. and Neptune, R. R. (2010). *Pre-swing deficits in forward propulsion, swing initiation and power generation by individual muscles during hemiparetic walking.* J Biomech **43**(12): 2348-55.

Piazza, S. J. and Delp, S. L. (2001). *Three-dimensional dynamic simulation of total knee replacement motion during a step-up task.* J Biomech Eng **123**(6): 599-606.

Raasch, C. C., Zajac, F. E., Ma, B. and Levine, W. S. (1997). *Muscle coordination of maximum-speed pedaling.* J Biomech **30**(6): 595-602.

Raschke, S. U., Orendurff, M. S., Mattie, J. L., Kenyon, D. E., Jones, O. Y., Moe, D., Winder, L., Wong, A. S., Moreno-Hernandez, A., Highsmith, M. J., D, J. S. and Kobayashi, T. (2015). *Biomechanical characteristics, patient preference and activity level with different prosthetic feet: A randomized double blind trial with laboratory and community testing.* J Biomech **48**(1): 146-52.

Rogers, B., Bosker, G. W., Crawford, R. H., Faustini, M. C., Neptune, R. R., Walden, G. and Gitter, A. J. (2007). *Advanced trans-tibial socket fabrication using selective laser sintering.* Prosthet Orthot Int **31**(1): 88-100.

Russell Esposito, E., Blanck, R. V., Harper, N. G., Hsu, J. R. and Wilken, J. M. (2014). *How does ankle-foot orthosis stiffness affect gait in patients with lower limb salvage?* Clin Orthop Relat Res **472**(10): 3026-35.

Schmalz, T., Blumentritt, S. and Jarasch, R. (2002). *Energy expenditure and biomechanical characteristics of lower limb amputee gait: The influence of prosthetic alignment and different prosthetic components.* Gait Posture **16**(3): 255-63.

Schrank, E. S. and Stanhope, S. J. (2011). *Dimensional accuracy of ankle-foot orthoses constructed by rapid customization and manufacturing framework.* J Rehabil Res Dev **48**(1): 31-42.

Seroussi, R. E., Gitter, A., Czerniecki, J. M. and Weaver, K. (1996). *Mechanical work adaptations of above-knee amputee ambulation.* Arch Phys Med Rehabil **77**(11): 1209-14.

Shandiz, M. A., Farahmand, F., Abu Osman, N. A. and Zohoor, H. (2013). *A robotic model of transfemoral amputee locomotion for design optimization of knee controllers.* Int J Adv Robot Syst **10**.

Shawen, S. B., Keeling, J. J., Branstetter, J., Kirk, K. L. and Ficke, J. R. (2010). *The mangled foot and leg: Salvage versus amputation.* Foot Ankle Clin **15**(1): 63-75.

Silverman, A. K. and Neptune, R. R. (2012). *Muscle and prosthesis contributions to amputee walking mechanics: A modeling study.* J Biomech **45**(13): 2271-8.

Slowik, J. S. and Neptune, R. R. (2013). *A theoretical analysis of the influence of wheelchair seat position on upper extremity demand.* Clin Biomech **28**(4): 378-85.

South, B. J., Fey, N. P., Bosker, G. and Neptune, R. R. (2010). *Manufacture of energy storage and return prosthetic feet using selective laser sintering.* J Biomech Eng **132**(1): 015001.

Sumiya, T., Suzuki, Y., Kasahara, T. and Ogata, H. (1997). *Instantaneous centers of rotation in dorsi/plantar flexion movements of posterior-type plastic ankle-foot orthoses.* J Rehabil Res Dev **34**(3): 279-85.

Suzuki, Y. (2010). *Dynamic optimization of transfemoral prosthesis during swing phase with residual limb model.* Prosthet Orthot Int **34**(4): 428-38.

Thelen, D. G. (2003). *Adjustment of muscle mechanics model parameters to simulate dynamic contractions in older adults.* J Biomech Eng **125**(1): 70-7.

Thelen, D. G. and Anderson, F. C. (2006). *Using computed muscle control to generate forward dynamic simulations of human walking from experimental data.* J Biomech **39**(6): 1107-15.

Tintle, S. M., Forsberg, J. A., Keeling, J. J., Shawen, S. B. and Potter, B. K. (2010a). *Lower extremity combat-related amputations.* J Surg Orthop Adv **19**(1): 35-43.

Tintle, S. M., Keeling, J. J. and Shawen, S. B. (2010b). *Combat foot and ankle trauma.* J Surg Orthop Adv **19**(1): 70-6.

Tsai, C. S. and Mansour, J. M. (1986). *Swing phase simulation and design of above knee prostheses.* J Biomech Eng **108**(1): 65-72.

Van Gestel, L., Molenaers, G., Huenaerts, C., Seyler, J. and Desloovere, K. (2008). *Effect of dynamic orthoses on gait: A retrospective control study in children with hemiplegia.* Dev Med Child Neurol **50**(1): 63-7.

Vaughan, C. L. and O'Malley, M. J. (2005). *Froude and the contribution of naval architecture to our understanding of bipedal locomotion.* Gait Posture **21**(3): 350-62.

Ventura, J. D., Klute, G. K. and Neptune, R. R. (2011a). *The effect of prosthetic ankle energy storage and return properties on muscle activity in below-knee amputee walking.* Gait Posture **33**(2): 220-6.

Ventura, J. D., Klute, G. K. and Neptune, R. R. (2011b). *The effects of prosthetic ankle dorsiflexion and energy return on below-knee amputee leg loading.* Clin Biomech **26**(3): 298-303.

Waters, R. L., Perry, J., Antonelli, D. and Hislop, H. (1976). *Energy cost of walking of amputees: The influence of level of amputation.* J Bone Joint Surg Am **58**(1): 42-6.

Wentink, E. C., Prinsen, E. C., Rietman, J. S. and Veltink, P. H. (2013). *Comparison of muscle activity patterns of transfemoral amputees and control subjects during walking.* J Neuroeng Rehabil **10**: 87.

Wickiewicz, T. L., Roy, R. R., Powell, P. L. and Edgerton, V. R. (1983). *Muscle architecture of the human lower limb.* Clin Orthop Relat Res(179): 275-83.

Wilken, J. M., Rodriguez, K. M., Brawner, M. and Darter, B. J. (2012). *Reliability and minimal detectible change values for gait kinematics and kinetics in healthy adults.* Gait Posture **35**(2): 301-7.

Winters, J. M. and Stark, L. (1988). *Estimated mechanical properties of synergistic muscles involved in movements of a variety of human joints.* J Biomech **21**(12): 1027-41.

Wu, G. and Cavanagh, P. R. (1995). *Isb recommendations for standardization in the reporting of kinematic data.* J Biomech **28**(10): 1257-61.

Wu, G., Siegler, S., Allard, P., Kirtley, C., Leardini, A., Rosenbaum, D., Whittle, M., D'Lima, D. D., Cristofolini, L., Witte, H., Schmid, O. and Stokes, I. (2002). *Isb recommendation on definitions of joint coordinate system of various joints for the reporting of human joint motion--part i: Ankle, hip, and spine. International society of biomechanics.* J Biomech **35**(4): 543-8.

Yang, J. F. and Winter, D. A. (1984). *Electromyographic amplitude normalization methods: Improving their sensitivity as diagnostic tools in gait analysis.* Arch Phys Med Rehabil **65**(9): 517-21.

Zajac, F. E. (1989). *Muscle and tendon: Properties, models, scaling, and application to biomechanics and motor control.* Crit Rev Biomed Eng **17**(4): 359-411.

Zajac, F. E., Neptune, R. R. and Kautz, S. A. (2002). *Biomechanics and muscle coordination of human walking. Part i: Introduction to concepts, power transfer, dynamics and simulations.* Gait Posture **16**(3): 215-32.

Zajac, F. E., Neptune, R. R. and Kautz, S. A. (2003). *Biomechanics and muscle coordination of human walking: Part ii: Lessons from dynamical simulations and clinical implications.* Gait Posture **17**(1): 1-17.

Ziegler-Graham, K., MacKenzie, E. J., Ephraim, P. L., Travison, T. G. and Brookmeyer, R. (2008). *Estimating the prevalence of limb loss in the united states: 2005 to 2050.* Arch Phys Med Rehabil **89**(3): 422-9.

Zmitrewicz, R. J., Neptune, R. R. and Sasaki, K. (2007). *Mechanical energetic contributions from individual muscles and elastic prosthetic feet during symmetric unilateral transtibial amputee walking: A theoretical study.* J Biomech **40**(8): 1824-31.

Vita

Ellyn Cymbre Ranz attended Washington University in Saint Louis where she received her Bachelor of Science in Biomedical Engineering and Master of Science in Mechanical Engineering in December, 2010. She subsequently joined an orthopedic biomechanics lab at the Washington University School of Medicine where she worked as a research technician until entering the Graduate School at The University of Texas at Austin in August, 2011. The focus of her graduate research has been examining elements of mobility restoration approaches for individuals who have experienced traumatic lower-limb injuries, including assistive devices, surgical techniques and rehabilitation therapies. The overarching goal of this research is to improve rehabilitation outcomes for individuals who have experienced traumatic lower-limb injuries.

Permanent address (or email): ellynranz@utexas.edu

This dissertation was typed by the author.